KfK 2836
Mai 1979

Proceedings of the Joint CERN-KfK-Workshop on Physics with Cooled Low Energetic Antiprotons

Karlsruhe, Federal Republic of Germany, March 19-21, 1979

Editor: H. Poth
Institut für Kernphysik

Kernforschungszentrum Karlsruhe

KERNFORSCHUNGSZENTRUM KARLSRUHE

Institut für Kernphysik

KfK 2836

PROCEEDINGS OF THE JOINT CERN - KfK - WORKSHOP ON PHYSICS WITH COOLED LOW ENERGETIC ANTIPROTONS

Karlsruhe, Federal Republic of Germany,

March 19-21, 1979

Editor: H. Poth

Kernforschungszentrum Karlsruhe GmbH, Karlsruhe

Kernforschungszentrum Karlsruhe GmbH
und CERN, Genf
ISSN 0303-4003

Preface

The workshop on Physics with cooled low energetic antiprotons was jointly organized by CERN and the Kernforschungszentrum Karlsruhe. Two important developments motivated this meeting.

Until now only little is known about the antinucleon annihilation and the low energy antinucleon interaction. Recently, however, strong evidence was found for unexpectedly narrow $\bar{N}N$ states at low energies, but the meager intensity of the present antiproton beams does not allow a more detailed study. The existence of narrow states around the nucleon antinucleon threshold is an essential ingredient to nuclear potential and quark models and the study of the nucleon-antinucleon system at low energies establishes an important bridge between nuclear and elementary particle physics. The understanding of the annihilation provides a deeper insight into the internal structure of nucleons and antinucleons.

The considerable improvement in phase space cooling and the development of a high intensity antiproton source for the CERN $\bar{p}$-SPS project opened up a new possibility to increase the intensity and quality of low energy antiproton beams by several orders of magnitude.

These facts have created strong interest in low energy antiproton physics and inspired the organizers to arrange this meeting. The purpose of this workshop was to discuss the scheme of a low energy antiproton ring (LEAR) and to work out the experimental possibilities offered by such a facility. Furthermore it was intended to elaborate and suggest a list of experimental and machine requirements and a time schedule for this project.

Three working groups were established covering the machine aspects, physics with LEAR in its first stage and physics with LEAR as a collider and were convened by G. Plass, K. Kilian and U. Gastaldi respectively. They took up their work already before the workshop and physicists were encouraged to present their ideas in joint sessions of these groups held at CERN. These presentations (in most

cases only copies of the transparencies) were compiled as $\bar{p}$ - LEAR Notes and are available upon request.

At the Karlsruhe meeting the previous discussions were resumed by the conveners and discussions were continued in parallel and plenary sessions. Invited speakers were asked to summarize the discussions at the end of the workshop. These Proceedings contain the conceptual study of the machine, related machine topics and the summary talks on the physics aspects. The intermediate summary of the conveners are not put in, since new ideas and the results of the discussions in Karlsruhe are to be included and the conveners are encouraged to present this more elaborate resume to the next CERN PSC Committee. These papers are also filed as $\bar{p}$ LEAR-Notes and they are all listed at the end of these Proceedings.

The Organizing Committee wishes to express its warmest thanks to the lecturers for their interesting and inspiring talks and to all participants for their active contributions to the workshop.

The editor expresses his thanks to Miss U. Diehl, Miss V. Lallemand und Mrs. Ch. Neff for their help during the meeting and the preparation of these Proceedings.

The editor

Organizing Committee

A. Citron, Karlsruhe
P. Dalpiaz, Torino
P. Falk-Vairant, CERN
R. Klapisch, Orsay
H. Poth, Karlsruhe
V. Soergel, CERN/Heidelberg
and the conveners of the working groups
U. Gastaldi, Mainz
K. Kilian, Heidelberg
G. Plass, CERN

CONTENT

PS/DL/Note 79-1
20 January 1979

CONCEPTUAL STUDY OF A FACILITY FOR LOW ENERGY ANTIPROTON EXPERIMENTS

Status report in preparation of the Karlsruhe Workshop on Physics with Cooled Low Energy Antiprotons, 19 to 21 March 1979, by

W. Hardt, L. Hoffmann, P. Lefèvre,
D. Möhl, G. Plass and D. Simon
CERN, Geneva, Switzerland

TABLE OF CONTENTS

1. INTRODUCTION

The idea to add to the Antiproton Accumulator [1] (AA) which is being built at CERN, a facility for experiments with low energy antiprotons [2),3)] has received enthusiastic support from many members of the CERN physicists community. It would provide improvements by several orders of magnitude in experimental conditions (rate, momentum definition, pion contamination) and open new fields of experimentation.

In this study the following scheme is considered : antiprotons would be taken at suitable intervals from Antiproton Accumulator, injected anticlockwise into the PS, decelerated, and injected into a small storage ring (LEAR for Low Energy Antiproton Ring) where they would be available for various types of experiments.

Experiments with an external $\bar{p}$ beam are amongst the most important so far proposed and the use of this ring as "stretcher", providing a $\bar{p}$ beam with a high duty cycle, is considered here as its main purpose. The storage ring could eventually also be used for collision experiments, for work with an internal target or other purposes. Some typical options are commented in Chapter 5.

2. AVAILABILITY OF ANTIPROTONS

The construction of a facility for low energy $\bar{p}$ experiments will bring the number of $\bar{p}$ facilities at CERN to three : SPS, ISR, LEAR. The question whether enough $\bar{p}$ can be produced to support three lines of physics must be answered.

The SPS will always have top priority, irrespective of whether it runs protons or antiprotons. It is currently assumed that the SPS will run as $p\bar{p}$ collider for about three months per year and the normal annual shutdown of the CERN machines is of the order of 2 months. ISR and LEAR can then be allowed to run during the remaining seven months in parallel with SPS proton physics and sharing the remaining protons with other customers. Some allowance must also be made for the further development of stochastic cooling and stacking techniques.

Although details of the PS/SPS schedule for the years beyond 1980 are not yet fixed, the proton economy can be approximately evaluated as follows. The normal duration of the SPS cycle is about 12 s, of which filling by 5 batches from the PS will take about 2.5 s. During the remaining 9.5s the PS can produce 4 bursts of 26 GeV protons.

One sees that for about 80% of the time the PS is available for the combination of LEAR and ISR $\bar{p}$ physics, and other users, during about six months per year (allowing one month for AA machine development). As will be shown later (Chapter 4.3) LEAR can produce an external $\bar{p}$ beam of more than 10^6 $\bar{p}$/s (time average) by using two of the four bursts available from the PS, leaving the other two for other users (25 GeV physics)

It appears too early to discuss the sharing of the six months per year available between ISR and LEAR but one can imagine that LEAR (and 25 GeV physics) operation would alternate with ISR filling. It is currently assumed [4] that ISR would stack during five days and then run on for as long as is useful.

The reader will realize two implications of the above :

- the AA is assumed to run continuously like any other fully operational machine, rather than being "part of an experiment" as sometimes thought previously ;
- 25 GeV physics will see the amount of PS time available seriously decrease due to the $\bar{p}$ programme.

3. SURVEY OF POSSIBLE SCHEMES

For the project of the high energy $p\bar{p}$ facility, the 3.5 GeV/c $\bar{p}$ from the AA are being brought to the PS for acceleration to 26 GeV/c prior to injection into the SPS. Similarly, the $\bar{p}$ for the low energy facility would be decelerated in the PS and then be transferred to a storage ring located in one of the existing experimental areas.

The preferred experimental area is the South Hall, which provides the required surface area and adequate infrastructure for the storage ring as well as for experiments installed on it or along ejected $\bar{p}$ beams from it. It is possible to transfer the $\bar{p}$ from the PS to the South Hall (by going through the tunnel of the old linac) by modifying equipment in the PS used for the inflection of 50 MeV protons, without requiring additional straight section space. This is an important consideration as straight section space is an invariant and extremely rare quantity in the PS. Also, 50 MeV protons and H^- ions obtained from the old linac could be brought to the $\bar{p}$ storage ring through the same channel.

It has been suggested to also consider the use of the ICE ring, (in its present location), which might possibly be the cheapest way to obtain a low energy $\bar{p}$ facility of limited potential. We discard this suggestion here because of its inherent limitations and because of the arguments given in the previous paragraph : the infrastructure for an experimental area around ejected $\bar{p}$ beams from the ICE ring would have to be created, and a new ejection point and external beam, including major civil engineering work would have to be implemented on the PS in order to bring the $\bar{p}$ which turn in counterclockwise direction in the PS, into ICE. It appears more interesting to use ICE with a $\bar{p}$ beam derived from a target in the ex-neutrino tunnel and so bridge the time in between now and the operation of LEAR.

Figure 1 shows a layout of LEAR in the PS South Hall. We assume four fixed sector magnets with strong focusing elements in between. The magnets should preferably be laminated in order to permit a reasonable acceleration rate, but an existing solid core magnet (g-2 ring) could in the limit also be used to start with. The focussing properties of the machine would be modified as required by the various experimental purposes envisaged (cp. Chapter 5).

4. THE PROPOSED LOW ENERGY $\bar{p}$ FACILITY

4.1 Typical lattice

It is not trivial to design a lattice for this small ring that permits to have long free straight sectors and to shift the transition energy out of the working range.

In Table 1 possible lattice parameters for a low energy stretcher ring are listed. More work is needed to optimize the lattice. However, the model presented here should suffice to permit cost and performance estimates. The bending radius of the magnet quadrants is chosen corresponding to the envisaged momentum range of the ring, 0.1 to 1.7 GeV/c. For comparison, parameters are given in Table 2 for a ring with a bending radius of 7m, which is the bending radius of the g-2 ring magnet now used for the ICE set-up.

4.2 Acceleration

It is proposed to include an acceleration cavity in the machine. On the one hand this will permit to attain energies lower than 50 MeV, and on the other hand, the beam could be transferred from the PS at a fixed energy higher than 50 MeV, the advantage being a constant and correspondingly smaller emittance at transfer. The energy would then be adjusted in the storage ring as required for the experiments.

Finally, H^- would only be available at 50 MeV from the old linac ; for experiments at any other energy acceleration in the storage ring would be a prerequisite.

The required frequency range would be in the band which the cavities of the PS can be tuned to. There are still cavities of the old PS RF system available. A laminated magnet permitting a reasonable acceleration rate would then be essential.

4.3 Slow ejection from a stretcher

It was initially though that each batch of $\bar{p}$ was to be separately stacked and cooled in the AA. A slow ejection of a duration similar to the cooling time, at least one hour, would then be necessary and this appeared as a major obstacle to the realization of a stretcher ring. Two ideas have helped to open the impass :

- it was realized that it will be possible to create in the AA a stack of $\bar{p}$ of a desired density from which small batches can be skimmed off ("unstacked") by the RF system at suitable intervals, the stack being continuously replenished.
- The proposal of "stochastic ejection" [5),6)], i.e., an ejection process stimulated by RF noise, opens a way to producing spills of hitherto impossible duration.

The problem is then reduced to the one of finding a set of paramaters which will yield useful $\bar{p}$ rates in the ejected beam and a high duty cycle.

The expected rates look roughly as follows :
the AA is designed to make available about 6.10^{11} $\bar{p}$/day or 7.10^6 $\bar{p}$/s as a time average if the PS runs for $\bar{p}$ production exclusively *). We make the

---

*) 1 PS pulse per 2.6s is assumed in the AA design study [1)]. This cycle is dictated by the present assumptions about the speed of momentum cooling. The PS could provide one pulse every 2s approximately.

assumption that $\bar{p}$ production for LEAR will be done in parallel with SPS and 25 GeV proton physics and that about 40% of the above $\bar{p}$ production rate can be obtained (cp. Chapter 2). Assuming furthermore a total $\bar{p}$ transfer efficiency of 60% from the AA through the PS and LEAR into the external $\bar{p}$ beam, (5 ejection and injection operations with an average efficiency of 90%), one obtains an average rate at the experiment of $7 \times 0.4 \times 0.6 \times 10^6 = 1.7 \cdot 10^6$ $\bar{p}$/s.

The expected duty cycle will depend on the success of stochastic ejection. As the filling of LEAR once it has become routine, should only take a few seconds for preparing the settings, and spills of a few hundred seconds appear possible according to theoretical work, a duty cycle of 90% or more can be expected. Tests made at the PS have so far shown the mechanism to work, but the demonstration of very long spills requires special running conditions of the PS at low energy and these will be available for spring 79. Taking a very pessimistic view one would expect at least 15 to 20% duty cycle, typical of the beams in the East Hall, using in the limit a classical resonant extraction.

4.4 Vacuum

The residual gas pressure is an obvious limit to the beam lifetime in a storage ring, in particular at low energies. It has, however, been demonstrated in the ICE experiment that the effect of multiple scattering can be cancelled by stochastic cooling at a pressure of a few 10^{-9} Torr. Hence, for stretcher operation only, a "normal" vacuum system, rather than ISR type, would be sufficient.

For the operation of LEAR as $p\bar{p}$ collider (option 5.1) an extreme vacuum will be required in order to reduce the background in the interaction region. As the vacuum system is one of the basic components of the machine which cannot easily be changed later, it is proposed to provide for an ISR type vacuum system in the initial design of LEAR.

4.5 Cooling

It seems that cooling will become indispensable for the optional uses of LEAR, but it is also advantageous for the stretcher operation for two reasons :

i) cooling could allow to extend the limits imposed by adiabatic anti-damping when decelerating further down ;

ii) cooling alleviates the vacuum requirement (see Chapter 4.4)

A crude estimate shows that with stochastic cooling, cooling rates of an interesting order of magnitude can be obtained : the minimum cooling time for perfect mixing and negligible noise is given by the bandwidth W used and the number of particles N

$$\tau_{emitt} \geq \frac{N}{W}$$

and one obtains the order of ten seconds for the stretcher mode. This means that deceleration by a factor 2.7 in momentum (with compensation of the adiabatic blow-up) would take about 10 seconds, and this seems quite acceptable. The cooling rate would also compensate Coulomb scattering at about 10^{-9} Torr down to approx. 200 MeV/c. For electron cooling, cooling times about one order of magnitude smaller have been obtained at Novosibirsk.

It appears at the moment that the installation of a cooling system will have to be delayed for reasons of availability of manpower and budget.

4.6 Deceleration in the PS

The low energy $\bar{p}$ facility will require beam in two different conditions : small batches of $\bar{p}$ if used in stretcher mode (cp. 4.3), or the full stack of the AA (6 10^{11} $\bar{p}$) if used for some of the options. The batches must contain more than 10^9 $\bar{p}$, the lower limit for safe operation of the PS instrumentation (with some minor modifications).

4.6.1 RF matching

i) Transfer of small batches for the stretcher

The small batches are obtained in the AA by creating a stack of a few 10^3 $\bar{p}$/eV density and unstacking a momentum bite, typically about 1 MeV wide, such that a few 10^9 $\bar{p}$ can then be ejected. The required RF bucket is about the same as used in the unstacking procedure for the SPS, only the density of the $\bar{p}$ bunch is smaller. The precise parameters can, of course, only be determined once the AA has run.

Several transfer schemes are possible with the radius ratio of 10/2·5/1 between PS/AA/LEAR. As an example assume that the normal bucket of 6 mrad in the AA is compressed to a length smaller than $2\pi \times 10$m to fit into one h = 10 PS bucket. In Table 5, last column, the available and the required buckets areas are listed. The bunch can conveniently be

decelerated down to $\beta = 0.5$ ($\simeq$ 0.6 GeV/c) until it meets the frequency limit (f_{min} = 2.5 MHz) of the PS cavities.

If one wants to decelerate down to 50 MeV, the harmonic number 20 must be used in the PS. In this case the unstacking bucket must be chosen to be smaller than 4 mrad in order to be able to decelerate the beam in one PS bucket.

The required RF voltages in the PS are given by

$$\frac{U_{PS}}{U_{AA}} = \left(\frac{R_{PS}}{R_{AA}}\right)^2 \frac{h_{AA}}{h_{PS}} \cdot \left|\frac{\eta_{PS}}{\eta_{AA}}\right|$$

The AA beam being bunched at full voltage (14 kV), 7 kV and 3.5 kV will be needed in the PS for harmonic number 10 and 20 respectively. For the lower value, some improvement of the system may be needed.

ii) Transfer of the full AA stack

For the modes where one wants to put the whole AA beam with a bucket area of 72 mrad into one bucket of LEAR, one will proceed in a way similar to transferring $\bar{p}$ to the SPS. The beam must be unstacked into a number of batches e.g., 10. These would be transferred into the PS buckets at a suitable PS harmonic number, decelerated either one by one or all in one PS cycle, and injected into LEAR by a multi-turn injection process.

4.6.2 Transverse acceptances

The transverse beam emittances are limited by the AA ejection channel and can be expected to be about the same in i) and ii).

Proton beams have been decelerated in the PS for injection into ICE from 800 MeV down to as low as 50 MeV with no losses other than to be expected from adiabatic growth of the emittances, and a total blow up less than a factor of two on the well compensated stop bands in the domain of strong space charge [9].

To work out the beam emittances that can be decelerated without loss we assume that emittances of 40π mm mrad horizontally and 20π mm mrad vertically can be safely handled and transferred. Actually the acceptance of the PS chamber is larger (say hor. x vert. = 100π x 40π) but it is impossible to eject and transfer such large beams.

In Table 5 the required beam properties at 3.5 GeV/c (AA ejection) are summarized as a function of the final energy after deceleration.

For the purpose of comparison the table includes the design properties of the AA beam at transfer (after 24h of accumulation). One notes that even for deceleration to the lowest energy the PS transverse acceptances are safely larger than the AA beam with 6×10^{11} $\bar{p}$ leaving enough margin for possible blow-up on stop bands.

4.7 Beam transfer from the PS to LEAR

Several possibilities exist to feed LEAR with a $\bar{p}$ beam from the PS. As an example we mention one solution where the $\bar{p}$ beam is fast ejected from ss 26. The beam transfer line is chosen parallel to the old linac and passes through the Linac building (Fig. 1).

The transverse emittances of the PS beam are assumed to be $\leq$ 40 and $\leq$ 20π mm mrad in the horizontal and vertical plane, respectively. The ejection septum (with an aperture of 70 x 45 mm^2) is supposed to deflect the $\bar{p}$ beam 70 mrad.

The transfer line ($\sim$ 100m) can transport $\bar{p}$ with a momentum $\leq$ 1.7 GeV/c using standard PS elements. High vacuum (without windows) is required to transport $\bar{p}$ of low momentum. Some special elements (collimators, etc.) and instrumentation have to be envisaged. A large part of the equipment from the ICE transfer line could be used.

Some civil engineering work is required for passage through the Linac building.

4.8 Experimental area

In the South Hall, two experimental areas may be available if two (or three) of the five test beams are abandoned.

The $\bar{p}$ beam ejected from LEAR could feed simultaneously two experiments by using a splitter magnet. By means of a bending magnet placed in one branch, one could in addition feed alternately a third experiment.

Two vertical steering magnets placed in front of the splitter magnet would make possible the adjustment of the intensity in each branch between 0 and 100% with low losses.

The elements needed are supposed to exist, except the external splitter magnet and the necessary instrumentation.

Some power supplies have to be moved from the East Area to the South Generator Building. Cooling water and general services which may be required exist in the South Area.

4.9 Cost

For a cost estimate, we assume that this facility be treated like an experiment, or a series of experiments, in one of the 25 GeV areas, whose normal services and infrastructure are available free of charge : beam transport, power supplies, water, etc. It is also assumed that available control computers are used (e.g., those available in the South Hall in the New Linac Control Room) as well as obsolete quadrupoles from the PS. Only items that are acquired specifically for the present purpose are accounted for.

Under these assumptions we arrive at costs of about

7.5 MFr for a new ring

5 MFr for a ring using the magnet and a few other components of the ICE ring.

The cost of cooling equipment and the options (Chapter 5) are not included in these figures.

5. OPTIONAL USES OF THIS FACILITY

The use as a beam stretcher is the prime motive for the construction of this facility. Some other uses have also been proposed and the present, still very preliminary, status of the technical considerations is summarized in this Chapter.

5.1 Luminosity in $p\bar{p}$ collision operation

To work out an upper limit for the luminosity we assume head-on collisions *) of a proton and an antiproton bunch of 6×10^{11} particles (each design figure for the AA beam after 24 hours of stacking) at 1.7 GeV/c.

The luminosity obtainable depends on the transverse beam size and on the amount of bunching which in turn is limited by the available RF, by longitudinal and transverse space-charge effects, and by intra-beam scattering. It is given by

$$L = \frac{N^2 f_{rev}}{A_{int}}$$

---

*) The alternative of having long bunches or coasting beams with separation of $\bar{p}$ and p beam and crossing in the interaction region will be investigated.

In an optimised collider, designed to the beam-beam limit [7] the luminosity is given by

$$L = \frac{f_{rev}\ \gamma\ N\Delta\nu}{(1+\beta^{-2})r_p\beta_v^*}$$ (see Appendix 2 for a glossary of symbols)

and the beam parameters summarized in Table 3, (especially $\beta_v^* = 5m$) and $\Delta\nu = 5\cdot10^{-3}$ yield an upper limit for the luminosity of

$$L = 1.5 \times 10^{29} cm^{-2} sec^{-1} \quad \text{at } 1.7 \text{ GeV/c.}$$

The beam satisfies the classical criteria for longitudinal and transverse stability (cp. App. 1). However, the luminosity depends critically on the assumed tight bunching (< 1/10)and small momentum spread ($\Delta p/p < 10^{-4}$). This necessitates a strong RF system and strong momentum cooling. In this context one can argue that several hours could be spent for cooling each injected batch.

The small momentum spread may also lead to fast beam decay due to intra-beam scattering. It is not yet clear whether the existing theory of this effect [8] is applicable to the present problem, and this matter is being investigated.

We estimate that a luminosity about one order of magnitude below the above limiting value could be realistically expected to start with. Note that for the lattice, Table 2, with the larger magnets, the luminosity would be lower by at least 5 because the circumference is larger, β_H, β_V bigger and the acceptance smaller.

Assuming a layout as indicated in Fig. 1, protons could be rather easily obtained from a septum magnet to be installed in ss 2 of the PS. The fast ejection kickers and orbit deformation magnets are already available in the PS, and only the septum magnet need be added.

5.2 Operation with an internal target

Two things are needed in order to run LEAR with an internal target (gas jet or foil) :

i) strong transverse cooling (stochastic or electron beam) is necessary in order to compensate the beam blow-up due to multiple scattering.

ii) A low β value at the target is necessary in order to reduce the losses due to single Coulomb scattering, and may also ease the design of the jet target.

In Table 4 some parameters for a modified working point giving $\beta_V = 0.2m$ and $\beta_H = 2m$ are summarized. The largest scattering angle which does not lead to losing the $\bar{p}$ out of the beam, is then 7 mrad rather than 2.5 mrad for the working point of Table 1, and losses are reduced by a factor of 6. Still smaller β values may be possible using a special low β insertion.

5.3 Overlapping beams

It is proposed to have two beams (H^- and $\bar{p}$) circulate in the same ring in the same direction. If the two species are kept by the same RF system the difference in mean radial position at the interaction point and in velocity will be given by

$$r = \alpha_p \gamma_t^2 \left(\frac{1}{\gamma_t^2 - \gamma^2}\right) \frac{\Delta m_o}{m_o}$$

and

$$\frac{\Delta\beta}{\beta} = \left(\frac{1}{\gamma_t^2 - \gamma^2}\right) \frac{\Delta m_o}{m_o}$$

(see App. 1 for glossary of symbols)

With $\Delta m/m = 10^{-3}$, $\alpha_p = 1.9m$, $\gamma_t^2 = -5.3$, $\gamma \simeq 1$

one obtains

$$\frac{\Delta\beta}{\beta} = 1.6 \times 10^{-4}$$

and

$$r = 1.6 \text{ mm}$$

Assuming the same parameters as in the collider mode this deviation in average position seems negligible as it represents less than 10% of the beam radius. The luminosity will be the same as in colliding beam mode multiplied by the velocity spread ($\Delta v/\beta c$) in the c.m. system.

The H^- ions of 50 MeV energy could be obtained from the old PS linac if an H^- source was installed instead of the present proton source. H^- sources have in fact been developed and are operational in other laboratories (NAL, LAMPF, RHEL). If a layout as in Fig. 1 was used, the H^- beam could be transferred from the old linac into the $\bar{p}$ transfer line by a 180^o bend beyond the end of the linac.

The H^- lifetime due to stripping on the rest gas at 10^{-10} Torr is between 1 and 10s in the momentum range of LEAR. It will therefore be essential to devise an injection scheme that permits frequent H^- refilling without disturbing the circulating $\bar{p}$.

6. REFERENCES

1) Design study of a $p\bar{p}$ colliding beam facility, CERN/PS/AA 78-3.
2) Chairman's report, CERN workshop on Intermediate Energy Physics, R. Klapisch, PS-CDI/77-50.
3) Memorandum to PS and SC Committees, A. Astbury, P. Dalpiaz, U. Gastaldi, K. Kilian, E. Lohrmann, B. Poth, M.A. Schneegans, 6.2.78;
   U. Gastaldi, K. Kilian, D. Möhl, Deceleration of Antiprotons for Physics experiments at low intensity, Proceedings, 10th Internat. Conf. on High Energy Accelerators, Serpukov 1977.
4) ISR operation with Antiprotons, compiled by P.J. Bryant, CERN/ISR-BOM/78-18.
5) Stochastic extraction, a low ripple version of resonant extraction, S. v.d. Meer, CERN/PS/AA 78-6.
6) Remarks on stochastic extraction, W. Hardt, PS/DL/Note 78-5.
7) M. Sands, The Physics of Electron Storage Rings, SLAC Report 121, 1970.
8) A. Piwinski, Intra beam scattering, Proceedings 9th Internat. Conf. on High Energy Accelerators, Stanford, 1974, p.405.
9) P. Lefevre, Deceleration de 800 MeV à 50 MeV dans le PS, PS/DL/Min 79-1.

TABLE 1

PRELIMINARY STRETCHER RING LATTICE WITH ρ = 3.5m BENDS

Momentum range	0.1 - 1.7 GeV/c
Circumference	62.8 m
Length of SS	10 m
Free length (regular lattice)	5.5 m
Number of SS	4
Maxima of lattice functions	$\beta_H \simeq$ 10m (5m in bends)
	$\beta_V \simeq$ 25m (15m in bends)
	$\alpha_p \simeq$ 2.2m (1.5m in bends)
Aperture of vac. chamber	$a_H = \pm$ 70 mm $a_V = \pm$ 32 mm
Beam apertures	$a_{H\beta} = \pm$ 45 mm
	$a_{H\rho} = \pm$ 45 mm
	$a_V = \pm$ 27 mm
Acceptances	E_H = 200 π mm mrad
	E_V = 30 π mm mrad
	$\Delta p/p = \pm$ 2.2 %

	1.7 GeV/c	0.1 GeV/c
Bending field	16 KGauss	0.9 KGauss
Integrated quad gradient (old PS quadrupoles)	411 G/cm.m	24 G/cm·m

Q values $Q_H \simeq 2.75$ $Q_V \simeq 2.75$

Transition energy $\gamma_t^2 = -(2.3)^2$

TABLE 2

PRELIMINARY STRETCHER RING LATTICE
WITH ICE (0 GRADIENT) BENDING MAGNETS

Momentum range	0.3 - 1.7 GeV/c	
Circumference	≃ 85 m	
Length of SS	10.4 m	
Free length of SS (regular lattice cell)	5.5 m	
Number of SS	4	
Maximum of lattice functions	β_H = 18 m (12 m in bends)	
	β_V = 25 m (18 m in bends)	
	α_ρ = 3.5 m	
Aperture of vac. chamber	$a_H = \pm$ 70 mm	$a_V = \pm$ 32 mm
Acceptances	E_H = 100 π mm mrad	
	E_V = 27 π mm mrad	
	$\Delta p/p = \pm$ 1.2 %	
	1.7 GeV/c	0.3 GeV/c
Bending field	8 KGauss	1.4 KGauss
Integrated gradient in quads (old PS quadrupoles)	≃ 400 Gm/cm	70 Gm/cm
Q values	$Q_H \simeq 2.75$	$Q_V \simeq 2.75$
	$\gamma_t^2 = -5.3$	

TABLE 3

COLLIDING BEAM PROPERTIES

1. Lattice parameters	
Lattice functions (average) in interaction region	
$\beta_H \simeq \beta_V$(m)	5
Momentum compaction α_p (m)	1.9
Transition energy γ_t^2	$-(2.3)^{-2}$
2. Beam parameters and luminosity	
Momentum (GeV/c)	1.7
No of particles ($N_{\bar{p}} = N_p$)	6×10^{11}
Beam size (2 rms) hor.xvert. (mm^2)	29 x 10
Corresponding emittances $E_h x E_v$ $(\pi mm\ mrad)^2$	$170\pi x\ 20\pi$
Bunched beam momentum spread $\pm\Delta p/p$	1×10^{-3}
Bunch length (total m)	5
Luminosity ($cm^{-2}sec^{-1}$)	1.7×10^{29}
3. Auxiliary quantities	
RF voltage/turn (kV)	60
Frequency, h=1 (MHz)	4.2
Off energy function $1/\gamma^2-1/\gamma_t^2$	0.42
Beam beam tune shift $\Delta\nu$	5×10^{-3}
Laslett space-charge limit N_{ic}	2.2×10^{13}
Tolerable impedance/n at n^{th}	
Revolution harmonic : $\lvert Z_n/n \rvert (\Omega)$	120

TABLE 4

MODIFIED WORKING POINT FOR INTERNAL TARGET OPERATION

Lattice function	
maxima	β_H = 30 m β_V = 30 m α_p = 1.8 m
in center of straight sectors	β_H = 2.1 m β_V = 0.3 m α_p = 0.8 m
in bending magnets	β_H = 27 m β_V = 6 m α_p = 1.6 m
Acceptances	E_n = 80π mm mrad E_V = 25π mm mrad
	$\Delta p/p$ = ±2.2 %
Maximum acceptable angles at center of SS	Θ_H = 6 mrad
	Θ_V = 9 mrad
	$\sqrt{\Theta_H \Theta_V}$ = 7.5 mrad
Q values	Q_h = 3.25 Q_V = 3.25 γ_t = 3.02

TABLE 5

PS ACCEPTANCES REFERRED TO 3.5 GeV/c

Energy after deceleration		Maximum acceptable beam at 3.5 GeV/c			
		Transverse emittance		longitudinal emittance	
pc (GeV)	T (GeV)	E_H (πmm mrad)	E_V (πmm mrad)	A (mrad) h = 20	A (mrad) h = 10
1.7	1.0	19	9.5	63	89
0.64	0.2	7.3	3.6	28	40
0.55	0.15	6.3	3.1	26	-
0.44	0.1	5	2.5	25	-
0.31	0.05	3.5	1.7	23	-
AA design values		1.4	1	6*) 30	15

Acceptances of $E_h = 40\pi$ mm mrad, $E_v = \frac{1}{2}E_h$ at transfer to the stretcher have been taken together with adiabatic scaling $E\beta\gamma$=const. The longitudinal PS acceptance has been worked out assuming stationary PS buckets supplied by the maximum available RF voltage (200 kV) and the usual PS frequence (h=20). For h=10 A is larger by $\sqrt{2}$.

*) If the AA bunch is transferred into one single PS bucket the area matching 6 mrad of the AA is 30 mrad at h = 20 in the PS and 15 mrad at h = 10. For deceleration with h = 20 it is proposed to use an unstacking bucket of 4 mrad in the AA which leads to bucket of 20 mrad in the PS.

APPENDIX 1

FURTHER COMMENTS ON THE COLLIDER OPTION

The parameters of Table 3 meet the condition (for $k_B=1$)

$$A_{int} = \frac{\pi}{4} hw = \frac{N^2 f_{rev}}{4L}$$ (see Appendix 2 for glossary of symbols)

with a beam size that fits into the aperture. Also the intensity is below the Laslett limit :

$$N = \frac{\pi h(h+w)}{r_p \beta_v} \beta^2 \gamma^3 \Delta Q$$

at 1.7 GeV/c. The assumed momentum spread can be contained in a 5m long bunch with an RF voltage

$$U = \frac{\pi}{2} |\eta| \beta^2 \gamma \left(\frac{\Delta p}{p} \frac{1}{y}\right)^2 938 \text{ MV} \simeq 60 \text{ kV}$$

(y = bunch $\Delta p/p$ / bucket $\Delta p/p \simeq 0.13$ for
B = bunch length / bucket length = 5/63)

This spread meets the longitudinal stability limit (local Keil-Schnell criterion)

$$\left|Z_n/n\right| \leq \frac{B\eta p\beta}{I} (\Delta p/p)^2$$

for a coupling impedance $Z_n/n \leq 120\Omega$ (25Ω seem to be obtained in PS and ISR).

We note that strong cooling will be necessary to reduce the momentum spread to a value which permits the tight bunching assumed.

The assumption $\beta_V^* \simeq \beta_H^* \simeq 5$m needs some further comment. For head-on collision the optimum luminosity (p. 10) can only be reached if the bunch length ℓ is $\ell \lesssim \beta$ or in other words there is no use in making $\beta < \ell$. The value $\ell = 5$m corresponds to the free length of the straight section and is also a lower limit of what can be obtained with a reasonable RF system.

Finally for our model lattice the average values of β_V and β_H over the straight section are close to 5m so that no special insertion is necessary.

APPENDIX 2

GLOSSARY OF SYMBOLS

A	Bunch area in units of $\Delta(\beta\gamma)\cdot\phi_{RF}$
A_{int}	effective colliding beam interaction area $A_{int} = \frac{\pi}{4} hwk_B = \frac{\pi}{4} a_V a_{H\beta} k_B$
$a_{H\beta}$, a_{Hp}, a_V	peak amplitudes (2σ) for horizontal betatron motion, synchrotron motion and vertical betatron motion respectively.
$a_H=(a_{H\beta}^2+a_{Hp}^2)^{\frac{1}{2}}$	horizontal beam half-width (2σ)
B	bunching factor = average current over peak current
E_H, E_V	horizontal, vertical emittances, respectively $E_H = \pi a_{H\beta}^2/\beta_H \qquad E_V = \pi a_V^2/\beta_V$
$f_{rev}=\frac{\beta c}{2\pi R}$	revolution frequency
h_{PS}, h_{AA}	harmonic numbers for RF systems in the PS and AA respectively
k_B	number of bunches per beam
L	luminosity
ℓ	total bunch length
$N(N_p,N_{\bar{p}})$	number of particles (protons, antiprotons) per beam
Q_H, Q_V	number of horizontal, or vertical, betatron oscillations per turn
ΔQ	Laslett tune shift (single beam)
$2\pi R$	circumference of machine
r_p	classical proton radius ($1.53\cdot10^{-18}$m)

r	horizontal (radial) deviation from equilibrium orbit
U	RF peak voltage (amplitude)
W	bandwidth of stochastic cooling system
y	bunch height/bucket height
$\lvert Z_n \rvert$	modulus of beam equipment coupling impedance at frequency $n \cdot f_{rev}$
α_p	$r/(\Delta p/p)$ momentum compaction function
β_H, β_V	horizontal, vertical reduced instantaneous wavelength for betatron motion
β^*, β_H^*, β_V^*	beta values in the interaction region
β, γ	relativistic velocity, total energy $\beta = v/c \qquad \gamma = (1-\beta^2)^{-\frac{1}{2}}$
γ_t	γ at transition energy
η	off-momentum function $(\Delta f/f)/(\Delta p/p) = \frac{1}{\gamma^2} - \frac{1}{\gamma_t^2}$
$\Delta\nu$	beam-beam tuneshift
ρ	magnetic bending radius

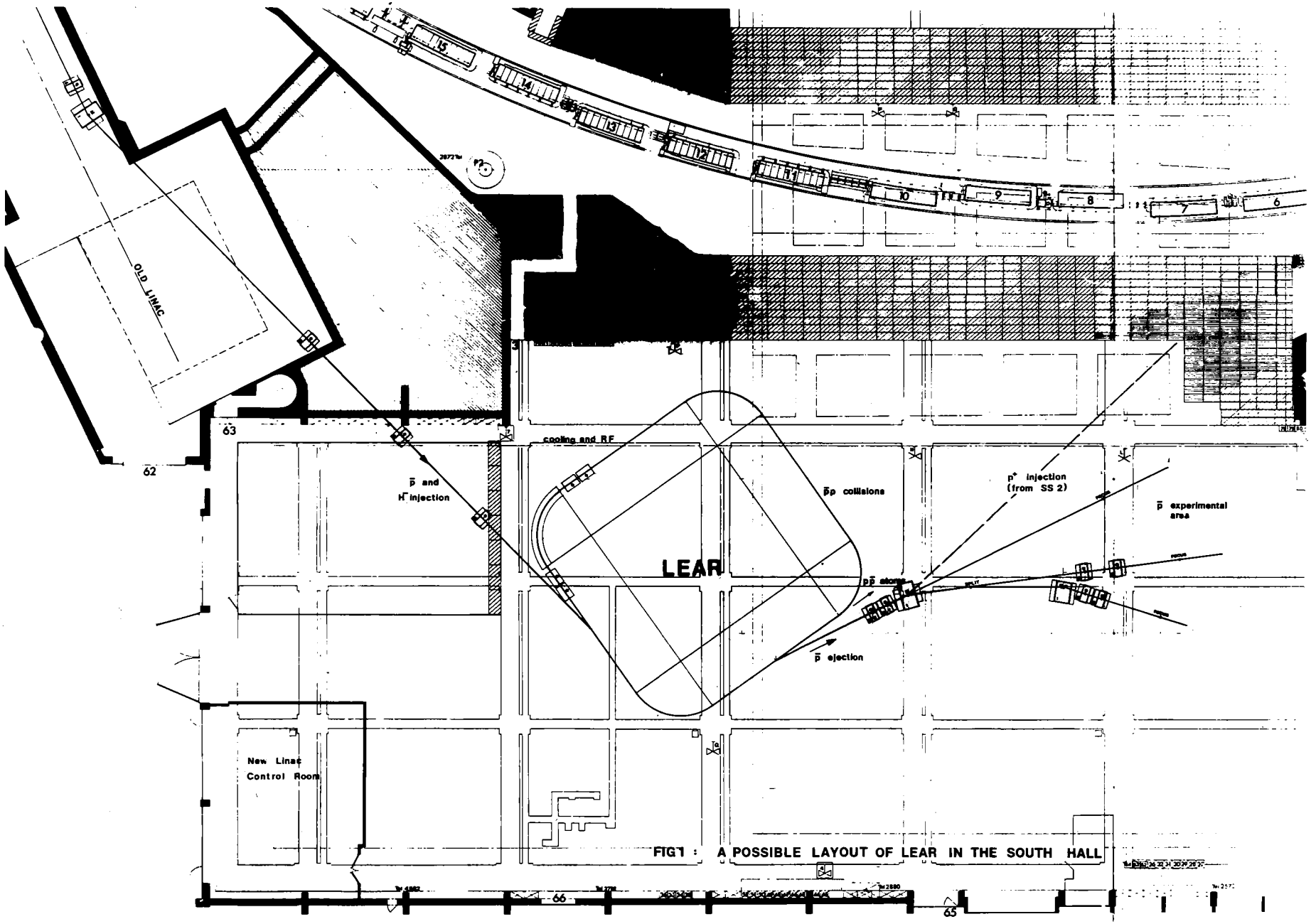

FIG 1 : A POSSIBLE LAYOUT OF LEAR IN THE SOUTH HALL

LEAR Note 73
PS/DL/Note 79-5
May 15, 1979

POSSIBILITIES AND LIMITS WITH COOLING IN LEAR

D. Möhl

CERN, Geneva, Switzerland

Table of contents

Talk given at the "Workshop on Physics with Cooled Low Energy Antiprotons" Karlsruhe, March 19-21, 1979

1. INTRODUCTION

As the cold antiproton beam from the accumulator (AA) is used, further cooling in the low energy ring is not a prerequisite for the simpler modes of operation. However, "post-cooling" in LEAR by stochastic and/or electron techniques is advantageous:

i) to improve beam lifetime (compensation of slow beam decay by multiple scattering on the rest gas, diffusion on high order resonances, etc. factor 40 gain in ICE),

ii) to relax RF requirements (by Δp cooling),

iii) to make lossfree deceleration possible down to lowest energies (despite of the adiabatic increase of phase space volume),

iv) to keep the beam cool in the presence of an internal jet target (compensation of multiple scattering on the target),

v) to prepare a frozen i.e. highly monochromatic and collimated beam for special experiments,

vi) to be able to tightly bunch the beam for the collider mode.

The aim of this talk will be to explain the basic limitations and the relative merits of the two cooling methods to non-specialists. Those familiar with cooling may skip all except perhaps the end of section 2 and of section 3 which give some numbers for LEAR.

2. STOCHASTIC COOLING

2.1 Principle and limitations (qualitative)

To be self-contained (as the organizers of this conference suggest), let us recall the principle of stochastic cooling [1-4] with emphasis on limiting phenomena.

To cool betatron oscillations a transverse pick-up station (sensor, Fig. 1) measures the average error in position of each successive sample of beam particles. A correction signal is derived and arrives on a kicker (corrector) at the same time as the corresponding group of particles. The sample

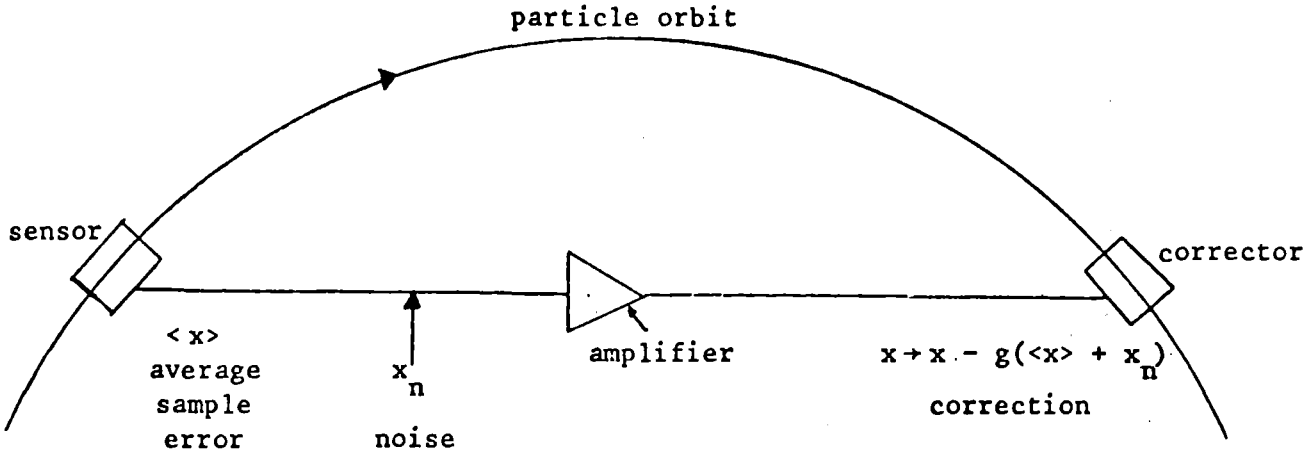

Figure 1

length is determined by the resolution time T_s of the system which in turn is related to the bandwidth W by $T_s = 1/(2W)$.

Speaking of beam samples, the approximation is as follows: since the kicker voltage can only change by a small amount during the time T_s, particles passing at $t = \pm T_s/2$ will get a similar kick and are treated as belonging to the same sample as the test particle passing at t. In this approximation the system can only correct the average position error $< x >$ of each sample. If the same particles stay together, cooling stops once their positions are symmetrically distributed around the zero error position (for just two particles per sample, particle 1 could be 10 cm above, particle 2 10 cm below the medium plane without giving a vertical correction signal).

In reality due to the dispersion in revolution frequency $\left[\Delta f/f = |\eta|\Delta p/p \ , \ \eta = \{ 1/\gamma^2_{\text{transition}} - 1/\gamma^2\}\right]$ faster particles will continuously overtake the slower ones, the sample population changes (mixing), the error reappears and cooling continues until ideally all particles have zero error. This mixing due to momentum spread is a prerequisite of cooling and one of the fundamental limits on cooling rate is given by the speed at which rerandomisation takes place (mixing limit).

A second limitation results from the unavoidable presence of noise in the low level part of the system (PU, preamplifier). This noise is amplified and appears on the kicker together with the correction signal. As the noise is random whereas the correction is correlated with the test

particle, it can be shown that the cooling effect dominates for small enough amplification (slow cooling) whereas noise heating prevails at too large gain (noise limit).

So far, we have concentrated on transverse cooling. Momentum cooling is similar in principle. The corrector is an acceleration/deceleration gap. The sensor is either a horizontal position pick-up (Palmer method). In this case the system has to disentangle the contribution of $\Delta p/p$ to the beam size from the betatron oscillation. Alternatively, the filter method of Thorndahl detects $\Delta p/p$ via the concurrent difference $\Delta f/f = |\eta| \Delta p/p$ in revolution frequency as observed with a current pick-up and a filter system. Mixing and noise limit apply in a similar fashion to all transverse and longitudinal cooling methods, although the filter technique is less sensitive to noise then the other methods.

Two more restrictions are obvious from Fig. 1 : as the signal has to arrive on the kicker at the same time as the corresponding particles, the cooling path length has to be readjusted when the particle velocity (i.e. the beam momentum) is changed. This can be done by remotely switchable delays (as practiced in ICE) but the required complexity makes it wise to limit the system to a few strategic energies in LEAR.

Finally, for betatron cooling, where the sensor detects position (x) and the correction readjusts angle (x'), the latter has to be spaced a quaterwave length or an odd multiple of betatron quaterwaves downstream of the former. A reshuffling of the transverse system in LEAR will therefore probably be necessary when the working point is changed as it may be desirable passing e.g. from the stretcher to the jet target operation.

2.2 Numbers for noise and mixing limits, application to LEAR

A simple semiquantitative derivation (due to Hereward) of the equation for the optimum cooling time constant [1-4]

$$\tau_o = \frac{N}{W g_o} = \frac{N}{W} (\Gamma + \nu) \qquad (2.1)$$

is sketched in Table 1; N is the total number of particles in the coasting beam, W is the bandwidth, $g \leq 1$ the fraction of the sample error corrected per turn, g_o its optimum (giving fastest initial cooling), $\Gamma \geq 1$ the "mixing parameter"

and $\nu \geq 0$ the "noise parameter"; $\nu \gg \Gamma$ corresponds to the noise, $\Gamma \gg \nu$ to the mixing limit.

The value of Γ can be estimated requiring

$$\underbrace{1/g}_{\substack{\text{No. of turns to correct} \\ \text{sample error in absence} \\ \text{of mixing}}} \gtrsim \underbrace{T_s/\Delta T_{rev}}_{\substack{\text{No. of turns for rms migra-} \\ \text{tion by one sample length} \\ \text{(rerandomisation time)}}}$$

which expressing $\Delta T_{rev}/T_{rev} = |\eta| \frac{\Delta p}{p}$ yields

$$\Gamma^{-1} = g_o \approx W T_{rev} \eta \left.\frac{\Delta p}{p}\right|_{total} \qquad (\Gamma \gg \nu)$$

More precise derivations and values of Γ may be found in references 3, 4, 5.

TABLE 1 : EVALUATION OF COOLING RATE

Change of error x for one passage of test particle

$$x_c = x - g\,(\langle x\rangle + x_n)$$

Work out $\Delta x^2 = x_c^2 - x^2$:

$$\Delta x^2 = -2g\,x\,(\langle x\rangle + x_n) + g^2(\langle x\rangle + x_n)^2$$

Take the sample average

$$\langle\Delta x^2\rangle = -2g\langle x\rangle^2 - 2g\,\langle x\rangle\,x_n + g^2(\langle x\rangle^2 + 2\langle x\rangle\,x_n + x_n^2)$$

For many passages, replace these quantities by their expectation values for random samples (mixing) of the beam. For $N_s \gg 1$

$$E(\Delta\langle x^2\rangle) = x^2_{rms.c} - x^2_{rms} = \Delta x^2_{rms}$$

$$E(\langle x\rangle^2) = \frac{1}{N_s} x^2_{rms}$$

$$E(x_n\langle x\rangle) = 0 \quad \text{(no correlation between noise and correction)}$$

where all rms are the beam rms values.

Hence

$$\frac{\Delta x_{rms}}{x_{rms}} \approx \frac{1}{2}\frac{\Delta x^2_{rms}}{x^2_{rms}} = \frac{-g}{N_s}\left[1 - \frac{g}{2}\left(1 + \frac{x_n^2}{\langle x\rangle^2}\right)\right]$$

For bad mixing, replace 1 in inner bracket by $\Gamma > 1$. Introduce $N_s = N f_{rev}/2W$, $\nu = x_n^2/\langle x\rangle^2$ to get

$$1/\tau = -f_{rev}\frac{\Delta x}{x} = \frac{2gW}{N}\left[1 - \frac{g}{2}(\Gamma + \nu)\right]$$

with maximum

$$1/\tau_o = W/\left[N(\Gamma + \nu)\right] \quad \text{for} \quad g_o = 1/(\Gamma + \nu)$$

Further from Table 1, we interpret

$$\nu = x^2_{noise} / x^2_{signal} \qquad \{x^2_{signal} = E(\langle x \rangle^2); \text{ Table 1}\} \qquad (2.3)$$

as the noise to signal power ratio at the amplifier input. The noise limit may thus be interpreted as requiring

$$\underbrace{g^2 x^2_{noise}}_{\text{Noise power on corrector}} \lesssim \underbrace{g\, x^2_{signal}}_{\text{Coherent signal power on corrector}}$$

which for $g = g_o = \nu^{-1}$ yields equation (2.3).

Note that the "error current" (x_{signal} x beam current) is proportional to $\sqrt{N}$ (Table 1), νN is therefore constant (assuming constant noise current). Hence, in the noise limit the cooling time (2.1) is independent of the intensity.

Equation (2.1) is illustrated in Fig. 2 (see reference 4) where some measured cooling rates have been included.

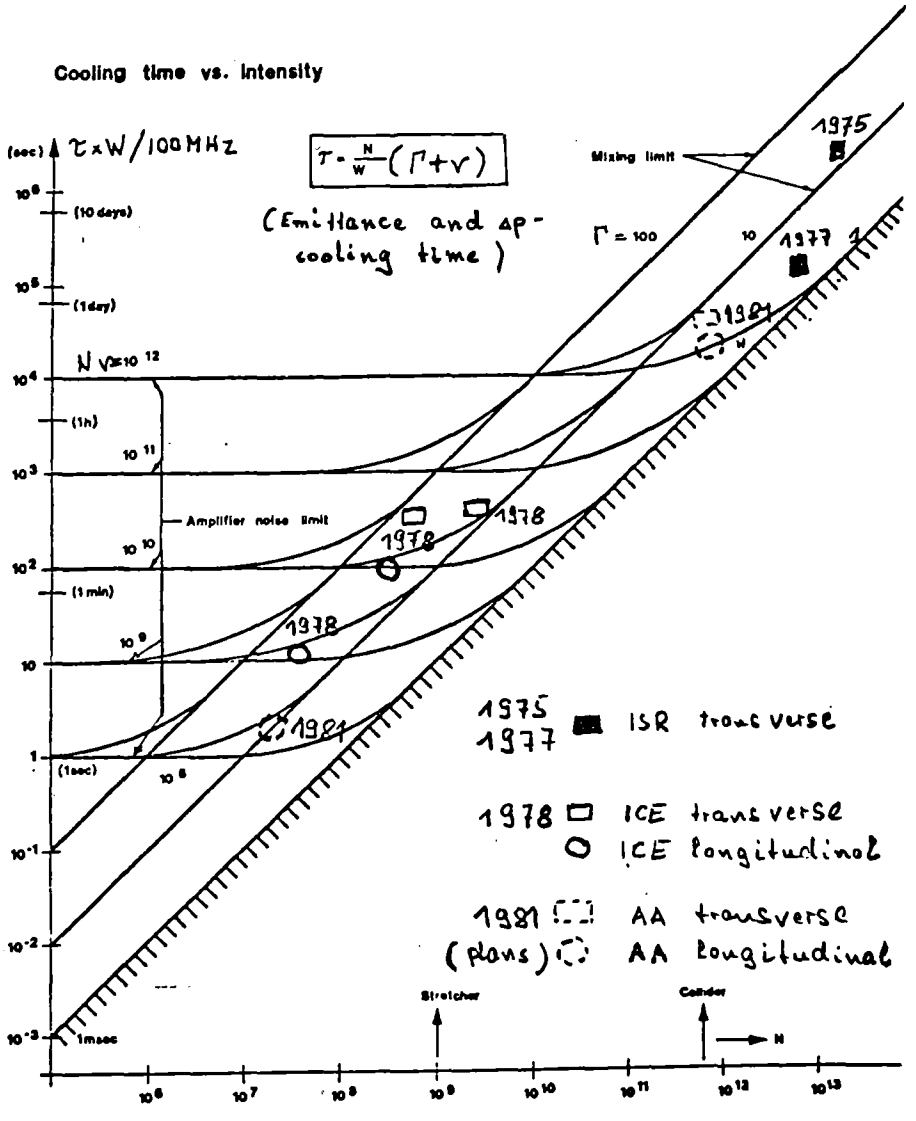

Figure 2

The parameters Γ and νN have to be worked out for the different beam and cooling system parameters. Γ can be estimated from (2.3) whereas ν = noise power/signal power has to be expressed by the preamplifier noise, the pick-up characteristics and the beam size. For transverse cooling one has (cf. ref. 6) :

$$\nu N \approx \frac{T_{rev}\, P_n'}{e^2\, n_{PU}\, R_{PU}} \left(\frac{6d}{a}\right)^2$$

$P_n' = 2kT \simeq 10^{-20}$ Watt/Hz at $T = 290^\circ K$
(preamplifier noise power/bandwidth)

$n_{PU}\, R_{PU}$: total pick-up impedance

d : PU plate spacing

a : effective beam size.

Note that in the mixing limit, cooling becomes more efficient (Γ small, equation (2.2)) as

i) the bandwidth increases $\{ \tau \propto W^{-2} \}$

ii) the momentum spread is large $\{ \tau \propto (\Delta p/p)^{-1} \}$
(advantage of betatron prior to momentum cooling)

iii) the intensity is low $\{ \tau \propto N \}$

The energy dependence enters weakly through the factor $\eta\, T_{rev}$. It is advantageous to have a large off momentum function $\eta = \frac{1}{\gamma^2_{transition}} - \frac{1}{\gamma^2}$ and the LEAR lattice has been chosen to have small and negative $\gamma^2_{transition}$ such that the terms forming η add.

In the noise limit, cooling improves as

i) the number of sensors and/or their impedance is large (x_{signal} large) $\{ \tau \propto x^{-2}_{signal} \propto (n_{PU}\, R_{PU})^{-1} \}$

ii) the preamplifier (and pick-up) noise is small $\{ \tau \propto x^2_{noise} \}$

iii) beam size and momentum spread are large $\left\{ \begin{array}{ll} \tau \propto a^{-2} & \text{for betatron,} \\ \tau \propto (\Delta p/p)^{-2} & \text{for Palmer cooling} \end{array} \right\}$

The energy enters as the signal current power is proportional to the beam current $I \propto \beta$. As a consequence noise is more important at low momentum in LEAR.

Table 2 gives an example of a transverse cooling system for LEAR. Parameters for momentum cooling follow from similar consideration and similar (perhaps somewhat more favourable) cooling times are to be expected. Note that for the "hot" beam of 10^9 $\bar{p}$ ($\Delta p/p \gtrsim 10^{-3}$, large beam size), initial cooling times of a few minutes are possible with a system of 300 MHz bandwidth and 250 Ω pick-up impedance (requiring a length of 1 to 1.5 m for the PU tank). With a 1000 MHz/500 Ω system these times could be reduced to 0.3 min. When the momentum spread or the emittance decreases by 10, these time constants increase by 5 to 10. In the collider mode at 5×10^{11} $\bar{p}$ the cooling time is of the order of 1 h. for the large beam (1000 MHZ/500 Ω system) and probably about 10 hours with the required tight bunching of 10 (or the smaller momentum spread).

TABLE 2 : TRANSVERSE STOCHASTIC COOLING IN LEAR

Momentum	p = 2 GeV/c	Off energy function	η = 0.4
Revolution frequency	f = 4.3 MHz	Preamplifier noise	3 dB at 270°K

Number of particles N	10^9						5×10^{11}	
Cooling system bandwidth W (MHz)		300			1000		1000	
Total pick-up impedance (Ω)		250			500		500	
Beam size / PU plate spacing	0.8	0.8	0.25	0.8	0.8	0.25	≲ .15	
Momentum spread Δp/p (per mille)	1	0.1	1	1	0.1	1	1	0.1
Mixing parameter	18	180	18	5	50	5	5	50
Noise/signal ratio	18	18	180	9	9	90	1	1
Emittance cooling time constant τ (min)	2	12	12	0.3	1	1.5	45	450
Limit (Γ = mixing, ν = noise)	Γ, ν	Γ	ν	ν	Γ	ν	Γ	Γ
Beam size	large	small Δp/p	small transverse	large	small Δp/p	small transverse	large Δp/p	small Δp/p

3. ELECTRON COOLING

The principle of electron cooling [7] is well known: electrons produced in a gun travel together with the protons over part of the proton storage ring and absorb proton oscillation energy by Coulomb interaction. It is instructive to look at the "electron rest frame" moving with the average electron velocity (which equals the average proton velocity to tight tolerances). In this frame, the process is similar to the energy loss dE/dx of a fast proton passing matter and loosing energy to the atomic electrons.

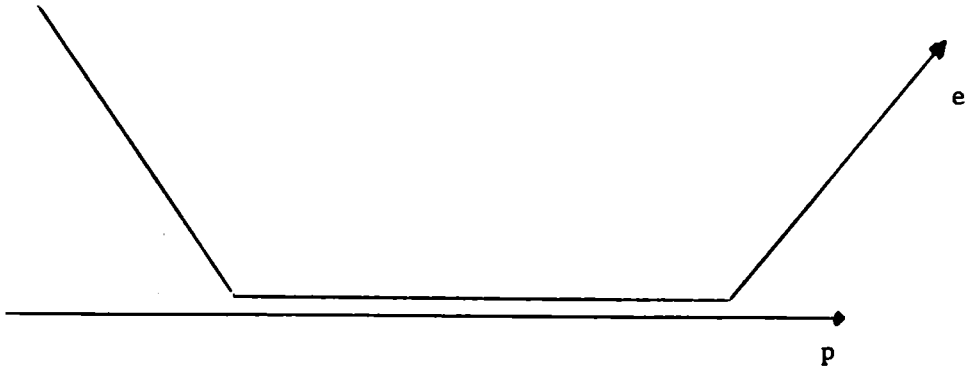

Figure 3

Ideally, equilibrium of the temperatures $T = \frac{1}{2} m (\Delta v)^2 = \Delta p^2/2m$ (non-relativistic) in the rest frame - like in a mixture of two gases - leads to a transverse proton velocity spread

$$\Delta V = \sqrt{\frac{m}{M}}\, \Delta v$$

(capital letters refer to proton, small case to electron properties).

Assuming both beams had originally a similar emittance $E \propto (\Delta V)^2$ the proton emittance will (ideally) be reduced by $M/m \approx 1836$. In a similar way the equilibrium proton momentum spread corresponding to the "typical" electron beam temperature of 0.2 eV can be estimated from

$$\frac{(\Delta P)^2}{2M} = \frac{(\Delta p)^2}{2m} = 0.2 \text{ eV}$$

giving e.g. $\Delta p/p = 6 \times 10^{-5}$ at 0.3 GeV/c.

The simple theory [8] which neglects the longitudinal magnetic field used to guide the electrons and which takes only binary collisions (i.e. collisions involving one electron and one proton at a time) leads to the following relation for the cooling time

$$\tau = (k/L) \frac{\beta^4 \gamma^5}{j \eta_c} \theta^3 \qquad (3.1)$$

Here $k/L \approx 0.02$ {Amp.s cm^{-2} mrad^{-3}}

$L \approx 20$ is the Coulomb logarithm

j the electron current density (in Amp/cm^2)

η_c cooling length/proton ring circumference

and

$$\theta_p^2 \approx \left(\frac{\Delta V_\perp}{\beta c}\right)^2 + \left(\frac{1}{\gamma}\frac{\Delta p}{p}\right)^2$$

$$\approx \left(\frac{E_h}{R/Q_h} + \frac{E_v}{R/Q_v}\right) + \left(\frac{1}{\gamma}\frac{\Delta p}{p}\right)^2$$

is the proton beam "divergence", θ_e the corresponding divergence for the electron beam, and

$$\theta^2 = \theta_e^2 + \theta_p^2$$

the effective divergence between electrons and protons.

Equation (3.1) is sketched in Figure 4 assuming parameters similar to the Novosibirsk experiment [7] i.e. $j = 0.5$ A/cm^2, $\eta_c \simeq 0.02$ and taking $\theta = 2 \times 10^{-3}$. At momenta below, say, 0.5 GeV/c, the current density has to be reduced to keep the proton tune shift due to electron space-charge small enough. This gives the deviation from the $\beta^4\gamma^5$ law at low energy.

One notes that cooling times of the order of 0.1 s to 1 s seem feasible at momenta up to 1 GeV/c (if the gun voltage can be pushed to 240 kV as it corresponds to this momentum). This is much faster than required for LEAR and a simpler gun with, say, 10 times less current density seems adequate at first sight. On the other hand, if the beam is hotter (θ larger) than assumed, the cooling speed decreases rapidly.

FIGURE 4

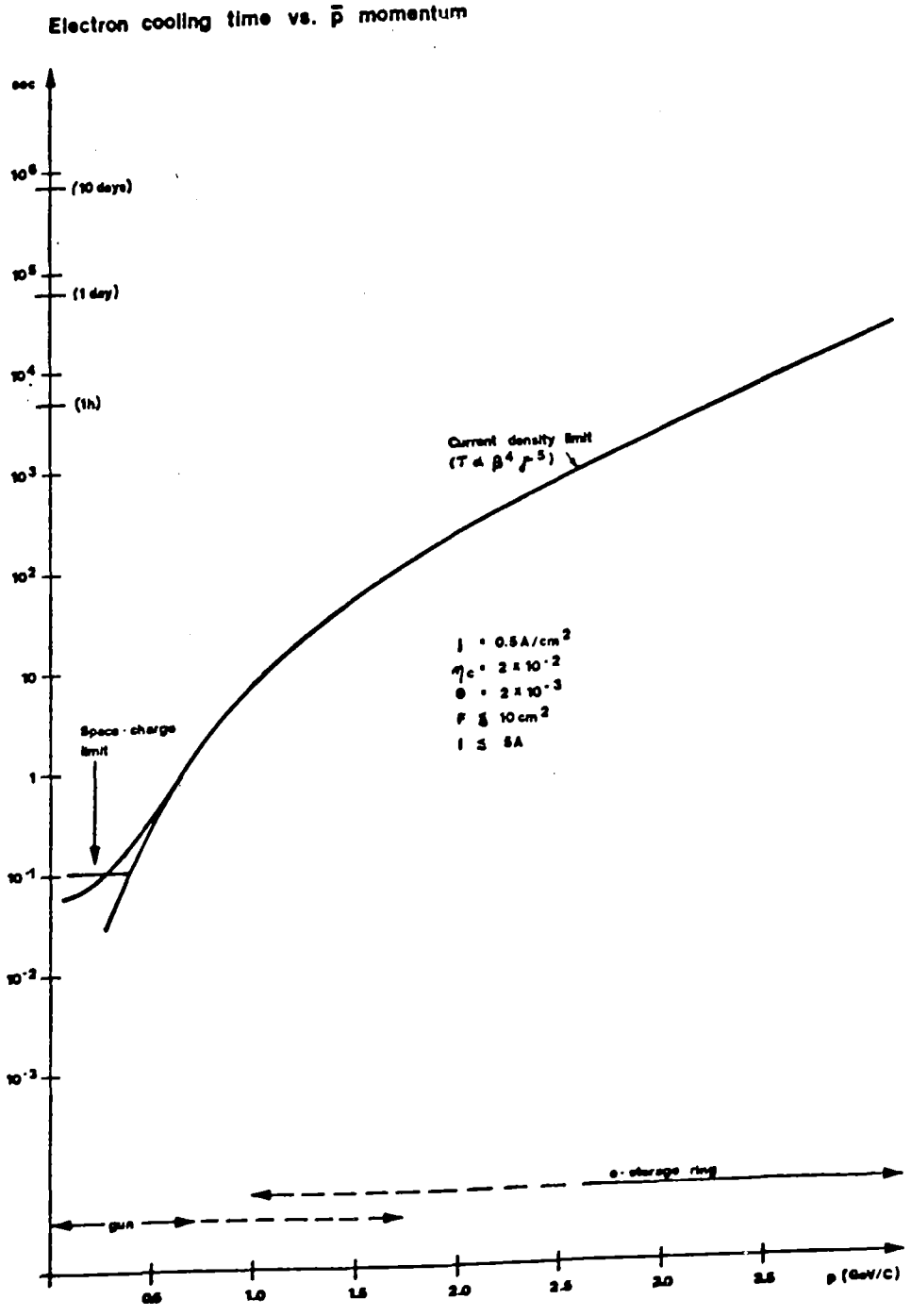

One notes the tendency that electron cooling gets easier as the proton beam is small (small θ and small electron beam size to match the proton beam). This is rather in contrast with the limits for stochastic cooling discussed above which favour a fat proton beam.

Finally, we note from Figure 5 which reproduces a Novosibirsk measurement [7] the tendency that the equilibrium beam size increases with proton intensity. At 10^9 particles, a $\Delta p/p$ of, say, 10^{-4} seems possible extrapolating from this measurement ($p \simeq 0.3$ GeV/c). In a similar way one can hope for an equilibrium beam size of a few millimeters ($N = 10^9$, $p = 0.3$ GeV/c).

FIGURE 5

Final $\Delta p/p$ vs. intensity (electron cooling) (extrapolated from reference 7)

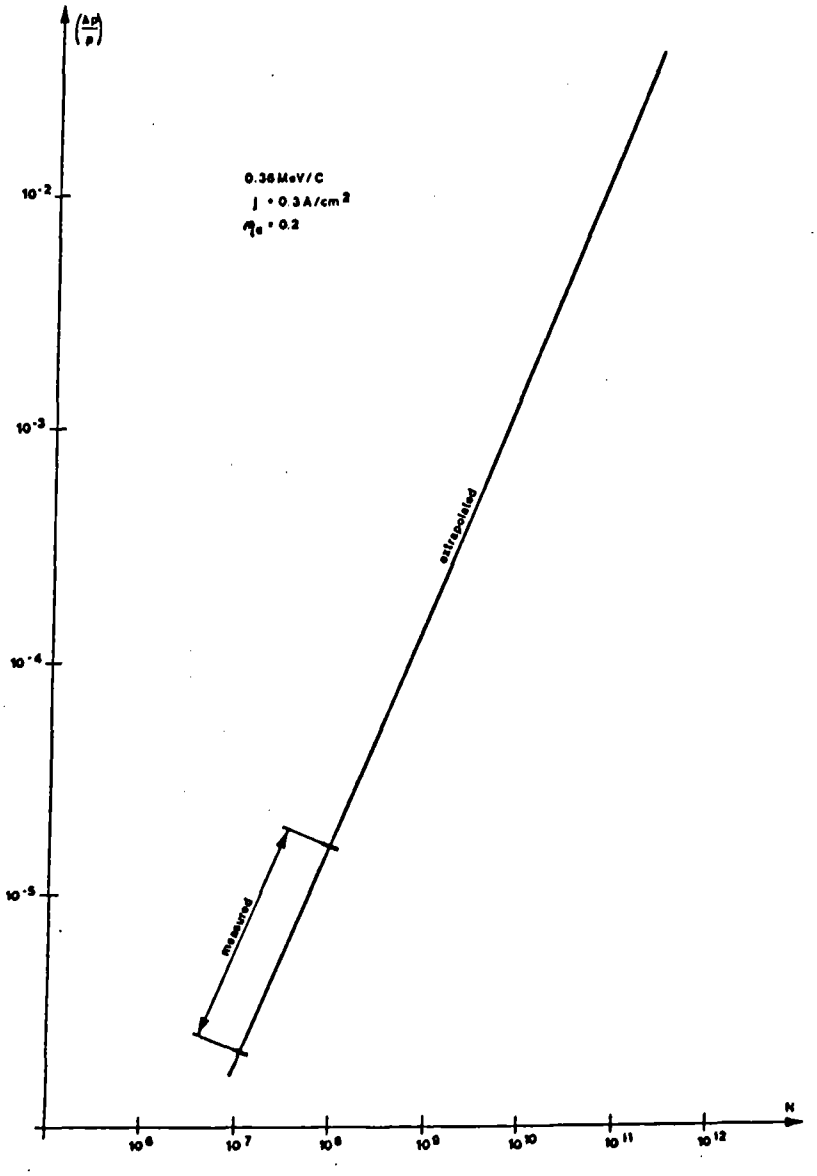

4. RELATIVE MERITS

A qualitative comparison is given in Table 3. One notes that both methods are to a large degree complementary. Stochastic cooling seems well suited to precool and condition the hot beam, especially at high energy where electron cooling is difficult. The electron method looks favourable for post-cooling to the minute temperatures desired for some experiments. At present, it appears that both techniques could coexist in LEAR provided enough straight section space can be made available.

TABLE 3

COMPARISON BETWEEN STOCHASTIC AND ELECTRON COOLING

	Stochastic	Electron
Energy dependence	Weak (possible at all LEAR energies)	Strong (difficult in LEAR above 1 GeV/c)
Intensity dependence	Strong (proportional to N)	Weak
Dependence on beam size and $\Delta p/p$	Likes hot LEAR beam	Likes cold beam
Hardware	Needs fast low level electronics, total of 3 systems for E_H, E_V and $\Delta p/p$ cooling.	Needs high power electron beam. Single device for cooling in all planes
Change of energy	Needs adjustable delays	Needs different electron energy
Change of proton working point	May need reshuffling of components	No change in principle but retuning of proton Q-shift and orbit correctors
Typical cooling time in LEAR at 10^9 p		
- simple system:	150 s at 2 GeV/c (fat beam)	1 to 10 s at $p \lesssim 1$ GeV/c
- advanced system:	15 s at 2 GeV/c (cold beam)	0.1 to 1 s at $p \lesssim 1$ GeV/c

5. CONCLUSION

The initial operation does not have to rely on cooling in LEAR. In a later stage a moderate (slightly upgraded "ICE type") stochastic system could keep the beam temperatures at "comfort level" thus improving LEAR performance and its range of application. The addition of a relatively low current (1/10 of the Novosibirsk values ?) electron device or an advanced stochastic system then seems suitable to freeze the precooled beam to lower temperatures as desired for high precision experiments. At energies above, say, 1 GeV/c where electron cooling becomes expensive the advanced stochastic system looks advantageous for beam freezing, at lower energies the potential for larger cooling strength of the electron system compares favorably. All cooling operations take time which (especially for stochastic cooling) may become a sizeable fraction of the LEAR cycle time.

REFERENCES

1. S. van der Meer, Stochastic damping of betatron oscillations, CERN/ISR-PO/72-31.

2. H.G. Hereward, Statistical phenomena - Theory, Proc. 1st Course Inter. School of Particle Accelerators, Erice (1976), CERN 77-13, p. 281.

3. F. Sacherer, Stochastic cooling theory, CERN Internal Report ISR/TH 78-11.

4. F. Bonaudi et al., To be published in Phys. Reports 1979.

5. S. van der Meer, Influence of bad mixing on stochastic acceleration, CERN Internal Note SPS/DI/pp 77-8, 5.5.1977.

6. L. Thorndahl, Stochastic cooling of momentum spread and betatron oscillations for low intensity stacks, CERN/ISR-RF/75-55.

7. Novosibirsk Group, CERN 77-08, and references given therein.

8. H.G. Hereward, in Proc. Saclay Study on Storage Rings, 1966.

HISTORICAL APPENDICES

1. History of stochastic cooling

Prehistory

Liouville	ca 1850	Invariance of phase space
Schottky	1918	Noise in DC electron beams

History

van der Meer	1968	Idea of stochastic cooling
ISR staff (Borer, Bramham, Hereward, Hübner, Schnell, Thorndahl)	1972	Observation of proton beam Schottky noise
van der Meer	1972	Theory of emittance cooling
Schnell	1972	Engineering studies
Hereward	1972-74	Refined theory, low intensity cooling
Bramham, Carron, Hereward, Hübner, Schnell, Thorndahl	1975	First experimental demonstration of emittance cooling
Palmer (BNL) Thorndahl	1975	Idea of low intensity momentum cooling
Strolin Thorndahl	1975	$\bar{p}$ accumulation, schemes for ISR using stochastic cooling
Rubbia	1975	$\bar{p}$ accumulation, schemes for SPS
Thorndahl	1976	Experimental demonstration of p cooling
Thorndahl	1977	Filter method of p cooling
Sacherer, Thorndahl van der Meer	1977-78	Refinement of theory; imperfect mixing, Fokker-Planck equations
ICE Team	1978	Detailed experimental verification
Herr	1978	Demonstration of bunched beam cooling.

APPENDIX

2. Some dates of the history of electron cooling
(First ten years at INP, Novosibirsk)
(from reference 7)

1966	First report by G. Budker (Saclay Symposium)
1966	First proton antiproton colliding beam proposal using electron cooling (G. Budker, A. Skrinsky, Saclay Symposium)
1967-70	Experimental study on the electron beam (I. Meshkov, R. Salimov, A. Skrinsky)
1968	Theoretical study of the kinetics of electron cooling (Y. Derbenev, A. Skrinsky)
1970	First $p\bar{p}$-project (VAPP-NAP-Group)
1972	Beginning of NAP-M design (N. Dikansky, D. Pestrikov, A. Skrinsky)
1974	The first successful electron cooling experiments (G. Budker, N. Dikansky, I. Meshkov, V. Parkhomchuk, D. Pestrikov, B. Sukhina, A. Skrinsky)
1976-77	Observation and study of the "fast cooling"
1976-77	Theory of "magnetized" electron beams with "flattened" distribution (Y. Derbenev, A. Skrinsky) (A possible explanation of the "fast" cooling).
1976	$p\bar{p}$-colliding beams projects (Novosibirsk for Serpukhov, Batavia, CERN).

$\bar{p}$ LEAR-Note 29
15.2.1979

REPORT ON THE CERN ELECTRON COOLER

M. Bell, J.E. Chaney, F. Krienen and P. Møller Petersen

CERN, Geneva, Switzerland

ABSTRACT

Basic design considerations and characteristics are discussed and a comparison with similar machines is made. Although cooling of 50 MeV antiprotons is in sight, results and performances until now necessitate a deeper understanding of the ionization of the rest gas. To this end the basic motion of the ionized gas is reviewed. It shows that quasi-neutral plasma build-up in the electron beam is probable. Its effect on the cooling is two-fold: the electron beam will be less cool, and the circulating antiprotons scatter more on the accumulated ionized gas. A possible solution for this problem is suggested in terms of operation in the pulsed mode.

Talk given at the
Workshop on Physics with Cooled Low-Energetic Antiprotons,
Karlsruhe, 19-21 March 1979

Geneva - 16 March 1979

REPORT ON THE CERN ELECTRON COOLER

M. Bell, J.E. Chaney, F. Krienen and P. Møller Petersen

CERN, Geneva, Switzerland

1. BASIC DESIGN CHARACTERISTICS

1.1 Introduction

The device may be considered as consisting of three basic parts: the electron gun; straight drift sections including bends; and the collector (see Fig. 1). The electron beam is immersed in a longitudinal magnetic field which extends from the gun to the collector; the gun operates in space-charge limited flow. Emphasis has been laid on obtaining the lowest possible temperature in the electron beam. Owing to high power requirements, this beam is decelerated when it enters the collector, which accepts the electrons in a tapered magnetic field. The electrons have, upon collection, a low velocity and in this way energy is efficiently recuperated.

1.2 Gun (Fig. 2)

The diameter of the cathode is 5 cm. At 60 kV anode potential, which is compatible with about 100 MeV protons, the current is about 8 A. The current is space-charge limited and the perveance is 6×10^{-7} A $V^{-3/2}$. The solenoidal magnetic field of about 700 G and uniform throughout assures fully confined flow of the electrons. We adopted the principle of resonant focusing[1], which assures that the electrons emerge rectilinearly from the gun. The flat cathode is surrounded by a Pierce shield, and followed by five anode rings, each with a bore of 6 cm.

The geometry has been optimized empirically with the help of a program developed, amongst others, for the calculation of the SLAC klystrons[2]. The program accepts any two-dimensional potential distribution imposed on the boundary of the problem and any magnetic field on the axis. It first solves the Laplace potential and does a first ray-tracking with a current density on the cathode given by Child's law. The Poisson solver redistributes the potential, a second ray-tracking redistributes the charge density, and so by iteration the problem is solved in about 300 sec CPU time. The program does not include ionization of the rest gas nor secondary emission.

The space-charged depression across the electron beam is of the order of 500 V, i.e. the peripheral electrons have an energy 500 eV higher than the axial electrons. The transverse temperature of the peripheral electrons is on the average about 1 eV, i.e. within errors the same as the theoretical minimum. We can run the gun at lower perveance by changing the magnetic field and redistribution of the potentials on the anodes. At half current the peripheral transverse temperature is 1.5 eV, and at quarter current the temperature is about 3 eV. Presumably the latter can be improved upon by further computer optimization.

1.3 Drift tube

In order to enter and to leave the (anti-) proton storage ring, the drift tube has two bends of 36 degrees each. The magnetic field in the bend is toroidal and matched to the adjacent solenoidal fields, so that the field strength on the geometrical centre line agrees. A small dipole field of 8 G, perpendicular to the plan of bending, is superimposed so as to minimize the small increase of transverse temperature. Furthermore, two vertical dipoles, of 150 G•m each are added in the proton line, upstream and downstream, in order to compensate the effect of the vertical component of the toroidal fields on the circulating protons.

The length of the drift tube along which the protons are cooled is 3 m, but the non-parallelism of the magnetic field lines in the junctions removes about 20% of the effective cooling length. The length of the gun straight section is 75 cm and that of the collector 70 cm. The over-all length from cathode to collector is 6 m. The diameter of the drift tube is 200 mm. For the time being, apart from tungsten cross-hairs which show the beam position, no other diagnostic means for observation of the electron beam behaviour have been incorporated. The problem with diagnostic means is that in general they adversely affect the transverse temperature of the electron beam.

1.4 Collector (Fig. 3)

The beam power at 60 kV is about 500 kW, hence it is essential to decelerate the electrons before they are collected. To this end the collector is held at 3 kV above cathode potential and the heat dissipation on the collector is then 25 kW [3]. In addition, the collector radius is made five times the electron beam radius. This reduces the peak specific

dissipation on the water-cooled collector to about 50 W cm^{-2}. The fanning out of the electron beam entails a tapering off of the magnetic field. The essential part is the magnetic shunt, i.e. a steel disk terminating the solenoidal field and from which plane the collector starts. The hole in the disk is about 8 cm.

The magnetic field penetrating the collector region can be further modified with five field-shaping coils, coaxial with the collector. A powerful design criterion is provided by the conservation of the generalized momentum p_θ conjugated to the θ coordinate of the motion. It leads to $r_0A_0 = rA$, in which the left-hand term is the radius times the magnetic potential at that radius of an electron before it enters the collector, whilst the product on the right pertains to the quantities at the point of impact on the collector. The above condition would reduce to zero the tangential velocity of the electron when it hits the collector.

The currents in the field-shaping coils are determined with the help of an extensive program, identical to the gun program but much improved with respect to the presentation of the magnetic field. An auxiliary program studies the fate of secondary-emission electrons produced from the collector. Three more electrodes are involved in the collection of the electrons. One is the "repeller", mainly responsible for the deceleration of the primary electrons, although it may capture some of them and also capture some fast secondaries. Another is the "spike", which reflects predominantly axial electrons towards the collector. The third electrode is the "mesh", i.e. a grid repelling some of the low-energy secondaries. The electrical schematic is shown in Fig. 4.

1.5 Comparison

At this stage it may be instructive to compare the basic design principles and parameters of the CERN, Novosibirsk, and Fermilab machines. The differences are very few, in so far as they are intentional. Clearly the aspect of the three machines is strikingly different, not only with respect to the size but also to the style (Table 1).

Table 1

	CERN	Novosibirsk [a]	Fermilab [a]
Cathode type	Dispenser	Oxide coated [b]	Dispenser
" surface	Flat	Flat	Spherical [c]
" emission	Space-charge limited	Temperature limited [d]	Space-charge limited
Focusing	Resonant	Resonant	Resonant
Beam diameter (cm)	5	1	5
Anode voltage (kV)	60	35	110
Beam current (A)	8	1	23
Proton kin. energy (MeV)	100	65	200
Cooling section (m)	3	1	5
Magnetic field (G)	700	1000	1000
Sector angle (degree)	36	45	90
Coll. deceleration	Non-resonant	Non-resonant	Resonant [e]
Coll. magn. field	Tapered	Tapered	Tapered [e]
Coll. diameter/beam diam.	5	>> 1	≤ 1 [f]
Coll. voltage (%)	95	97	?
Coll. curr. loss (%)	(g)	10^{-4}	?

Notes

a) Some of the numbers may not be up to date.

b) Oxide-coated cathodes are delicate to handle, but there is appreciably less outgassing.

c) Spherical cathodes require a tapered magnetic field, which is difficult to match.

d) Temperature-limited emission has the risk of non-uniform current density, but the outgassing rate is less.

e) The deceleration is the reverse of the acceleration in the gun.

f) The electron beam runs into a tapered cone and creates a (-ve) potential well which would suppress secondary emission.

g) At present the losses are higher than predicted; the cause for this is under investigation. One difference with the Novosibirsk machine seems that they decelerate the electrons before the magnetic field tapers off, whereas we do this simultaneously. Up to now, computer simulation has shown no difference.

2. HISTORY

The construction of the apparatus started in the summer of 1977. In general the progress was reasonable with the exception of the delivery of the high-voltage feedthrough insulators, which delayed the general assembly until the summer of 1978. Detailed mapping of the magnetic field has been made. Non-uniformities have been compensated with correction coils.

Low-voltage testing confirmed the 3/2 power law between current and voltage. We could measure the beam position by means of 20 μm tungsten cross-hairs which became incandescent where the electrons hit the wires. The contrast between light and dark was as little as half a millimetre. In these tests the electrons were decelerated so that most (92%) of the beam power was recuperated. The energy of the electrons landing on the collector was 6% of the anode voltage, and the fraction of the current which did not land on the collector was 2%.

The vacuum pressure reached in the initial stage was 10^{-9} Torr with the cathode cold, and 10^{-8} when hot. This was considered sufficient to produce the electron beam, although the electrons were probably not cool neough for the cooling process. The maximum d.c. anode voltage was 12 kV, and the maximum short-time anode voltage was 22 kV. The high voltage was limited by rising vacuum pressure, and in general a breakdown was imminent when the pressure rose to 10^{-7} Torr.

Owing to these vacuum problems, by the end of 1978 the system was opened for visual inspection. It was discovered that 3 brass washers had inadvertently been used to mount the cathode. Deposits produced by evaporation of zinc contained in the brass washers were clearly visible on the cool surfaces of the gun and could easily account for some of the high-voltage breakdowns and vacuum troubles. Inspection of the Pierce shield and the first anode facing it showed signs of charge impact. The back of the last anode, i.e. the one facing the collector, also showed signs of impacts, but none of these eroded the surface, indicating some sort of sustained discharge. The collector was found to be remarkably clean, but one of the minor internal stand-off insulators was cracked. In addition,

when dismantling the collector the position of the field coils was found to be incorrectly located. This could explain the discrepancy between the computed coil currents and those needed to optimize the electron beam collection.

3. PRESENT STATUS

A new cathode has been mounted, suspect parts have been cleaned or replaced, and an initial cathode conditioning has been done separately. Upon starting up, we reach a pressure of 2×10^{-9} when the cathode is hot. Most of the rest gas is hydrogen. After completing the electron gun assembly, bake out, and vacuum testing, the pressure was again measured by this time with the titanium sublimators switched on. We now reach 10^{-10} when the cathode is cold and 2×10^{-10} when the cathode is hot. The improvement of a factor of 10^2 with respect to the first cathode trials should enable us to reach operation at 30 kV. If this is so, then we will mount the gun in the ICE ring and start to cool 50 MeV protons. In tests made recently, 24 kV was reached at a pressure of 5×10^{-9}. According to the Russian experience a pressure of 10^{-10} is essential, so going by this assumption we may need more pump speed. On the other hand, the new cathode might in the long run clean up, so that the recommended pressure is obtained.

4. PARTICLE MOTION IN THE DRIFT TUBE

In the gun and in the collector one has to rely to a large extent on computer calculation. In the drift tube, considerable analysis is possible. We can do this for any charged particles, slow or fast, because they obey one and the same Hamiltonian.

The non-relativistic equation of motion for a particle with charge q is given by

$$H = \frac{p_r^2}{2m} + \frac{(p_\theta - qrA)^2}{2mr^2} + \frac{p_z^2}{2m} + q\phi \ ,$$

in which $p_\theta = mr^2\dot{\theta} + qrA$ is a constant of the motion. In a uniform magnetic field $A = \frac{1}{2} rB$. In a uniform space-charge field $\phi = -\rho r^2/(4\varepsilon_0)$, in which ρ is the charge density and ε_0 is the vacuum permittivity. Thus we find

$$\ddot{r} = -\frac{1}{m}\frac{\delta H}{\delta r} = \frac{\left(\dot{\theta}_0 + \frac{1}{2}\omega_c\right)^2 r_0^4}{r^3} - \frac{1}{4}\omega_c^2 r + \frac{q\rho}{2\varepsilon_0 m} r \ ,$$

where $\dot{\theta}_0$ is the initial angular velocity of the particle and r_0 is the initial radius; $\omega_c = qB/m$, the cyclotron frequency. The above equation in $\ddot{r}$ is of the type $\ddot{r} = a^2 r^{-3} - b^2 r$ and has an exact solution

$$r \cos\theta = R \cos\omega t + r' \cos\omega' t$$

$$r \sin\theta = R \sin\omega t + r' \sin\omega' t \ .$$

R, r′, ω, and ω′ will be expressed in B and ρ and the initial conditions, which we assume start at t = 0. Clearly we have $r_0 = R + r'$, $\theta_0 = 0$, $r_0\dot{\theta}_0 = R\omega + r'\omega'$, and $\dot{r}_0 = 0$. We note that the last condition is not necessarily restrictive. By inspection we find

$$\ddot{r} = \frac{1}{4}\Omega^2(R^2 + r'^2)^2 r^{-3} - \frac{1}{4}\Omega^2 r \ ,$$

where $\Omega = \omega' - \omega$, so that

$$\frac{1}{4}\omega_c^2 - q\rho/(2\varepsilon_0 m) = \frac{1}{4}\Omega^2$$

$$\left(\dot{\theta}_0 + \frac{1}{2}\omega_c\right)^2 r_0^4 = \frac{1}{4}\Omega^2(R^2 - r'^2)^2 \ .$$

From this we find

$$\omega' = \frac{1}{2}\left(\Omega - \omega_c\right)$$

$$-\omega = \frac{1}{2}\left(\Omega + \omega_c\right)$$

$$r' = \frac{1}{2} r_0 + \left(\dot{\theta}_0 + \frac{1}{2}\omega_c\right) r_0/\Omega$$

$$R = \frac{1}{2} r_0 - \left(\dot{\theta}_0 + \frac{1}{2}\omega_c\right) r_0/\Omega \ .$$

It is also possible to find an explicit formula for the θ-motion. The conserved conjugated momentum furnishes

$$\dot{\theta} = r_0^2\left(\theta_0 + \frac{1}{2}\omega_c\right)/r^2 - \frac{1}{2}\omega_c \ .$$

Now

$$r^2 = R^2 + r'^2 + 2Rr' \cos\Omega t \ ,$$

hence

$$\theta = \int \dot{\theta} dt = \tan^{-1} \left[\left(\theta_0 + \frac{1}{2} \omega_c \right) \Big/ \frac{\Omega}{2} \times \tan \frac{1}{2} \Omega t \right] - \frac{1}{2} \omega_c t \ .$$

It may be shown that $\langle \dot{\theta} \rangle_{av} = \omega'$.

Finally, the z-motion is simply given by $z = \dot{z}_0 t$.

We note that the frequencies ω' and ω are independent of the initial conditions and that for most practical purposes $\dot{\theta}_0 << \frac{1}{2} \omega_c$, so that r' and R are likewise independent of the initial conditions. For instance, the ionization products have in general a kinetic energy which is very small, for electrons typically of the order of $\frac{1}{2}$ eV and (+ve) ions even less.

Nevertheless the motion of the two particles is strikingly different, in the first place because of the large mass difference. Slow electrons spiral, with angular velocity $\omega \simeq \omega_c$ and small radius of gyration, around a guiding centre which rotates with the angular velocity $\omega' << \omega_c$. Slow (+ve) ions execute a quasi-harmonic oscillation with frequency $\omega \simeq -\frac{1}{2} \Omega$ across the electron beam. The plane of oscillation rotates with angular velocity $\omega' \simeq \frac{1}{2} \Omega$. In the above we have made the convention that Ω and ω_c have the same sign, which fixes the guiding centre to be (ω', r') and the electron spiral or the harmonic oscillation of the positive ion to be (ω, R). It is also easy to see that $\omega' r_0$, in the electron case, is numerically about the Alfvén velocity E_r/B, where E_r is the radial electric field strength.

In the second place the sign of the charge q provides a restriction: whereas (+ve) ions are always bounded in a (-ve) space-charge well, electrons can escape if the (-ve) space-charge well is so deep that $\Omega^2 < 0$. The solution is of course formally correct, only one has to fill in complex numbers for ω and ω'. The break-even condition $\Omega^2 = 0$ imposes a net (-ve) particle density

$$n_{BE} = \frac{1}{2} B^2 \varepsilon_0 / m \ .$$

However, it is easy to see that break-even for electrons is physically not realistic, because the associated potential well would have a depth much larger than the anode voltage. On the other hand, the escape of

(-ve) ions is a physical reality, as can be inferred from the above expression.

Furthermore, the motion of the fast beam electrons in the drift tube is, apart from a relativistic correction, identical to the formulas developed above. Again, the aspect of this motion is very much different from that of the slow electrons and from the low (+ve) ions. The screw-like fashion of the fast electrons is now much drawn out. The associated wavelength (pitch) will be $\lambda = 2\pi v/\Omega$, where v is the velocity of the electron. The rotation of the guiding centre has direct relation to the theoretical minimum transverse energy one can obtain. It is easy to show that the theoretical minimum $E_\perp = \frac{1}{2}\, m\omega'^2 r'^2$, and furthermore that $\omega' \simeq \simeq \rho/(2\varepsilon_0 B)$ and $r' \simeq r_0$. However, the self-magnetic field produced by the fast electrons reduces $E_\perp$ by a factor $(1 - v^2/c^2)^2$.

As mentioned before, the peripheral fast electrons have an energy appreciably higher than that of the axial fast electrons. The associated temperature, $E_\parallel$, with respect to the centre of mass of the axial electrons, is small: $E_\parallel = \frac{1}{2}\, mc^2\beta^{*2}$. The centre-of-mass velocity $c\beta^*$ is related to the depth of the potential well ϕ with good approximation by $c\beta^* \simeq \phi/p_0$, in which p_0 is the momentum of the axial electron. In our case, the theoretical minimum $E_\perp \simeq 0.7$ eV and $E_\parallel \simeq 1$ eV.

5. THE VACUUM PROBLEM

The previous section on the motion in the drift tube may shed some light on the understanding of the necessity for a good vacuum. It clearly has to do with the ionization of the rest gas colliding with the fast beam electrons. We saw that the motion of the slow electrons and the slow (+ve) ions is bounded in the transverse plane, whereas the ż-motion is conserved. We now discuss what can happen at either end of the drift tube.

The slow electrons, born in the drift tube, run at either end against a retarding electric field; hence they are totally reflected and stay trapped, at least initially. The electrons born in the gun region at a potential $\phi > \phi_c$, where ϕ_c is the collector potential, will penetrate the collector and then be reflected; for how long we do not know, because considerable scalloping may occur upon the repeated passages in the drift

tube. At a potential $\phi < \phi_c$ the electrons could be captured by the collector, but if not, their lifetime will be limited. Something similar will happen with electrons born in the collector region.

The slow (+ve) ions born in the gun or collector region see an accelerating electric field and will be captured at once on the cathode or on the collector. The ions born in the drift tube stand a good chance of being reflected at the ends, where the diameter of the drift tube narrows. A restriction in drift tubes creates a quadrupole-like electric field, entirely due to the space charge of the fast electrons. Now quadrupoles have typically a centre where two equipotential surfaces cross over (Fig. 5). If the potential at the centre is higher than the peripheral beam potential, (+ve) ions are reflected. So there is in principle no need for extraneous electrostatic repellers.

On the gun end of the drift tube this situation is shown up in the computer graphics. We also find reflections of the type described above in arbitrary constrictions in drift tubes (see Fig. 5). On the collector end we have not yet seen this phenomenon, perhaps because of the poor termination of the computer problem or because the collector opening is larger than the anode opening; but in principle, reflection could be there.

Comparing the two cases, there will be more electrons trapped than (+ve) ions. The unbalance is least when the drift-tube reflection for (+ve) ions is perfect, and is estimated to be between 2 and 4%. The percentage refers to the total ionization rate in the system. Clearly the percentage will be higher if some of the (+ve) ions born in the drift tube ooze out. However, in this respect, something can be done to remedy this technically.

We now discuss the rate with which space charge builds up. In order to have numbers, we assume we are working with a vacuum of 10^{-9} Torr throughout. The rest gas is assumed to be hydrogen. The anode voltage is 60 kV.

Gas density	$n_1 = 3.2 \times 10^{13}$ m^{-3}
Electron beam density	$n_2 = 1.9 \times 10^{14}$ m^{-3}
Electron velocity	$v = 1.2 \times 10^{8}$ m sec^{-1}
Ionization cross section	$\sigma = 0.6 \times 10^{-22}$ m^2
Recombination coefficient	$\alpha = 5 \times 10^{-19}$ m^3 sec^{-1}

Attachment coef. (-ve) ions	$\beta = 3 \times 10^{-22}$ m^3 sec^{-1}
Drift tube length	$L = 6$ m
Beam volume	12×10^{-3} m^3
Pump speed (2000 ℓ/sec)	6×10^{13} sec^{-1}

The fraction of the fast electrons producing ionization is $\sigma n_1 L \simeq 10^{-8}$, so this fraction is too small to impair the quality of the electron beam, even if similar processes such as scattering and excitation are taken into account.

The ionization rate $R_i = n_1 n_2 v\sigma \simeq (1/2)\ 10^{14}$ m^{-3} sec^{-1}. Clearly the gas population in the beam will be totally ionized in about one second. However, the ionization continues by diffusion of the surrounding gas into the beam. In a way, the electron beam works as a pump, but its pumping speed is small compared to the speed of the sublimators by a factor of 100. The ionization rate scales with the square root of the anode voltage.

Next we assume that both ionization products are 100% trapped in the electron beam. Hence we build up a neutral plasma of high density, n_3. The equilibrium will be reached when recombination equals ionization. Clearly we have $R_i = n_3^2 \alpha$ or $n_3 \simeq 10^{16}$ m^{-3}. This represents an increase in pressure inside the beam volume by a large factor, $n_3/n_1 \simeq 300$, so the pressure inside the beam would be 3×10^{-7} Torr!

The time constant for building up the equilibrium $\tau_p = (\alpha R_i)^{-1/2} \simeq$ $\simeq$ 200 sec. Clearly the plasma density scales with the square root and the build-up time with the inverse square root of the gas pressure.

The build-up of a neutral plasma in the electron beam is, as such, harmless. The charge density remains as it was before, so the temperature of the beam electrons will not be affected. There would be a small effect due to an increase of excitations of all sorts. But the fraction of fast electrons participating in these processes would be still very small.

The danger lies in the non-perfect trapping. As we have estimated, the best we can hope for is an unbalance of, say, $\Delta = 2\%$. The fraction Δ refers to the total ionization in the system. The rate of increase of (-ve) charge density would be $\Delta R_i \simeq 10^{12}$ m^{-3} sec^{-1}. Hence it takes about 200 sec to add a charge equal to the original charge. This time scales inversely with the gas density. The temperature of the fast electrons

will increase, because the resonant focusing is geared to a specific space-charge density and, in addition, $E_{\parallel}$ goes with the square of the depth of the potential well.

The question is now: Would there be equilibrium in the sense that, whilst (-ve) space-charge builds up, automatically an escape mechanism for slow electrons sets in, which tends to restore plasma neutrality? For instance (-ve) ions are not trapped, but the production rate $R_{\beta} = n_1 n_3 \beta \simeq 10^8 \text{ m}^{-3} \text{ sec}^{-1}$, which is negligible. An escape mechanism for excess slow electrons might conceivably be added to the system, but to hold such a precarious balance at the required precision must be quite difficult. Clearly if the vacuum were an order of magnitude better, all time constants would be improved. Hence switching the gun on and off every now and then would in principle be operational. In the case of a temperature-controlled oxide cathode this procedure would in fact be quite easy. The heat capacity is low, so that by temporarily switching off the cathode heating, the electron emission would rapidly cease. We can also think in terms of pulsing the anode voltage; this will be discussed in the next section.

6. PULSED OPERATION

We could expect a gradual build-up of quasi-neutral plasma from the time of switching on the beam current. So there could be several measureable beam quantities which would change during the build-up, and supply proof that the above reasoning is qualitatively correct. Even in the worst case, when all (+ve) ions disappear from the beam at once, we still have several seconds before the (-ve) charge density has doubled. Presumably there will be a current transient during the establishment of the anode voltage, but this can be trimmed to, say, a fraction of a millisecond. The current collection efficiency is shown up in the measurement of the anode current. This current would ideally be zero, so a steady increase with time would be a sensitive test.

The vacuum pressure is expected to behave as follows. Initially one would observe a pressure spike when the beam starts liberating the gas molecules that have settled on the collector during the previous period of rest. Then pressure builds up when not all charges are properly collected. Finally there will be a pressure spike when the beam is switched off and the (+ve) ions disperse to the wall of the vacuum system.

There are three ways in which the electron beam could be pulsed. One would consist in applying all the potentials except that of the cathode, which is held to ground in the off-state. In this case the switch should be rated for the full beam power. The second would consist in keeping the four auxiliary anodes at cathode potential in the off-state. In this case the off-state current would not be quite zero, but the power rating of the switch would be minimal. The third possibility would be to pulse collector and cathode simultaneously. It would mean pulsing the high-voltage Faraday cage, which is then at ground potential in the off-state. The power rating of the switch would also be quite small; in fact it would be determined by the current collection efficiency. It offers also the advantage that the electron beam velocity can be modulated at will. Nevertheless, the switching gear is not trivial; the appropriate switch would be a high vacuum tube (tetrode).

7. CONCLUSION

It seems that with the improved vacuum the required minimum energy of the electron beam can be reached, so that cooling tests on 50 MeV protons are within sight. We do believe, however, that there will always be some build-up of plasma, which at best does no harm. Pulsing the electron beam is a good diagnostic tool. Pulsing may even be a necessity for good cooling.

REFERENCES

1) J.R. Pierce, A gun for starting electrons straight in a magnetic field, Bell System Technical Journal 30, 825 (1951).

2) W.B. Herrmannsfeldt, Electron trajectory program, SLAC-166 (1973).

3) H.J. Wolkstein, Effect of collector potential on the efficiency of travelling-wave tubes, RCA Rev. 19, 259 (1958).

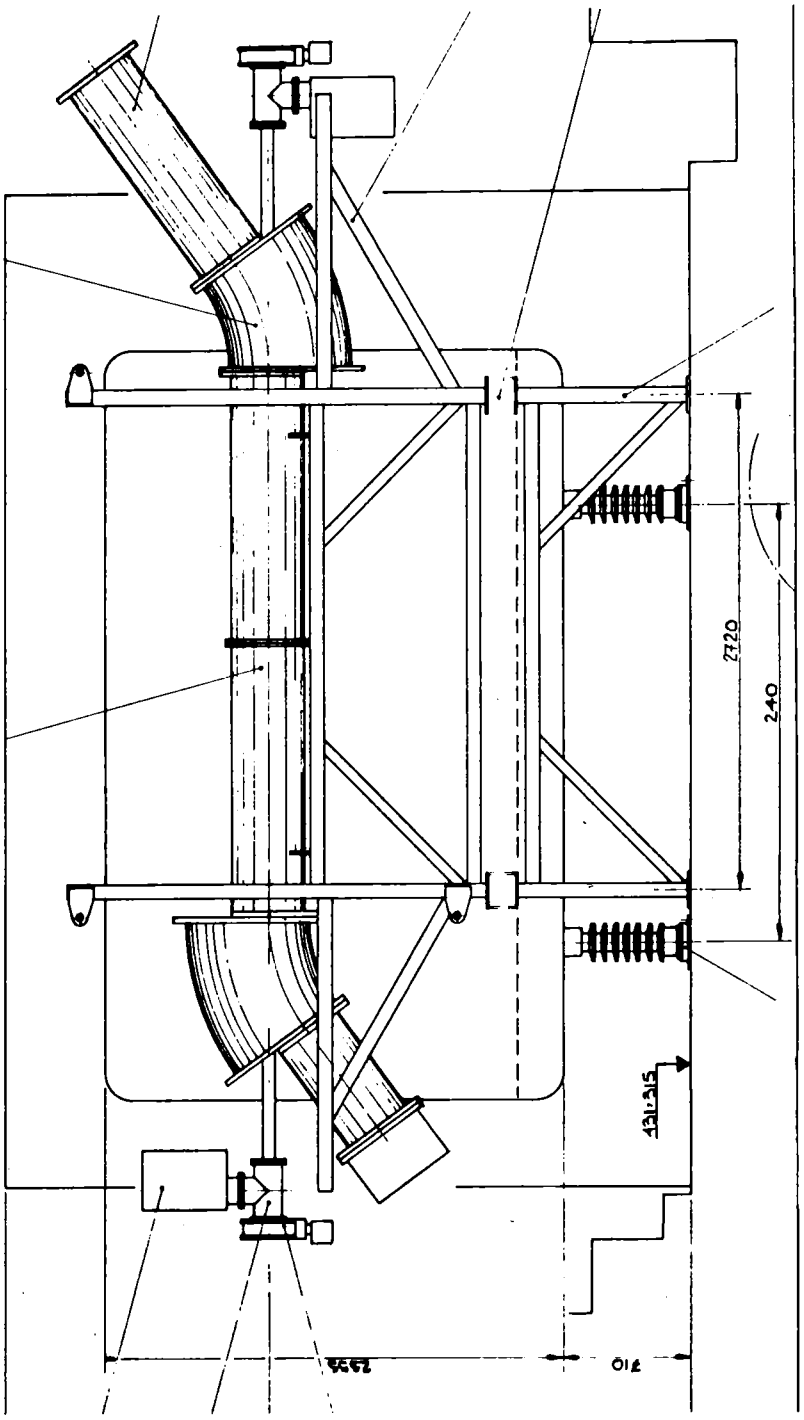

Fig. 1 General layout

1.	Cathode	W
2.	Pierce shield	Ta
3.	Heat sink	Mo
4.	Gas cooled base	Cu
5.	Cathode feedthrough	Al_2O_3
6.	Anode feedthrough	Al_2O_3
7.	Bellows	s.s.
8.	Anodes	Ti
9.	Anode	Cu
10.	Anode support	Al_2O_3

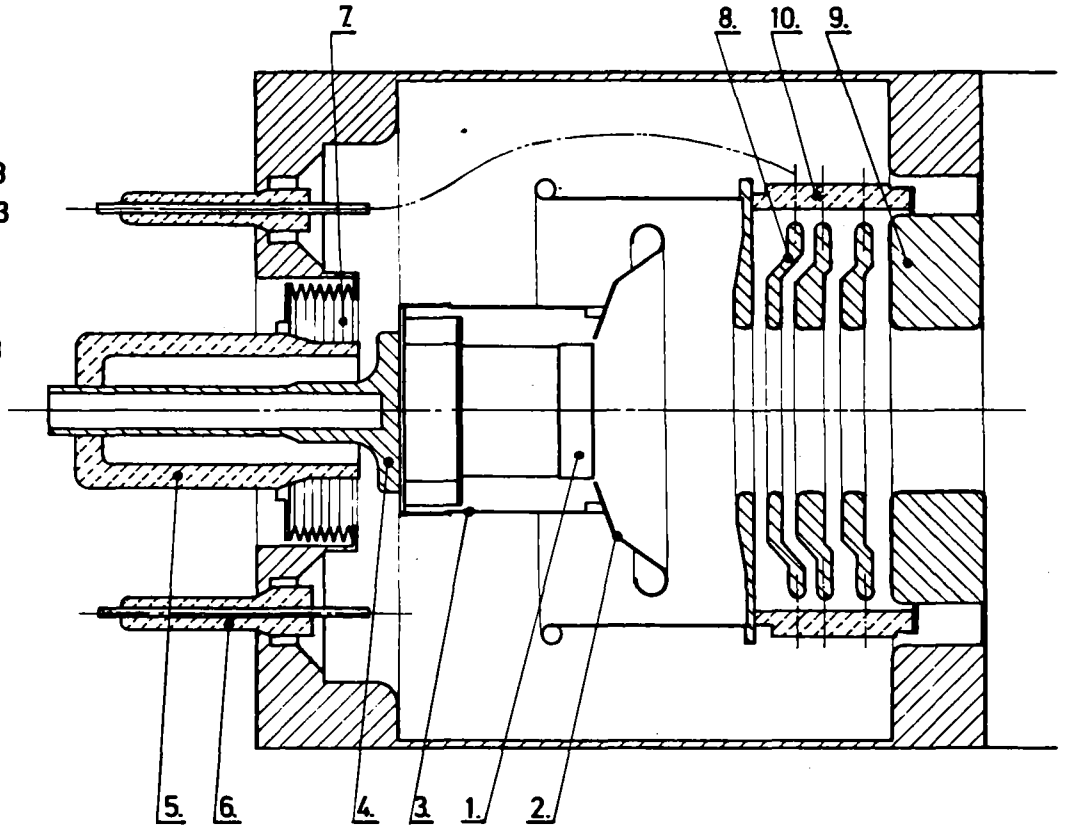

Fig. 2 Gun

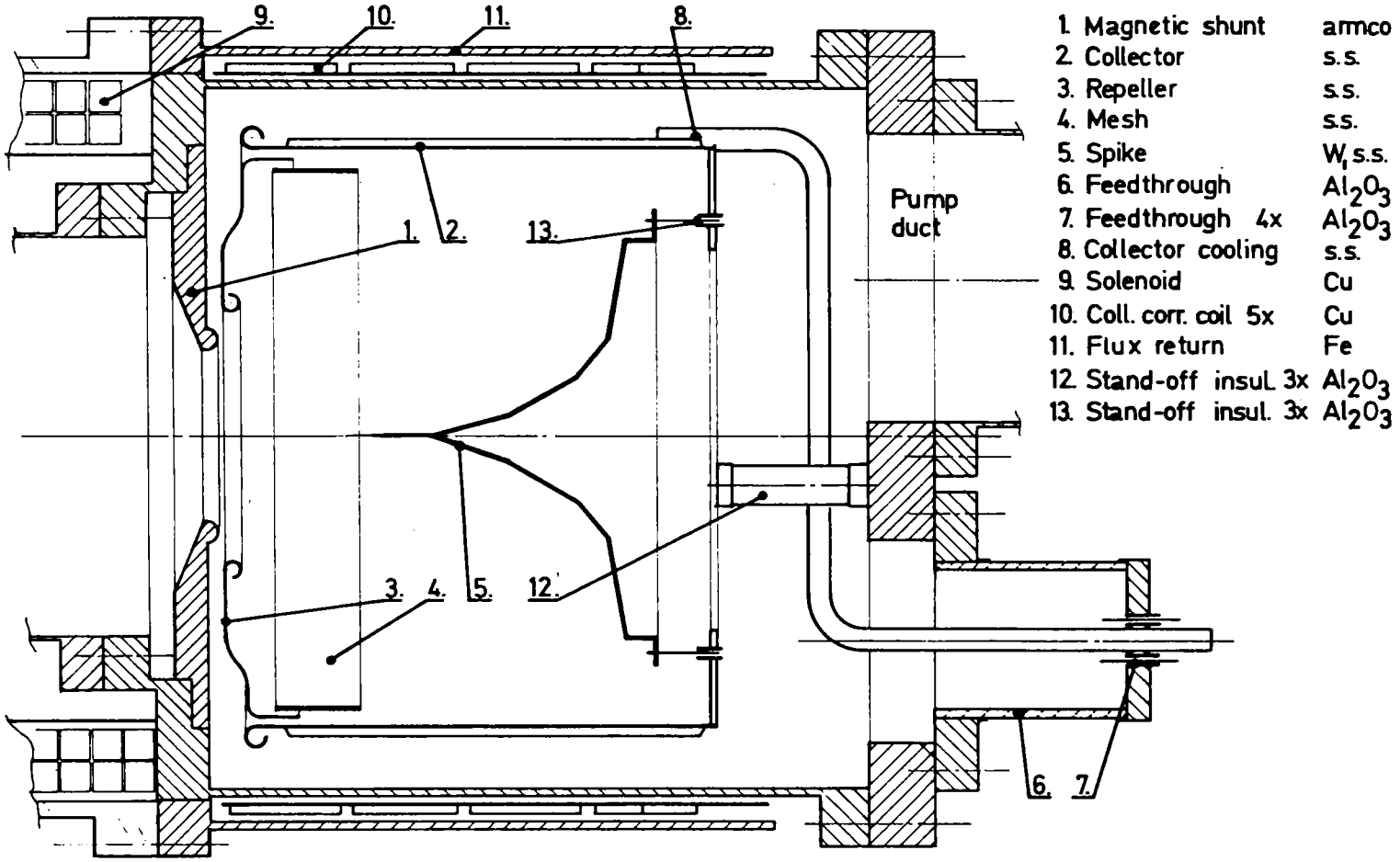

Fig. 3 Collector

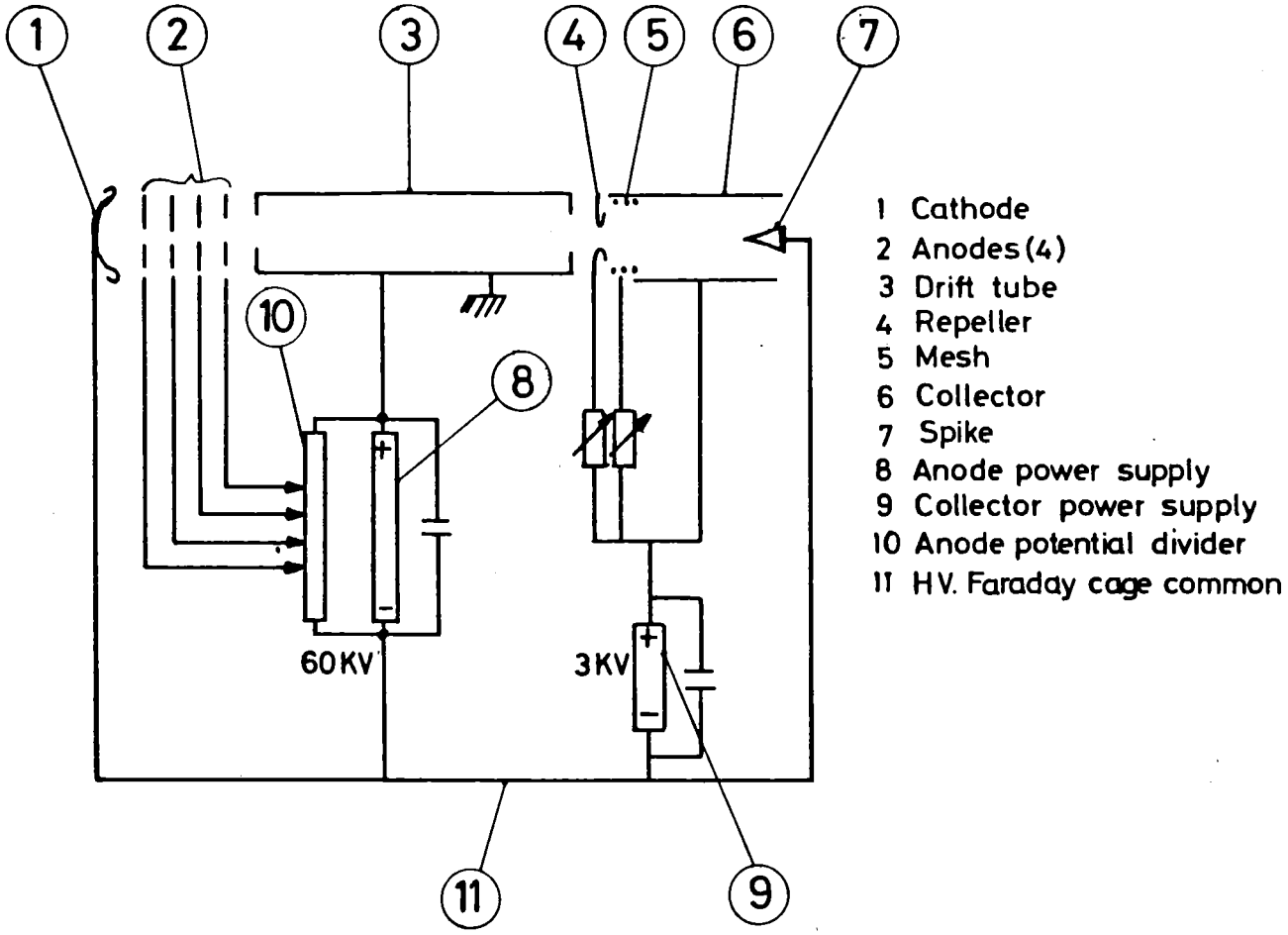

Fig. 4 Electrical schematic

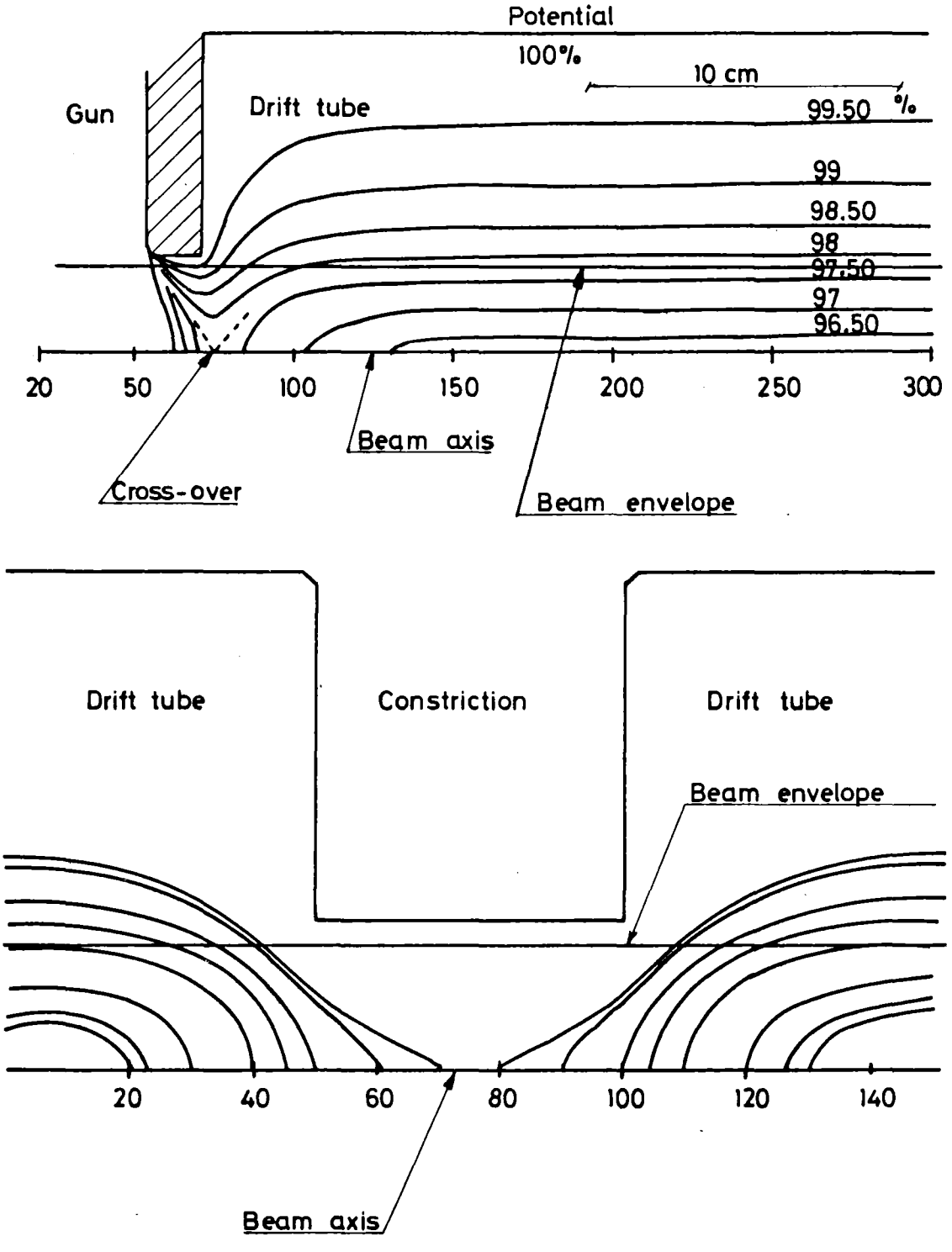

Fig. 5 Equipotential cross-over

PS/AA/Note 79-2
LEAR Note 52

THE CERN ANTIPROTON ACCUMULATOR (AA) *

H. Koziol
CERN, Geneva, Switzerland

The aim of this report is to give an overall view with weight on those aspects that are of interest to the present audience. It will be neither complete nor well balanced, such descriptions can be found in the design study (ref. 1) and in an up-to-date report (ref. 2). No further references will be given, they are all contained in the two quoted.

A glance at the history

It is the low density in transverse and longitudinal phase-space, i.e. wide angular distribution and large momentum spread, with which antiprotons emanate from a production target, that prevented their accumulation in a storage ring to anything like a useful intensity for colliding beam experiments. Before that can be done, their density in phase-space must be increased by a very large factor.

When G. Budker invented electron cooling in 1966, it was with just that application in mind: accumulation of large numbers of antiprotons for a 25 GeV $p\bar{p}$ collider.

In 1968, S. van der Meer invented stochastic cooling, a very different process. The motivation was also different: to reduce the emittance of the high-intensity beams circulating in the ISR and thereby increase the luminosity.

Both cooling methods were experimentally proven in 1974 and by 1976 they had been developed to a level that one could conceive large scale projects based on them.

---

* Talk given at the "Workshop on Physics with Cooled Low-Energy Antiprotons", Kernforschungszentrum Karlsruhe, 19-21 March, 1979

C. Rubbia then proposed a scheme where antiprotons, produced by the intense PS beam striking a target, would be cooled and accumulated over many hours and then transferred to the SPS. Collision with a counter-rotating proton beam would yield centre-of-mass energies up to 540 GeV supposedly enough to produce the long awaited intermediate bosons, $W^{\pm}$.

It should be noted, that the virtue of the antiproton in this scheme is its negative charge. It allows one to turn the SPS into a "poor man's collider", with only one magnet system for two counter-rotating beams. Two intense colliding proton beams would, of course, give a much higher luminosity. ISABELLE at BNL may provide that in several years' time.

Following C. Rubbia's proposal, CERN launched the $p\bar{p}$ project. ICE, a small experimental storage ring, was built in a record time of 9 months to study both cooling techniques. This was done successfully for stochastic cooling in the spring of 1978.

In parallel, a study group elaborated a viable scheme for producing, cooling, accumulating, accelerating and colliding antiprotons, which involves practically all CERN accelerators.

The $p\bar{p}$-project

In June 1978, the $p\bar{p}$-project was authorized. Fig. 1 shows its final lay-out, with all new construction shown in heavy lines.

The 26 GeV/c PS beam is brought onto a $\bar{p}$-production target. $\bar{p}$ of 3.5 GeV/c are injected into the AA and accumulated there over a period of a day. The $\bar{p}$-stack is then extracted in 12 batches that are returned, via a loop, to the PS for acceleration to 26 GeV/c, to be injected into the SPS above its transition energy.

When in 12 PS cycles all the $\bar{p}$ are loaded into the PS, they are accelerated, together with the protons, already injected before them, to an energy of 270 GeV. Contraction of the 12 $\bar{p}$ and 12 p bunches into 6 bunches each and a low-β insertion are required to reach the design luminosity of 10^{30} cm^{-2} sec^{-1}.

Two underground experimental halls house the equipment to observe the collision products.

Recently, the $p\bar{p}$-project has been extended to the ISR which will also receive $\bar{p}$ at 26 GeV/c into one of the two rings.

Finally, shown as a little speck in the PS South Hall, there is LEAR as a new pretender, wanting to feed on the 10^{-12} g of antimatter that the AA provides per day.

AA design criteria

Let us now turn to the central piece of the $p\bar{p}$-project, the Antiproton Accumulator. Its basic design criteria were:

- At the input end, 10^{13} ppp at 26 GeV/c in a 0.5 μsec burst from the PS, every 2.6 sec.

- At the output end, 6×10^{11} $\bar{p}$ to be accumulated in a day, to obtain the final luminosity of 10^{30} cm^{-2} sec^{-1} in the SPS.

From these boundary conditions, the main AA parameters follow rather logically (at least in retrospect):

6×10^{11} $\bar{p}$ per day corresponds to 1.8×10^{7} $\bar{p}$ per PS cycle (2.6 sec). Taking into account the losses that occur at various stages, this gives a nominal value of 2.5×10^{7} $\bar{p}$ per PS cycle.

With 26 GeV/c primary proton energy, the $\bar{p}$ production maximum is at 3.5 GeV/c, the AA nominal momentum.

The nominal momentum together with the fact, that in the PS the beam can be contracted to $\frac{1}{4}$ of the circumference, determines the AA circumference: $\frac{1}{4}$ that of the PS, i.e. 50π m.

The $\bar{p}$ production facility consists of a high efficiency target (small diameter, 3 mm, at the thermal limit) and a pulsed current-sheet lens ("magnetic horn"). With 10^{13} primary protons, and hitting a compromise between transverse emittance and momentum spread, the required 2.5×10^{7} $\bar{p}$

are produced into a horizontal and vertical emittance of 100π mm mrad each and into a $\Delta p/p$ of $\pm$ 7.5 $^{0}/_{00}$. This determines the acceptance of the injection line and the AA injection orbit. As we will see later, the total momentum acceptance of the AA must be much larger: 6%.

The accumulation process requires a very fast momentum pre-cooling, $\Delta p/p$ is reduced by a factor 9 in 2.2 sec, and a stack-cooling by a very large factor: 10^4 in longitudinal phase space density and 10^2 in each transverse plane. Altogether, the density in 6-dimensional phase space has to be increased by nine orders of magnitude!

Lattice

The requirements for stochastic cooling (see D. Möhl's contribution, this conference) lead to a peculiar lattice (Fig. 2). Good mixing means a strong dependance of revolution frequency on momentum, hence a large average value of the dispersion α_p. Large local values of α_p are required for spatial separation of injected beam and stack, as we will see later on. On the other hand, stack momentum cooling must be applied at $\alpha_p = 0$ to avoid transverse "heating" and injection/ejection is also facilitated by a small α_p at the septum.

The consequence is a FODO-lattice of 12 periods in 2 super-periods, where $\alpha_p = 0$ in the two long straight sections (Fig. 3). One is used for injection and ejection, the other mainly for stack momentum cooling.

We have to mention a further point of great importance and considerable technical complication. The fringe field of the fast injection kicker magnet, fired every 2.6 sec, would strongly perturb the stack, i.e., increase its horizontal emittance. Also, the rather violent action of the pre-cooling kicker would "heat up" the stack, i.e. increase its momentum spread. Finally, the pre-cooling pick-ups should only see the low-density, injected beam and must not be swamped by the strong signals from the high-density stack.

All these elements must therefore be equipped with effective magnetic shields. This is achieved with fast shutters that are normally closed, being opened only when the pre-cooled beam is brought from injection orbit to the top of the stack and also during extraction. A high α_p at these locations must spatially separate injected beam and stack to the extent

that there is a gap between them, wide enough to accommodate the shutters (Figs. 4 and 5). Obviously, this leads to impressive horizontal beam dimensions, as much as 70 cm, and corresponding monstruous vacuum chambers.

Cooling and stacking

Let us now look at the 2-step process of cooling and stacking (Fig. 4). After a conventional mono-turn injection with septum and fast kicker, the $\bar{p}$ beam circulates on an injection orbit that is off-centre, towards the outside, except in the long straight sections, where $\alpha_p = 0$. The initial $\Delta p/p$ of $\pm$ 7.5 $^{o}/_{oo}$ is pre-cooled to $\pm$ 0.83 $^{o}/_{oo}$ in 2.2 sec, using the filter method. The pre-cooled beam is then trapped in an rf-bucket and decelerated to the top of the stack, where it is released. At that moment a new $\bar{p}$ beam can be injected.

Stack momentum cooling requires a gain that varies approximately as the inverse of particle density over frequency or momentum. It is highest at the high-momentum end, so as to remove the freshly stacked particles in time to make room for the next pre-cooled beam. It then decreases until, in the high-density plateau, it just balances intra-beam scattering.

Particle density varies by a factor $\sim 10^4$ and therefore the gain has to vary by a similar factor. This can not be achieved with filters alone.

The solution was to split stack momentum cooling into 3 sub-systems, so that within each the gain variation is much smaller. Each sub-system has its own pick-ups with strongly position-dependent sensitivity, which provides part of the gain variation.

There is one "low frequency" system, working in the range from 150 to 500 MHz, that covers the top of the stack (fast removal). Another "low frequency" system covers the high-momentum tail of the stack. Both have pick-ups and kickers of the loop-coupler type and coaxial line filters. The third, "high frequency", system cools the high-density part of the stack and compensates intra-beam scattering. It works in the range from 1 to 2 GHz, has a slotted-structure pick-up and kicker and no filter.

Extraction

After about a day of cooling and stacking, the nominal 6 x 10^{11} $\bar{p}$

should be contained in the flat, high-density part of the stack, $3^{o}/_{oo}$ wide in $\Delta p/p$. Another 4×10^{11} $\bar{p}$ are contained in the low-and high-energy tails of the stack, making a total of 10^{12} $\bar{p}$.

It is only the high-density part that is extracted. One creates a small rf-bucket within the stack, of a size to contain 1/12 of the useful 6×10^{11} $\bar{p}$. Then one accelerates to the ejection orbit, which is the same as the injection orbit. Mono-turn ejection sends the batch of $\bar{p}$ towards the PS, for acceleration to 26 GeV/c and transfer to the SPS.

This process is repeated 12 times at 2.6 sec intervals. The high-density part of the stack has then disappeared, leaving 4×10^{11} low-density $\bar{p}$, and a new accumulation cycle starts.

Beam diagnostics

Observation of beam properties and behaviour during the complicated sequences of processes will be essential for the development of the AA to the desired performance. Because of the particular interest to LEAR, we list the main items:

Scintillator screens in the injection and ejection lines are used for beam guidance, also onto the $\bar{p}$ production target.

Fast beam transformers monitor intensity and transmission in the injection and ejection lines.

A dc beam transformer of very high resolution ($\pm$ 1μA) measures the circulating beam intensity.

The closed orbit is measured with electrostatic pick-ups, 12 for each plane.

Measurement of Q, the betatron tune, is performed by exciting transverse coherent oscillations (small kicker) and measuring their frequencies.

With moveable scrapers, beam size and amplitude distribution are measured in a destructive way.

Signals from the Schottky-noise pick-ups of the cooling systems deliver a wealth of information: Δf, Δp, Q, ΔQ, rms-betatron amplitudes.

A non-destructive profile monitor may be added later on.

Timetable

Civil engineering work is well on the way and all main components are on order. Construction should essentially be terminated in June 1980.

In July 1980, running-in begins with tests of the target/horn assembly ($\bar{p}$ yield) and exploration of the AA with 3.5 GeV/c protons. After a 2-month shut-down, we should develop, towards the end of 1980, the cooling and stacking procedures. Early in 1981, we expect to send the first $\bar{p}$ to the PS and a few months later they will also be transferred to the ISR and the SPS.

In the context of the present Workshop, some words of caution may be in order.

Firstly, the nominal performance figures for the AA should be regarded as an ultimate goal. With the many novel techniques that are involved, it may take a considerable amount of development to reach them.

Secondly, the AA was originally conceived as part of an experiment. Since then, the experimental programme based on $\bar{p}$ has expanded considerably and, as we see at this Workshop, is still expanding. It may also take some time of operational consolidation until one reaches the high degree of reliability that the users have come to expect from the CERN accelerators.

Acknowledgements

The project described in this report is the work of a large number of people in the several CERN-Divisions involved in the $p\bar{p}$ project.

R. Billinge has read the manuscript and suggested a number of improvements.

References

1. Design Study of a Proton-Antiproton Colliding Beam Facility, CERN/PS/AA/78-3, 1978, and references quoted there.
2. R. Billinge and M. C. Crowley-Milling. The CERN Proton-Antiproton Colliding Beam Facilities. Int. Conf. on Particle Accelerators, San Francisco, March 1979 (also: CERN/PS/AA/79-17, 1979), and references quoted there.

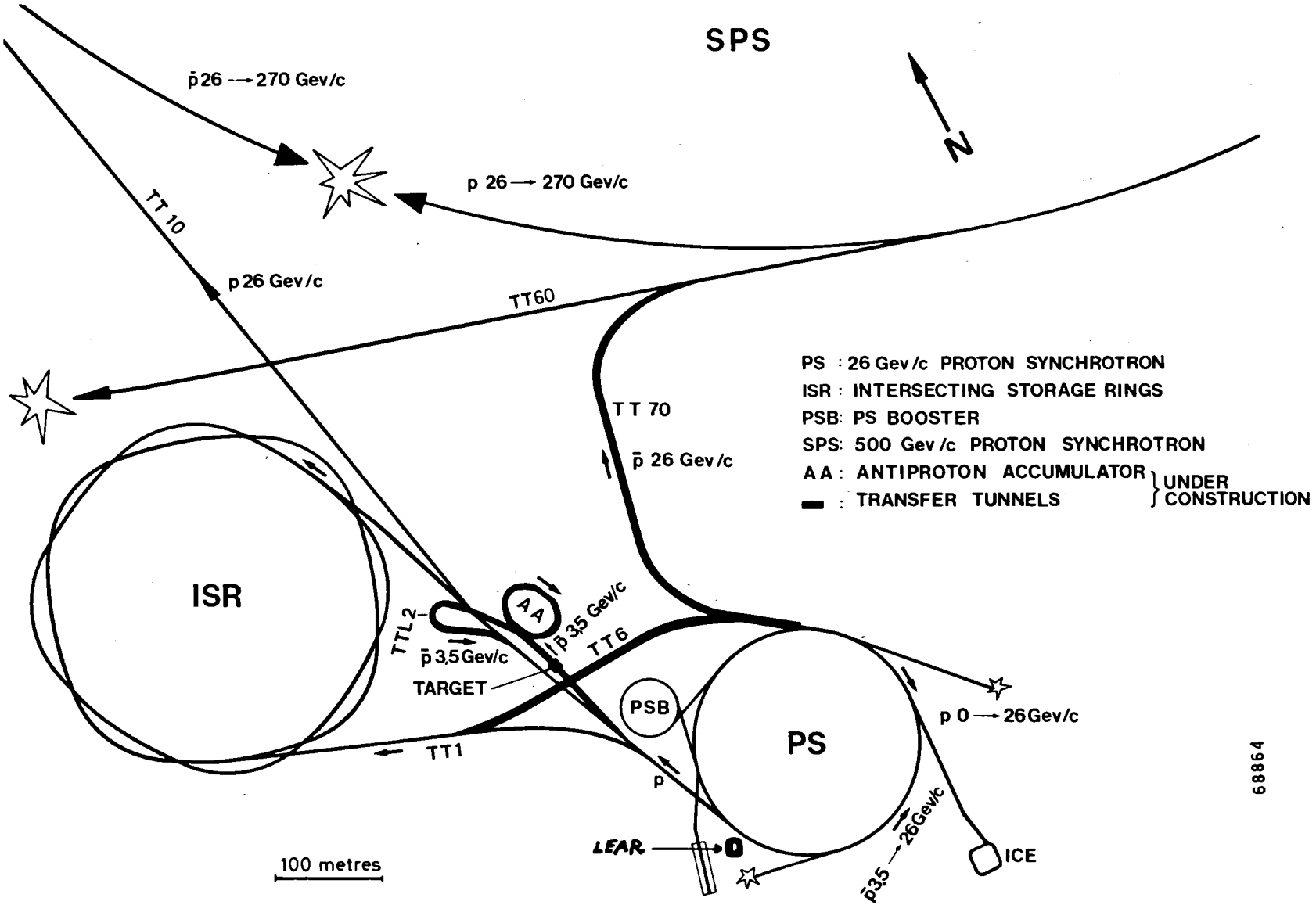

FIG. 1 OVERALL SITE LAYOUT

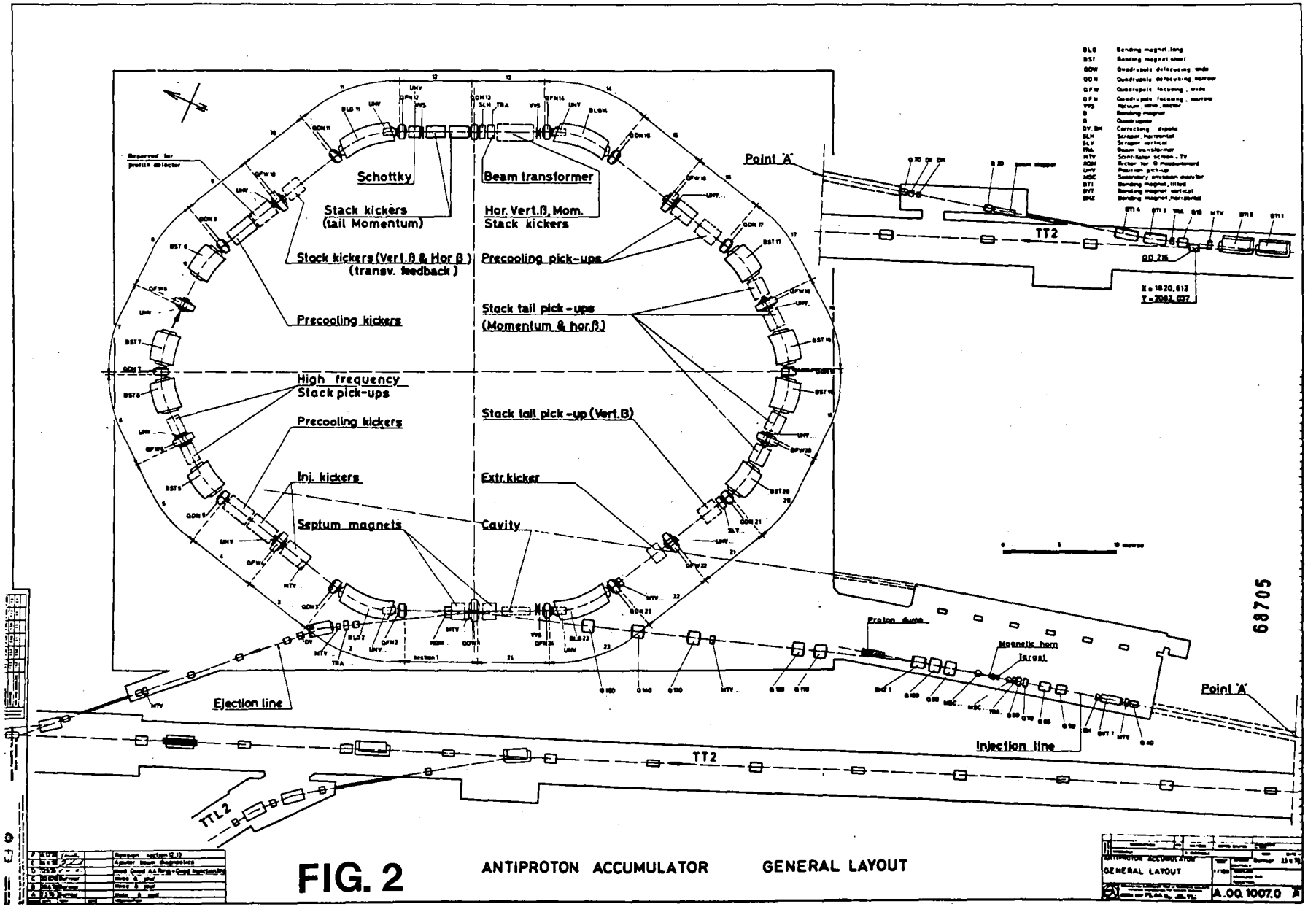

FIG. 2 ANTIPROTON ACCUMULATOR GENERAL LAYOUT

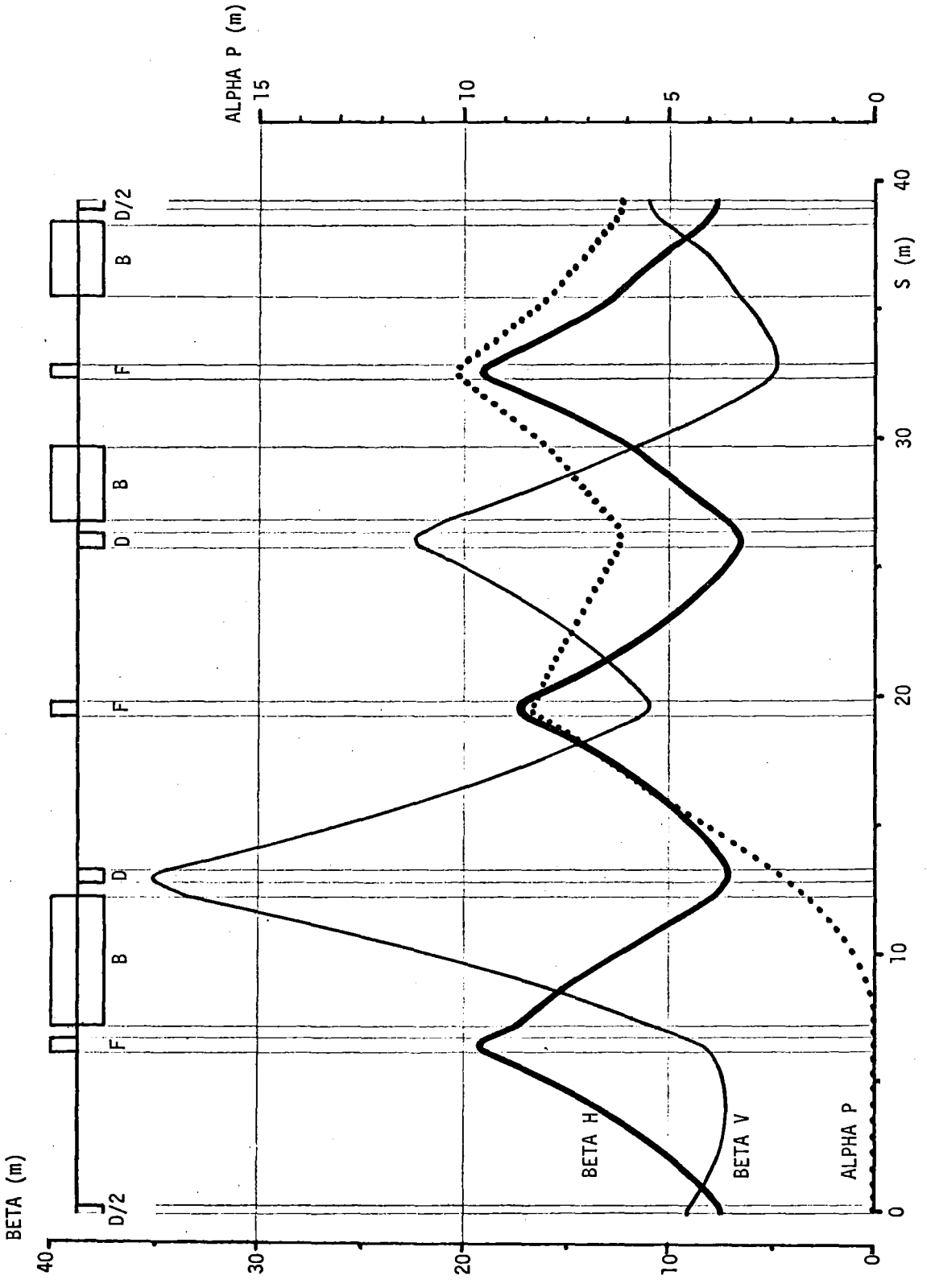
BETA (m)
ALPHA P (m)
S (m)
BETA H
BETA V
ALPHA P
D/2
F
B
D
F
B
D
F
B
D/2
0
10
20
30
40
5
15
0
10
20
30
40

FIG. 3

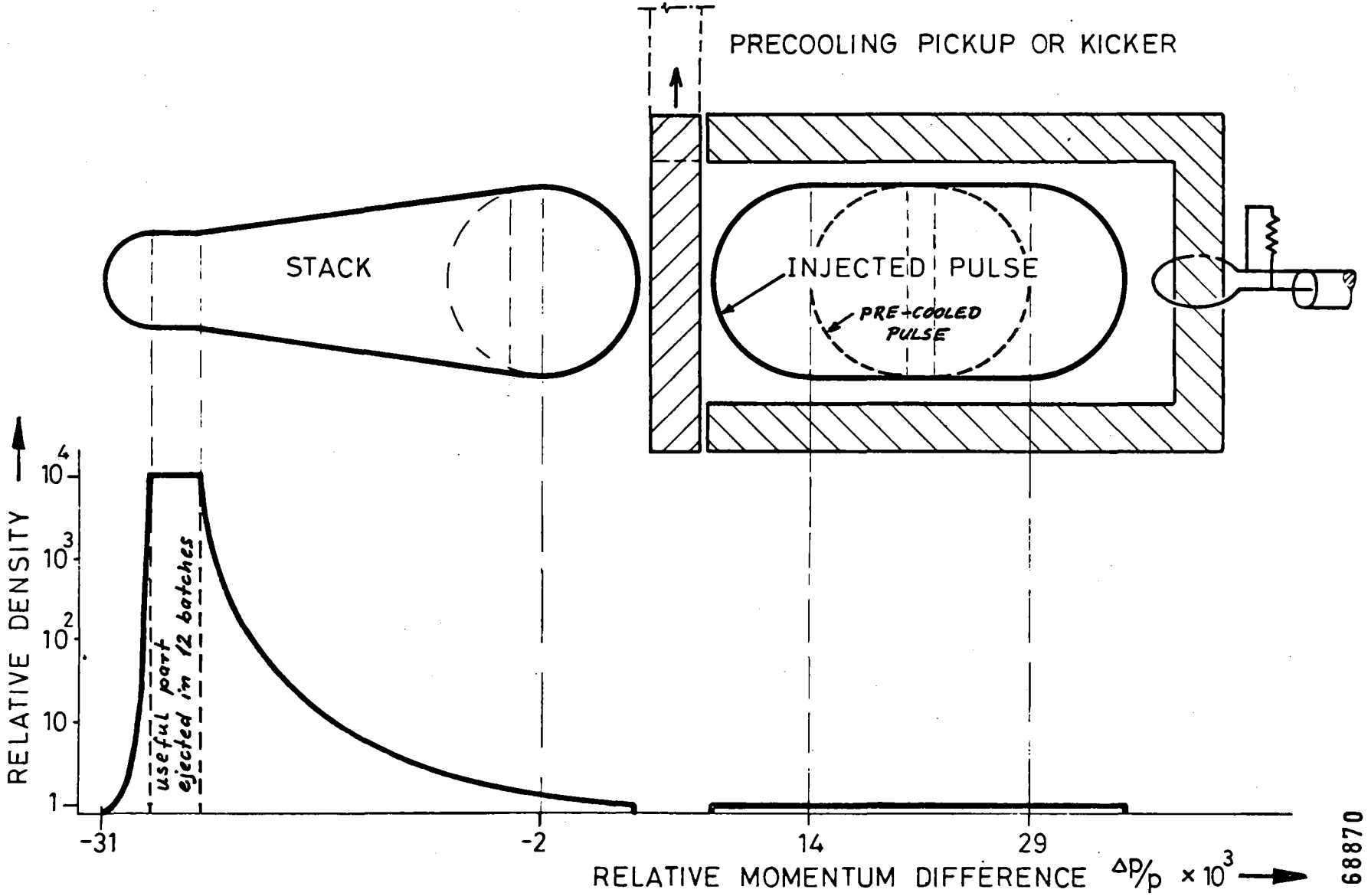

FIG.4 SCHEMATIC CROSS SECTION IN COOLING RING

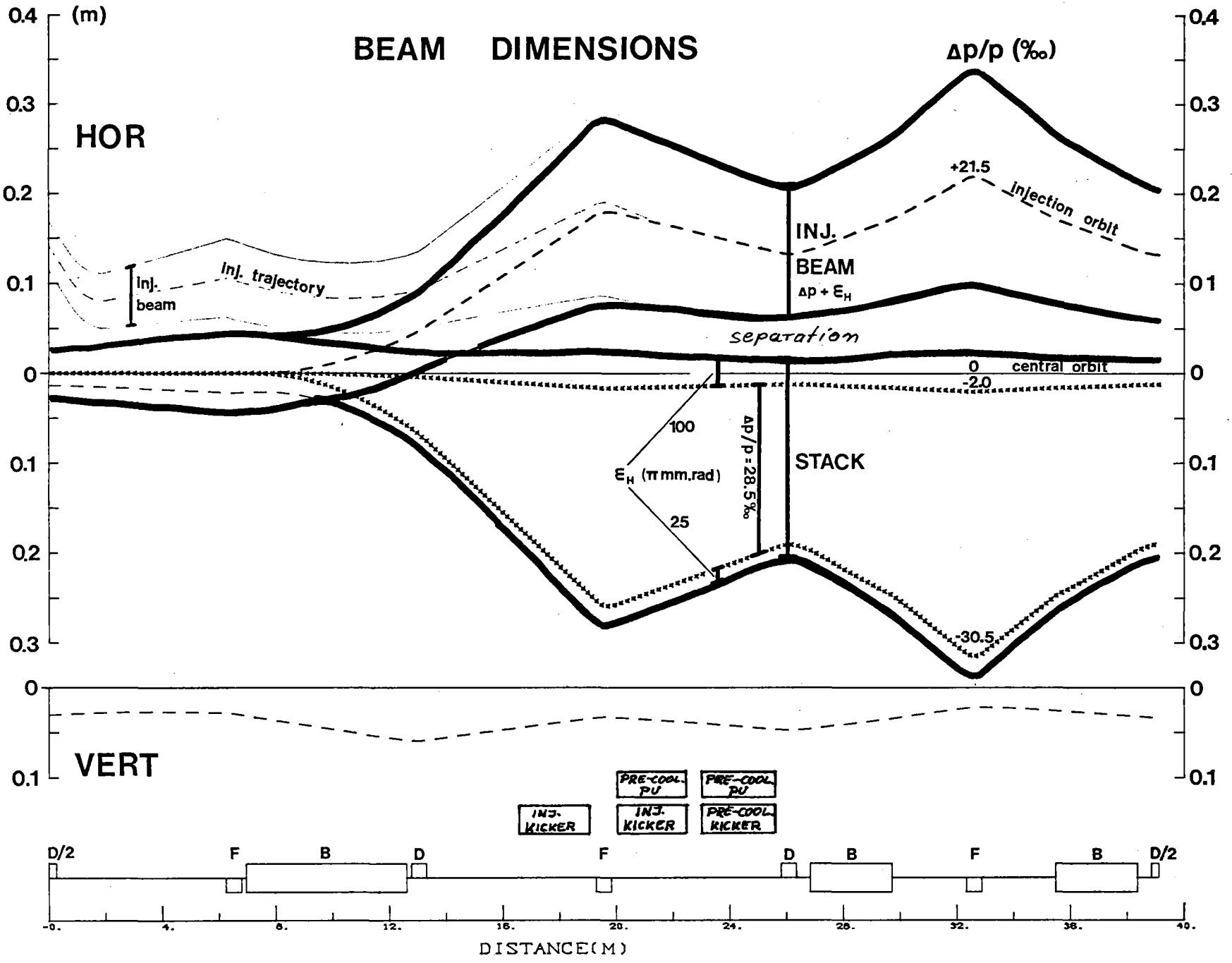
BEAM DIMENSIONS
(m)
Δp/p (‰)
HOR
VERT
Inj. beam
Inj. trajectory
+21.5
injection orbit
INJ. BEAM
Δp + ε_H
separation
0 central orbit
-2.0
-30.5
100
ε_H (π mm.rad)
25
Δp/p = 28.5‰
STACK
PRE-COOL. PU
PRE-COOL. PU
INJ. KICKER
INJ. KICKER
PRE-COOL. KICKER
D/2
F
B
D
F
D
B
F
B
D/2
DISTANCE(M)

FIG. 5

PS/AA/Note 79-3
LEAR Note 53

BEAM DIAGNOSTICS FOR LEAR*

H. Koziol
CERN, Geneva, Switzerland

It may appear premature to elaborate a set of beam diagnostic devices at a time when the machine itself is not yet well defined; however, there are several diagnostic devices that will be needed, whatever the final machine design may look like. It is preferable to include their space and other requirements from the beginning.

There are other devices, of which necessity and validity have to be assessed as machine design and definition of operational modes are progressing.

It pays off not to be stingy with beam diagnostics and to equip a new machine adequately from the beginning. This is particularly true for a machine as complicated and rich in operational modes as LEAR promises to be.

Based on experience with ICE, the experimental cooling ring, and with the AA (at least in its design stage), the following beam diagnostic systems are proposed, with an asterisk for those that are considered indispensable:

*	Scintillator screens & TV	: beam guidance
	beam loss monitors	: machine debugging
*	beam transformer	: circulating intensity
*	position pick-up electrodes	: closed orbit, Q
	Q-measurement	: Q, chromaticity
*	scrapers	: beam size, amplitude distribution
	non-destructive profile monitor	: beam size, density distribution
*	Schottky-noise pick-up	: Δf, Δp, Q, ΔQ, rms-amplitude
	directive couplers	: separate p and $\bar{p}$ intensity

As in the two aforementioned machines, a general difficulty in LEAR is the very low intensity, as compared to conventional accelerators and storage rings. Quite some development for low intensities has, however, been made for ICE and is being continued for the AA. One can thus be fairly confident that all of the above systems can be made to function satisfactorily at the foreseen LEAR beam intensities.

One by one, they shall now be presented and discussed in a projection-sheet style.

---

* Talk given at the "Workshop on Physics with Cooled Low Energy Antiprotons". Kernforschungszentrum Karlsruhe, 19-21 March, 1979.

SCINTILLATOR SCREENS + TV

Beam guidance at injection (position and approximate size).
Simple, cheap, reliable.

Mechanical insertion into beam path under 45°.
Observation with TV-camera.

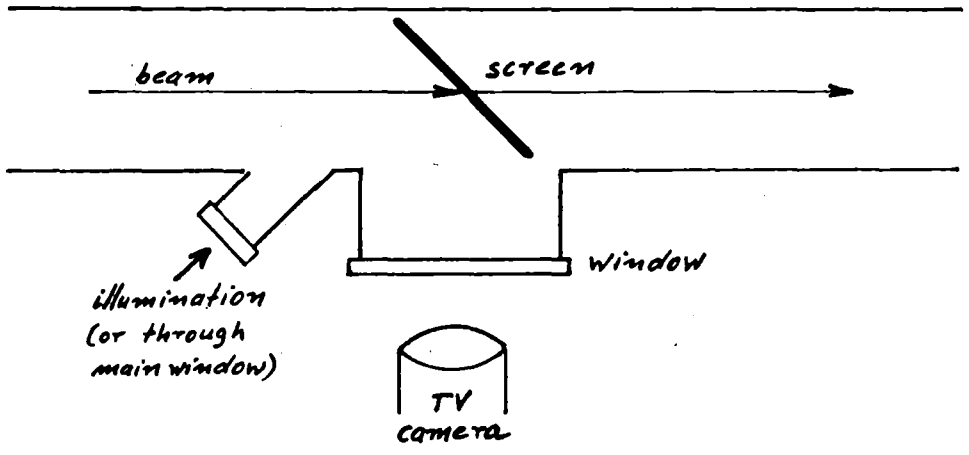

Material

ZnS + glue on metal plate: Lifetime $\sim 10^{16}$ p/cm² at min. dE/dx.
Not acceptable in good vacuum.

Preferred: Alumina (Al_2O_3), Cr-doped, red light.
Lifetime $> 10^{19}$ p/cm² at min dE/dx.

Sensitivity at min. dE/dx:

10^{10} p/cm²	standard PS camera
$5 * 10^8$	special Vidicon
$2 * 10^7$	+ cheap image intensifier

Strategic locations

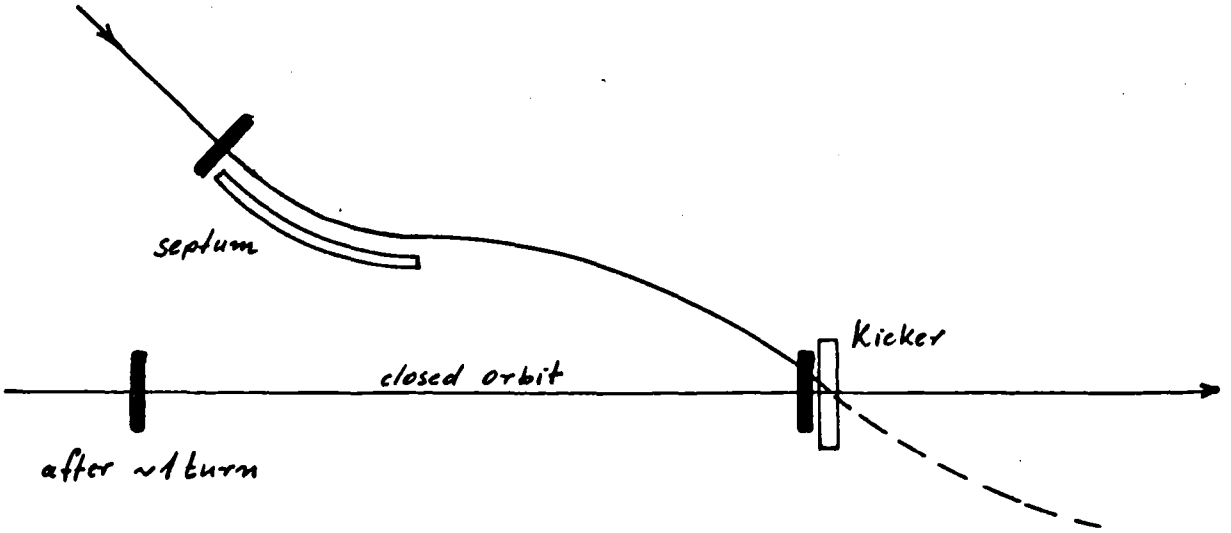

BEAM LOSS MONITORS

Valuable in debugging the machine, e.g.:

timing faults (BLM has time resolution of a few msec)
hardware faults like closed valve, wrong polarity, etc.
(loss location to ~ 1 or 2 m).

Ad hoc calibration by controlled loss.
Very sensitive + range of ~5 orders of magnitude by varying HV.

E.g. FNAL design, also on CPS-Booster.

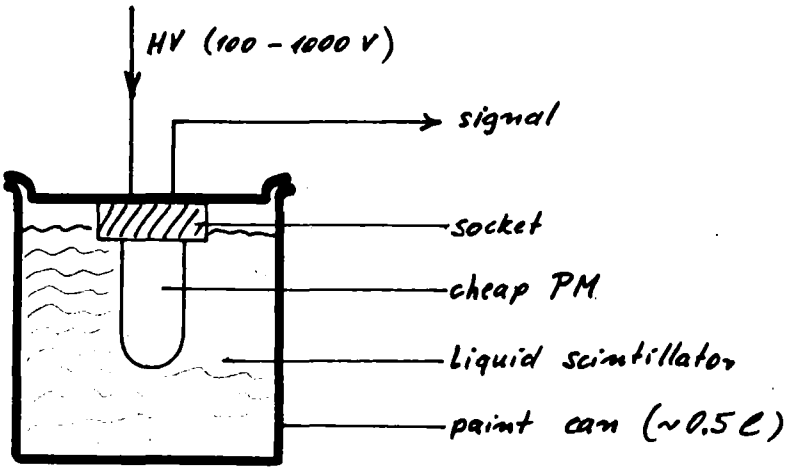

cost:

100 Fr/BLM

Several BLM's in strategic locations.
Observe signals on oscilloscope.

BEAM TRANSFORMERS

1. Fast BT bandwidth easily ≥ 100 MHz

Observation of injected beam and bunch-shapes in ring.
Probably very difficult at 10^9 p, 10^{11} probably OK.

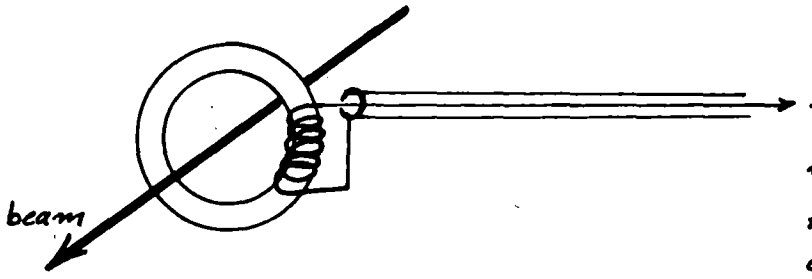

may be integrated to obtain low frequency components (0.01 Hz)

2. DC-BT as developed for ISR

For true dc-performance, use magnetic amplifier.

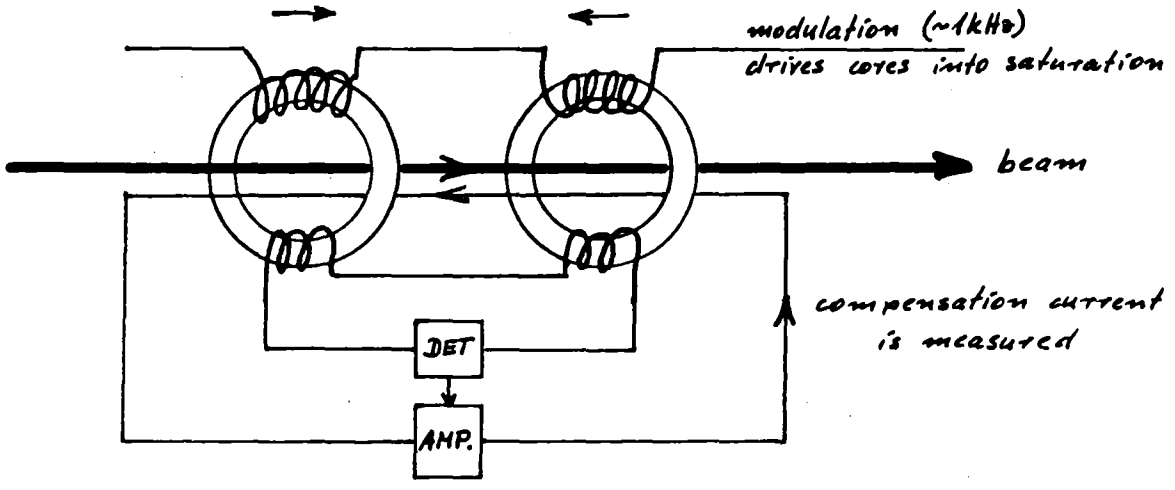

Resolution, with ~2 sec averaging:

50 μA on ISR (original)
6 μA on ICE
1 μA on AA (hoped for)

1 μA in LEAR at 100 MeV/c : 1.2×10^7 p
at 1700 MeV/c : 1.1×10^6 p

POSITION PICK-UP ELECTRODES

Look at bunched beams with conventional electrostatic PU's:

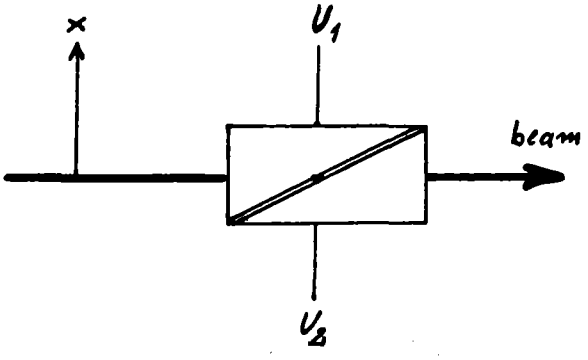

$$X = \text{const}\,\frac{U_1 - U_2}{U_1 + U_2}$$

With low intensity, as in LEAR; head-amplifier with high input-impedance, directly on chamber.

10^9 p: signal/noise good for ~1mm resolution.
bandwidth: ~30 MHz.

Number of PUs

For adequate closed orbit measurement in view of correction:

~3.5 PU/λ_β. Max. Q in LEAR is 2.75 → 9 PUs.

Location

regular distribution in lattice → 8 PUs each plane
avoid waste of straight section space → PU inside quad or bend
regular spacing in betatron phase
close to critical points

These requirements are conflicting. Select compromise when lattice final.

Signal treatment

All degrees of sophistication possible:

- from observation on oscilloscope + pocket-calculator
- to automatic gating, integration, acquisition, treatment and display of closed orbit on screen.

Q-MEASUREMENT

When the beam performs coherent transverse oscillations, the signals from the individual PU electrodes (V_1 or V_2) or their difference ($V_1 - V_2$) contain the frequencies

$$f_m = (m \pm Q) f_{rev}$$

Measure f_m and f_{rev}. m must be known from lattice.

1. Pedestrian's way, no special equipment needed.
Produce coherent oscillations by misadjusting injection.
Observe PU signals on oscilloscope. Envelope is lowest f_m

Determine f_m/f_{rev} by counting

over, say, 50 or 100 revolutions.
Resolution: $\sim \pm 0.001$

2. Excitation of coherent oscillations with special Q-kicker or pulsing injection kicker with reduced amplitude.

Determine envelope frequencies with filters and counters or by Fourier-analysis of PU signal sampled every revolution.

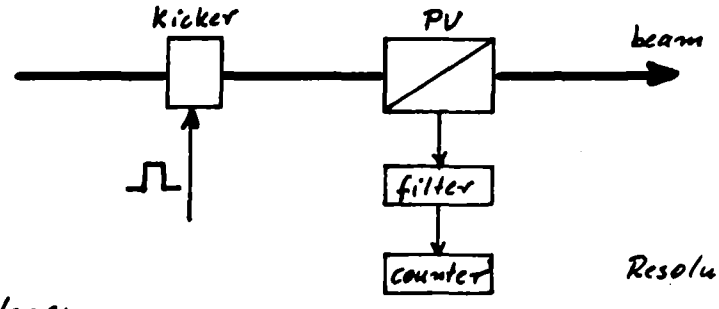

Resolution: $\sim \pm 0.001$

Advantage:
Can be done at any moment, repetitively, at momenta different from injection momentum.

SCRAPERS

Simple and reliable way to measure beam size (emittance) and amplitude distribution.
Disadvantage: destructive.

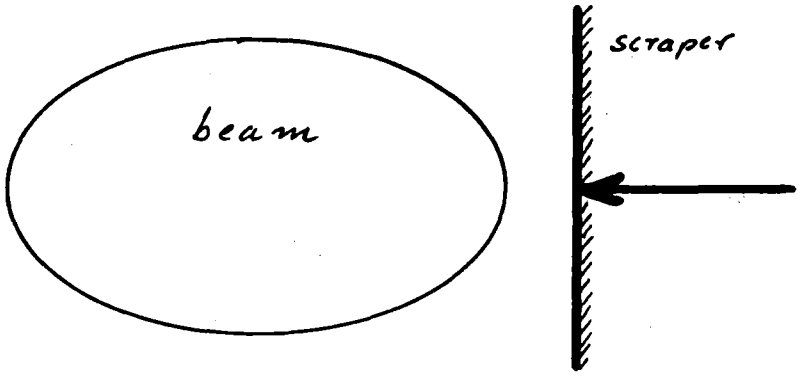

with beam transformer, measure remaining intensity as function of scraper position x

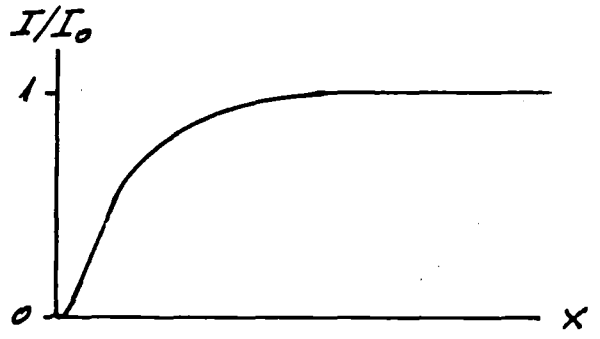

differentiate to obtain amplitude distribution

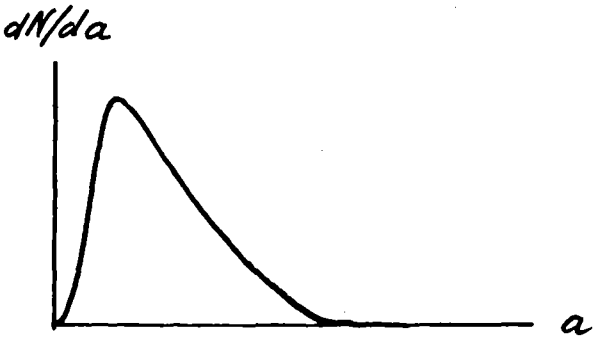

2 scrapers : 1 hor. + 1 vert.

To measure amplitude distribution : put hor. scraper where $\alpha_p / \sqrt{\beta_H}$ is small.

In the case of LEAR, it is better to move the scraper rather than to displace the beam (localized closed orbit distortion needs 2 or 3 dipoles).

NON-DESTRUCTIVE PROFILE MONITOR

advantages: non-destructive, fast, repetitive, convenient in use

disadvantages: complicated, expensive, needs a lot of space, may perturb beam

All available types use electrons from ionization by beam of residual gas or "gas curtain".

eg. Vosički-Stefanini profile detector on ICE:

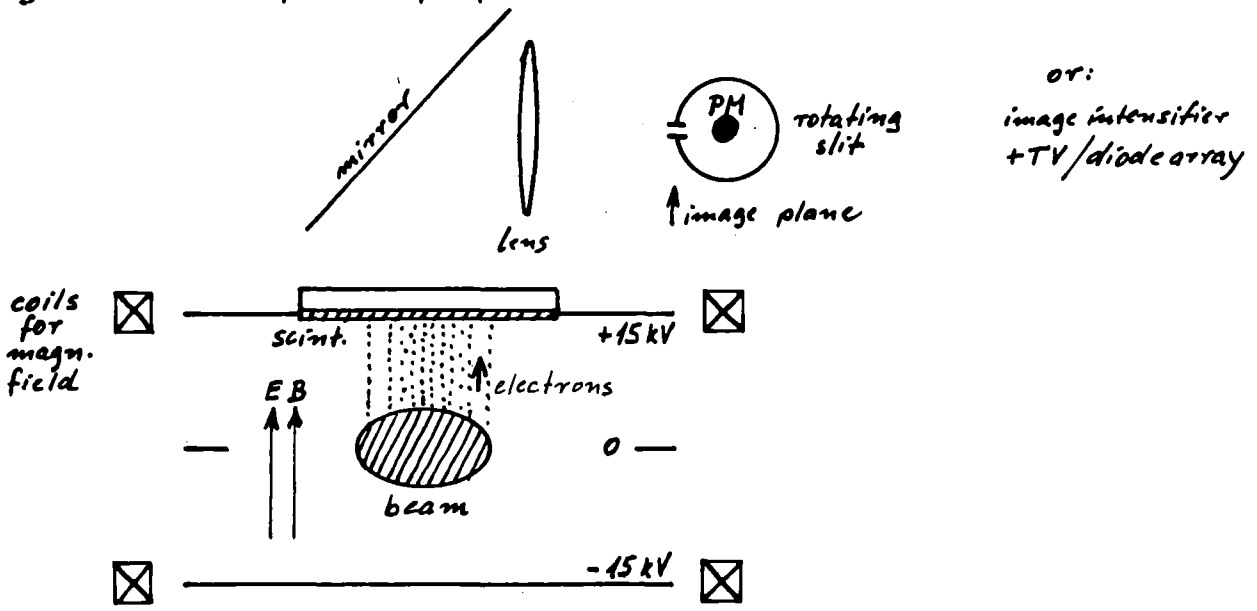

Electrons are extracted by electric field and focussed by magnetic field in same direction. They impinge on scintillator ("phosphor"), thin layer on quartz-plate, aluminized. This constitutes 1st stage of amplification. Observe light with image-intensifier tube or with PM behind rotating slit in image plane (ICE).

Typical example for ICE for good quality profile (good statistics):

$3 * 10^{-9}$ Torr $5 * 10^{8}$ p scan time: 200 msec

Scaling to LEAR (also around min. dE/dx, ~same circumference):

10^{-11} Torr 10^{9} $\bar{p}$ scan time: 30 sec

A scan time as long as 30 sec is a problem (background, e.g.). Non-destructive profile monitor needs higher gas pressure and/or higher intensity (collider mode).

SCHOTTKY-NOISE PICK-UP

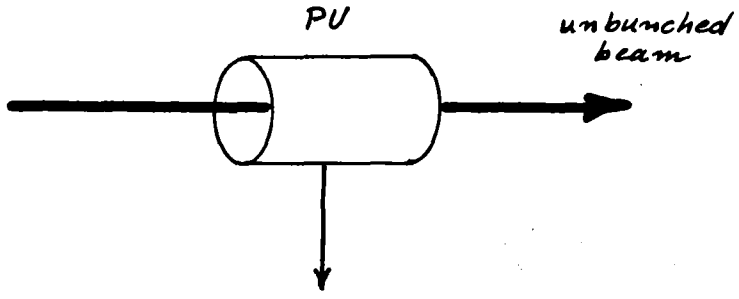

PU:
in practice use more sophisticated design:
loop-couplers, resonant PUs, etc.

signal contains all harmonics of f_{rev}

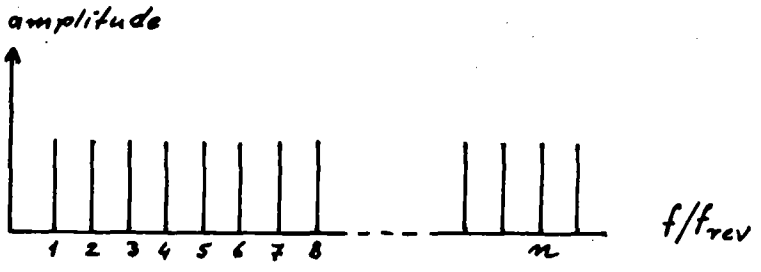

look at harmonic n with frequency analyzer: $\longrightarrow \Delta f_{rev}$

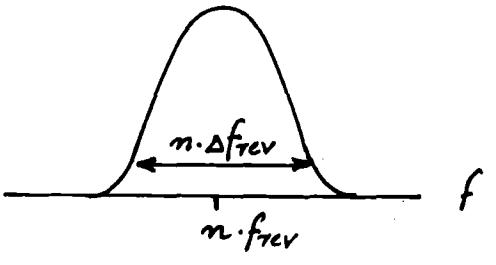

from Δf we obtain momentum spread:

$$\frac{\Delta p}{p} = \frac{1}{|\eta|} \cdot \frac{\Delta f}{f} \qquad \eta = \frac{1}{\gamma^2} - \frac{1}{\gamma_{tr}^2}$$

From area under above curve and electronics noise level, one can also obtain beam intensity (interesting at intensities below resolution of dc-beam transformer).

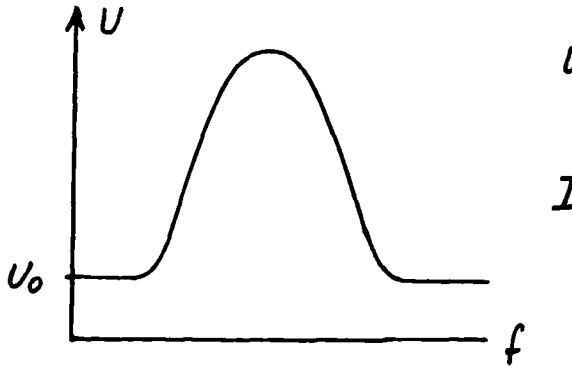

U_0 : intrinsic noise level, present without beam

$$I = \text{const} * \int_f (U^2 - U_0^2)\, df$$

calibration with BT at high intensity

By using position-sensitive PU one obtains in a similar way:
Q, ΔQ, rms-betatron amplitude.

DIRECTIVE COUPLERS

In $p\bar{p}$ storage + collider mode, beam transformer sees only sum of intensities, $I_p + I_{\bar{p}}$.

When p and $\bar{p}$ beam are bunched, directive couplers can see p and $\bar{p}$ bunches separately:

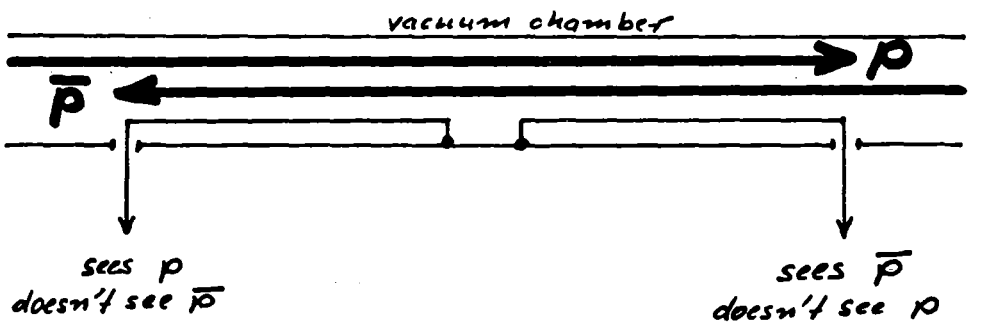

When beams are unbunched, analyze Schottky-noise from the 2 directive couplers.

Separation in case of $\bar{p} + H^-$ mode : not possible.
Look at typical decay of beam intensity with each type of particles separately.
Measure, with BT, 2-step intensity build-up with successive injection of H^- and $\bar{p}$ and assume that each constituent decays as before separately.

LEAR Note 64
PS/DL/Note 79-4
19.4.1979

SLOW EXTRACTION FROM LEAR

W. Hardt
CERN, Geneva, Switzerland

Presented at the $\bar{p}$ Workshop in Karlsruhe
(19-21.3.1979)

Introduction

Experience with slow extraction exists for many years.

Example of CERN PS :

- 1963 : first tests with integer resonant extraction
- since 1971 : third integer resonance extraction with spill time t_s of $\sim .3$ s.

At other synchrotrons t_s is also of the order of 1 s. With LEAR one would like to obtain $t_s \approx 10^3$ s.

As the number of particles N in the stretcher mode is $N \simeq 10^9$ and the revolution time $\frac{1}{f_{rev}} \simeq 1$ μs, that means to extract about 1 particle per revolution. There is hope to reduce the sensitivity of the spill modulation versus magnetic ripple by stochastic extraction [1].

Picture in horizontal phase space

Take normalized co-ordinates $Z = X + iP$ so that trajectories for linear machine elements (bends and quads only) become circles. As an example, consider third order resonant extraction for a slice of particles of the same momentum. In lowest order (ε^1) for the non-linear element - a sextupole specified by $\Delta P = SX^2$ - the change of Z over three revolutions can be written

$$\Delta Z = - i\varepsilon Z + i \exp(i\mu) \cdot \frac{3}{4} S \overline{Z^2} \qquad (1)$$

where $\begin{cases} \varepsilon = 3 \cdot 2\pi \left(Q - \frac{m}{3}\right) \text{ ; } Q = \text{tune for zero amplitude particles} \\ \mu = \text{phase distance of selected azimuth from the sextupole.} \end{cases}$

Of particular interest are azimuthal places with $i \exp i\mu = 1$. To them belong the fixed points $Z_{fp} = Z_K$

$$Z_K = \frac{4\varepsilon}{3S} \exp i \left(\frac{\pi}{2} + \frac{2K}{3}\right) \text{ ; } K = 0, 1, 2$$

There the equation of motion (1) can be obtained from the Hamiltonian

$$H = \frac{\varepsilon}{2}\left(X^2 + P^2\right) + \frac{S}{4}\left(3X^2 - P^2\right)P$$

At the fixed points we find $H_{fp} = \left(\frac{2\varepsilon}{3}\right)^3 S^{-2}$ and we can factorize

$$H = H_{fp} - \frac{S}{4}\left(P + \frac{2\varepsilon}{3S}\right)\left(P - \frac{4\varepsilon}{3S} + \sqrt{3}\,X\right)\left(P - \frac{4\varepsilon}{3S} - \sqrt{3}\,X\right)$$

showing that the separatrices are straight lines in this approximation

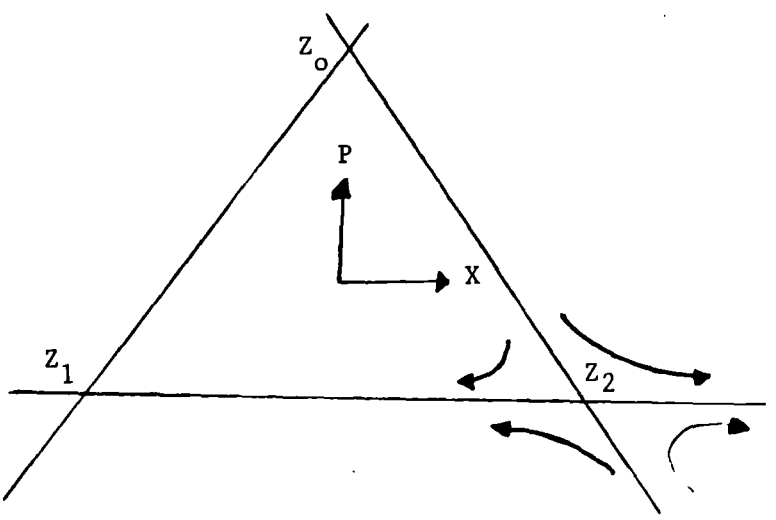

Fig. 1

In full beauty the separatrices become curved with increasing sextupole strength S so that the effective jump size and hence the extraction efficiency will have a maximum. The best jump size might be chosen smaller as it determines one factor of the emittance of the extracted beam. The other

factor is the distance in P direction between full and vanishing emittance, being proportional to the square root of the horizontal emittance.

The ideal ejection requires that the stable area shrinks monotonically squeezing particles onto the outgoing separatrices where they move outward with increasing jumps as can be seen from

$$\Delta Z = \Delta X = \left(X^2 - X_2^2\right) \cdot \frac{3}{4} S$$

by putting $Z = X + i P_2$ into (1) : $X_2 = \frac{2\varepsilon}{\sqrt{3}\, S}$; $P_2 = - \frac{2\varepsilon}{3S}$

The vertical emittance remains unaffected ideally, but the dynamics in momentum space deserve attention.

Picture in momentum space

We now consider a beam with a finite width in momentum space. Typically, prior to ejection, the beam is brought to the inner side of the design orbit whose Q value is tuned to the resonance. Then the beam is swept slowly to the outside, i.e. accross the resonance by one of the following processes :

i) a field decrease (conventional extraction from CPS),

ii) betatron acceleration by an induction core (possible for LEAR with reasonably small core),

iii) a diffusion process as proposed in [1].

Forgetting the details in horizontal betatron phase space, we can consider the resonance value x = 0 as a sink in Q-space. Let

$$x = (Q - Q_{res}) \text{ sign } \xi \simeq Q_{res} \, |\xi| \, \frac{p - p_{res}}{p} \; ; \; \xi = \text{chromaticity}$$

$\psi = \frac{\partial N}{\partial x}$: the particle density

$\phi = \frac{\partial N}{dt}$: the spill rate

ΔQ : beam width in Q-space

$v_s = \Delta Q / t_s$: average sweeping speed.

A constant spill rate requires a speed

$$v = \frac{N}{t_s}\frac{1}{\psi} \simeq v_s \quad \text{for} \quad \psi = \frac{N}{\Delta Q}$$

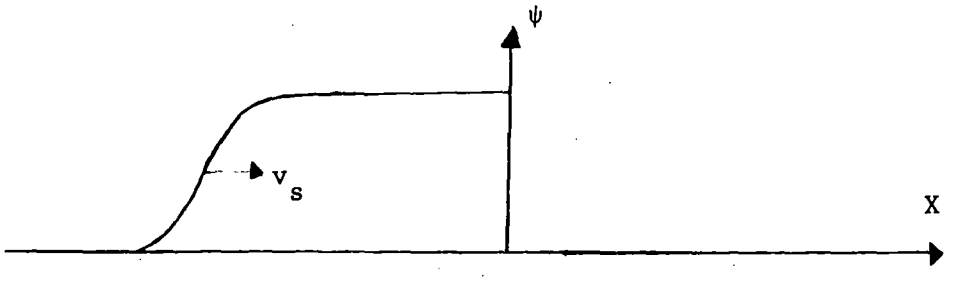

Fig. 2

The real instantaneous v will jitter around the average value v_s due to unavoidable magnetic ripple. If the (angular) ripple frequency is ω and the (small) ripple amplitude is δQ, the spill rate will be modulated with an amplitude

$$\frac{\delta\phi}{\phi} \simeq \frac{\delta Q\ \omega}{v_s}$$

The effective spill time will no longer be t_s but

$$t_{eff} = \frac{\left(\int \phi\ dt\right)^2}{\int \phi^2\ dt} \leq t_s$$

Several uncorrelated ripples yield

$$\frac{t_s}{t_{eff}} = 1 + \frac{t_s^2}{2} \sum_m \left(\frac{\omega_m\ \delta Q_m}{\Delta Q}\right)^2$$

imposing severe tolerances on the ripple amplitudes δQ_m. There are limitations on controlling the Q value. Servoing the spill is only possible for low ω_m as there is a considerable delay in the extraction mechanism. Fortunately very high ω_m are not important due to the inherent spread of extraction time for particles with different initial conditions in betatron space.

But when aiming at $t_s \simeq 10^3$ s something significantly better ought to be done compared to the conventional method. This could be method iii) or a combination of iii) and i) or ii).

Diffusion in a limited region of Q space (equivalent to frequency space) can be achieved by generating a noisy band around at least one harmonic of the particle revolution frequency. The particle density with diffusion D(x) is described by

$$\frac{\partial \psi}{\partial t} = \frac{\partial}{\partial x}\left(D\,\frac{\partial \psi}{\partial x} - v_s \psi\right) = -\frac{\partial \phi}{\partial x} \qquad (2)$$

If the resonance is not crossed too fast, the $x = 0$ value still acts as a sink for ψ but the beam modulation is less sensitive to the versus ripple. Analysis of eq.(2) shows that the ripple amplitude is allowed to be larger by the improvement factor

$$F = \frac{v_\omega}{\sqrt{2}\, v_s}$$

where $v_\omega = \sqrt{2D\omega}$ = phase velocity of the diffusion waves. It should be sufficient to make $D \neq 0$ only over a fraction of the initial beam width and in that region we might achieve a stationary distribution.

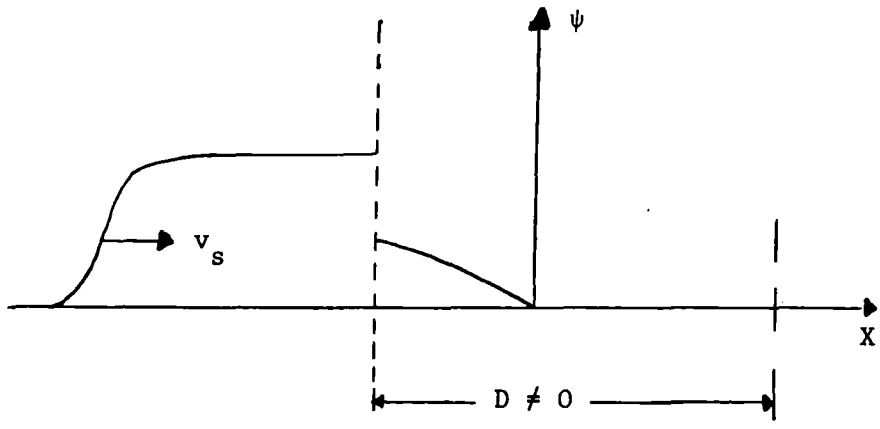

Fig. 3

At present, attemps are made to try the method at the CPS (at 10 GeV/c with $t_s \simeq 1.5$ s) since one can argue that the noise applied externally is only a rough description of a true diffusion which would lead to a random walk of individual particles instead of groups of particles.

In addition, another scheme, based on repetitive unstacking, will be described in LEAR Note 65.

Reference

1) S. van der Meer, Stochastic Extraction - A low ripple version of resonant extraction, CERN/PS/AA 78-6, March 1, 1978.

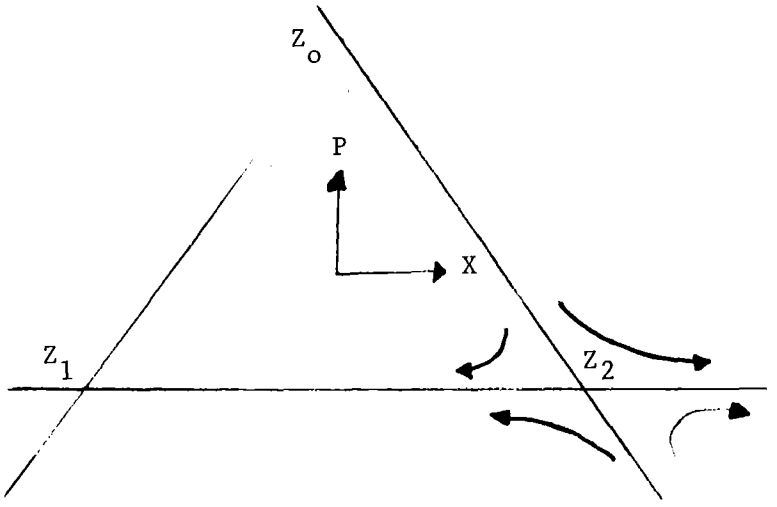

Fig. 1

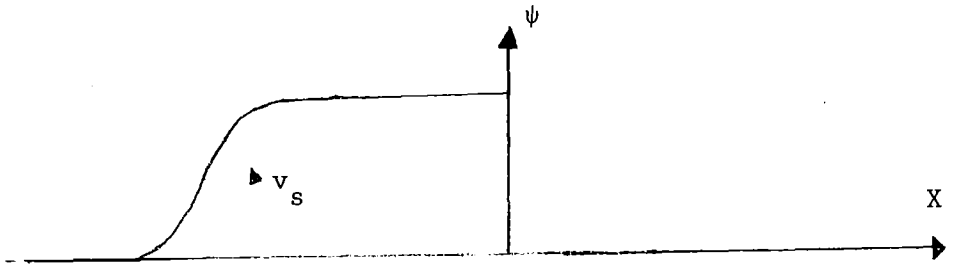

Fig. 2

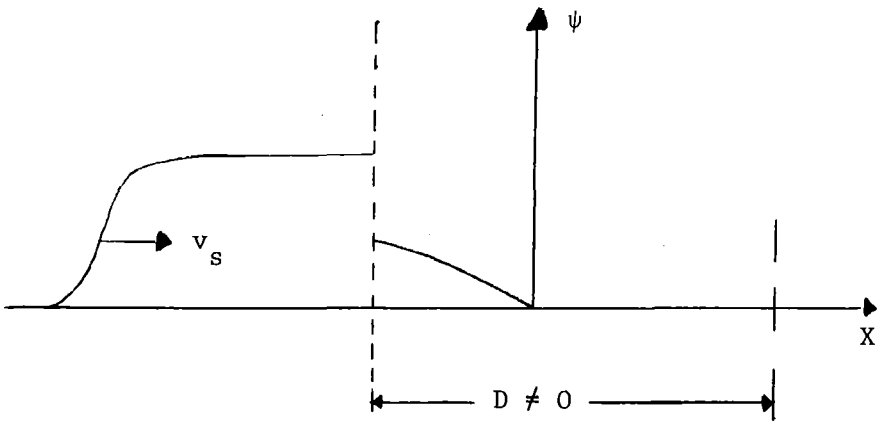

Fig. 3

$\bar{p}$ LEAR Note 61

$\bar{N}N$ ANNIHILATION AT LEAR

M.A. Schneegans*)
LAPP Annecy-le-Vieux, France

1. INTRODUCTION

I will try to summarize some proposals and ideas for possible experiments at the Low-Energy Antiproton Ring (LEAR) which were discussed at this Workshop, and to show what can be learned about $\bar{N}N$ annihilation. The limits of this field are difficult to set since it clearly overlaps with other subjects which will be covered by various speakers in their summary talks; in particular: baryonium resonances (*B. Povh*)[1] and bound states (*H. Koch*)[2]; $\bar{p}A$ atoms and protonium (*E. Klempt*); and "high-energy" aspects such as charmonium, etc. (*P. Dalpiaz*)[3].

What I call "high-energy" aspects of $\bar{N}N$ annihilation start in the LEAR energy range. From this point of view, annihilation appears as the main difference between NN and $\bar{N}N$. In fact, $\bar{p}p$ data show higher multiplicities at given s, narrower multiplicity distributions at given n, and larger p_T in exclusive channels. The "high-energy" aspects include jet production and the production of heavy objects such as the charmonium family. P. Dalpiaz will report on some interesting possibilities in this field, and I will speak no more about it.

Discussions on baryonium formation and protonium clearly cannot be separated from discussions on annihilation. Before reviewing experimental possibilities at LEAR, I shall briefly mention some theoretical and experimental features of $N\bar{N}$ annihilation, following partly reviews of I.S. Shapiro[4] and T.E.O. Ericson[5].

2. SOME THEORETICAL FEATURES

$N\bar{N}$ and NN interactions differ mainly in two ways:

- $N\bar{N}$ involves a much stronger nuclear attraction;
- $N\bar{N}$ undergoes annihilation.

---

*) Visitor at CERN, Geneva, Switzerland

$N\bar{N}$ attraction

Nuclear forces are different for NN and $N\bar{N}$ but are due to exchanges of the same light bosons:

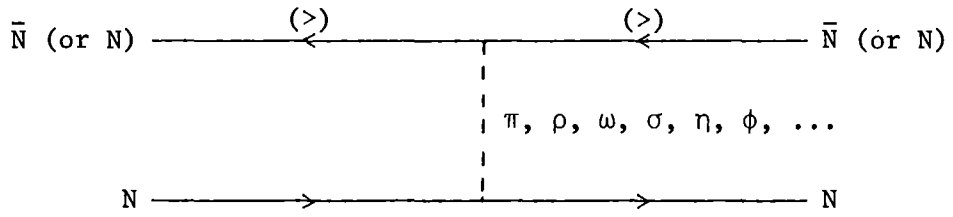

For NN, the couplings of the exchanged mesons are well known, using OBE potentials. For each boson exchange, the $N\bar{N}$ potentials must be related to the NN potentials by G parity:

$$V_{NN}(x) = (-1)^G V_{N\bar{N}}(x) \ .$$

In particular, potentials for ω exchange have opposite signs, which means that to the strong short-range NN repulsion due to ω exchange, there will correspond a strong short-range $N\bar{N}$ attraction due to the same boson exchange. This attraction makes possible the existence of several nuclear-type bound and resonant $N\bar{N}$ states, as opposed to NN, where only one loosely bound deuteron state exists, in addition to the singlet state.

Approximate solutions of the Schrödinger equation with known potentials can now be calculated and the spectra predicted. In particular, Shapiro et al. and Dover[4] made predictions using a Bryan-Phillips potential. In fact, a large number of states can be predicted between 1.7 and 7 GeV, of the types

- baryon-antibaryon (in particular hyperon-antihyperon)
- $2N\bar{N}$
- $2N2\bar{N}$

with relatively narrow width. In particular, a $2N2\bar{N}$ state is possible with a width of 20-30 MeV.

Constituent models and, in particular, various QCD models[6], also make many predictions regarding the existence, energy levels, and widths of quasi-nuclear states.

Up to now, absorption was neglected. Let us now add the effects of annihilation.

Annihilation

It is clear that annihilation of an $N\bar{N}$ pair tends to destroy the quasi-nuclear system by broadening and shifting the levels and by mixing the degenerate states.

If the annihilation was a long-range effect, we would have complete destruction of the OBEP approach.

Absorption is often treated as a perturbation (Dover, Shapiro)[4]:

$$\text{Range} \approx \frac{1}{M} \approx 0.2 \text{ fm}$$

$$\Gamma \approx v \times \sigma_{abs} \times \langle \psi^2(r) \rangle$$

(absorption rate) (average probability over volume)

Typical widths are then:

L	Γ(MeV)
0	100
1	10
2	1

Absorption can also be introduced as an additional potential: Gersten, Myrer and Thomas[4], for instance, conclude that even small depths of absorptive potential eliminate most bumps in σ. This is probably not true, since resonances have been observed. One can remark that not many have been seen up to now compared with the numerous predictions, so that some could have been rubbed out by annihilation.

The main question is: How can the large annihilation cross-sections that are observed be compatible with the existence of $N\bar{N}$ resonant states? According to Shapiro the answer is that even if shifts and broadening of the levels by annihilation cannot be calculated precisely, it can be shown that they are small, provided r_a/R is small, where r_a is the annihilation radius and R the size of the quasi-nuclear $N\bar{N}$ systems.

Annihilation at rest

A particular case is that of annihilation from the $N\bar{N}$ system at rest. Here we have annihilation from the atomic levels of the protonium ($\bar{p}p$ atom) or, more generally, of the antiprotonic atoms. For large orbits the strong nuclear interaction is negligible; we have a pure QED system.

For smaller orbits the nuclear interaction shifts and broadens the levels. The effect of absorption can be well calculated, assuming no $N\bar{N}$ resonance is present near threshold. In fact, the annihilation essentially alters the intensities of the X-rays emitted, so that measuring the yield of monochromatic X-rays, emitted when an antiproton stops in H_2 liquid or gas, can give the probability of $N\bar{N}$ annihilation from states of given L. Note that if only the annihilation products are detected, an integral width summed over all possible states in the protonium cascade can be obtained.

The presence of an $N\bar{N}$ resonance near threshold can partly modify the relative populations of the levels. On the other hand, in dense materials the Stark effect will mix near degenerate atomic states of opposite parity.

Let us conclude these generalities on $N\bar{N}$ annihilation by asking why is it so important to measure $\bar{N}N$ cross-sections and, in particular, annihilation cross-sections.

The NN forces are known from NN scattering phase-shifts and from deuteron structure. The NN scattering occurs at asymptotically large distances and the deuteron is loosely bound, so that they are both rather insensitive to the potentials. But $N\bar{N}$ has a spectrum of bound and resonant states well localized in the nuclear force region. Therefore, the energy-level spacing is very sensitive to the details of the potentials. These structures should show up in formation experiments; thus a good way to find them is to measure the energy dependence of all the cross-sections down to the lowest antiproton energy accessible.

Furthermore it is important to measure the energy dependence of the non-resonant annihilation cross-section for slow antiprotons, since a strong $N\bar{N}$ attraction should lead to a deviation of the 1/v law.

3. MAIN EXPERIMENTAL FEATURES OF σ_{annih}

- The measured annihilation cross-section is large. In fact, it is not far from the unitarity limit in each partial wave with orbital angular momentum L:

$$\frac{(2L + 1)\pi}{k^2},$$

where k is the c.m. momentum of the antiproton. This is verified between $p_{lab} \approx 0.3$ and 1 GeV/c.

- The elastic cross-section is smaller than the annihilation cross-section: $\sigma_{annih}/\sigma_{el} \approx 1.5\text{-}1.8$.

  Optical models can in general meet these two features and fit σ_{annih}.

- Resonances have been observed in certain annihilation channels and in σ_{tot}, σ_{annih}, and σ_{el}.
- Nothing is known below 300 MeV/c!
- $\sigma_{annih} = \sigma_{tot}(\bar{p}p) - \sigma_{tot}(pp)$ is not valid when we want σ_{annih} with some precision.

Figure 1 shows the situation for σ_{annih} as compiled by H. Muirhead and P.S. Gregory[7]. To obtain σ_{annih}, the subtraction method was used below 3 GeV/c:

$$\sigma_{annih} = \sigma_{tot} - (\sigma_{el} + \sigma_{inel}) .$$

Above 3 GeV/c, the fitting method was used.

It can be seen that no measurements exist below 300 MeV/c, that we have a gap between 0.6 and 1.2 GeV/c, and that even at higher energy the measurements should be improved.

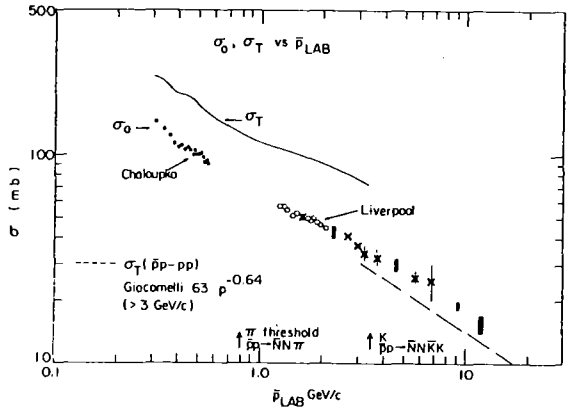

Fig. 1 Total (σ_T) and annihilation (σ_a) cross-sections for $\bar{p}p$ interactions versus antiproton laboratory momentum. The dots and open circles refer to data obtained by subtraction techniques using the curve σ_T as the basis. The crosses refer to individual contributions, the oblongs refer to estimates[7] of σ_a on several groups' data. The dashed line is a fit to the difference of total $\bar{p}p$ and pp cross-sections.

4. EXPERIMENTAL POSSIBILITIES AT LEAR

What can we expect to measure at LEAR in order to make substantial progress in $N\bar{N}$ annihilation?

We should have, at an early stage of LEAR development, an extracted beam[8,9] of any momentum down to 100 MeV/c with an intensity of the order of 10^6/s and $\Delta p/p \lesssim 10^{-3}$ if stochastic cooling is applied in LEAR, and $\Delta p/p \lesssim 10^{-5}$ if electron cooling is also available.

With such beams, the following measurements should be possible:

- Precise measurement of all cross-sections down to the lowest possible energy ($\lesssim$ 1 MeV?) with very good energy resolution and high statistics: σ_{tot}, σ_{el}, σ_{inel}, $\sigma_{ch.ex.}$, σ_{annih}, $\sigma_{annih \to all\ channels}$.
- Angular distributions in all annihilation channels in order to know the partial wave contributions. Statistics should be high even for small $d\sigma/d\Omega$.
- Polarization in all channels with a polarized jet target.
- Annihilation at rest in all channels with event-by-event X-ray signature of the atomic level concerned.
- Annihilation from baryonium states in coincidence with a transition γ-ray (and X-ray signature of the starting level).
- $\bar{p}A$ annihilation at rest and in flight.
- Annihilation in rare channels of particular interest:

$\sigma_{e^+e^-}$,	$\sigma_{Ve^+e^-}$	$\sigma_{2\pi^0}$	$\sigma_{neutrals}$
($\to$ G)	(Vector meson spectroscopy)	($\to$ p waves)	(Specific interests)

- Measurement of $\bar{n}p$ and $\bar{n}d$ cross-sections with $\bar{n}$ beams produced by anti-protons.

All these systematic studies will be done eventually, but right now we have many specific proposals for studying particular fields of physics with certain types of apparatus.

5. EXPERIMENTS PROPOSED AT LEAR

I will now review some of the possible experiments concerning $N\bar{N}$ annihilation, which have been proposed before and during the Karlsruhe workshop.

5.1 Experiments to measure cross-sections (σ_{tot}, σ_{annih}, σ_{el}, $\sigma_{ch.ex.}$) and study baryonium

- Proposal by F. Balestra et al.[10] to look for baryonic states near threshold with a streamer chamber. They will measure σ_{annih}, σ_{tot}, σ_{el} with angular distributions.
- Proposal by P. Pavlopoulos et al.[11] to look for baryonium states near threshold with a crystal ball. This study should give data on $\bar{p}p$ annihilation at rest and in flight if the apparatus is made sufficiently selective.
- Proposal by M. Macri and F. Silombra[12] to look for baryonium states and measure annihilation cross-sections at rest and in flight with a nearly 4π detector in a solenoid magnet. The detector would include drift chambers, X-ray detection, dE/dx, and TOF measurement. A field of 1 T should give a resolution for charged particles of $\Delta p/p \sim 1\%$.
- Proposal by J. Rafelski[13] to study $\bar{p}A$ annihilation in flight. Measuring all cross-sections and taking inclusive spectra into account should give good tests of the fireball model.
- Proposal by J. Bailey, U. Gastaldi and E. Klempt[14] to study annihilation of $\bar{p}p$ at rest, coincident with X-ray emission from the atomic cascade. The X-rays of a Balmer series can be used in an electronic trigger to study specific annihilation channels. Furthermore, narrow baryonium states can be looked for by detecting a transition γ-ray (to a quasi-nuclear level) in coincidence with annihilation from a 2p level (L X-ray). The set-up would consist of a cylindrical proportional chamber to detect X-rays, of drift chambers, and of a crystal ball detection system or π^0 detectors. In this way, a "complete" experiment on $\bar{p}p$ annihilation at rest can be performed.
- Proposal by U. Gastaldi[15] to measure σ_{annih}, $\sigma_{ch.ex}$ at <u>very low energy</u> with a parallel beam technique: $\bar{p}$ and p^+(or d^+) travel parallel with

δv controlled by the RF system. With such a scheme, one can reach an energy region where neither extracted beams nor jet targets may be used. The luminosity should be $L \approx 3 \times 10^{28}$ cm^{-2} s^{-1} and the annihilation rate ≈ 150 s^{-1}.

- Proposal by P. Birien and K. Kilian[16] to build a special spectrometer allowing the LEAR extracted beam to be used for measurement of some annihilation cross-sections down to very low energies ($\lesssim$ 1 MeV). Using the $\bar{n}$ production target as degrader, the antiprotons would be deflected and refocused and their time of flight measured.
- Proposal by C. Voci[17] and H. Poth[18] to make $\bar{n}$ beams with the LEAR extracted beam of antiprotons on an external production target ($N_{\bar{n}} \sim 10^3$/day in 40 μsr) or with antiprotons on an internal jet target ($N_{\bar{n}} \sim 4 \times 10^3$/day in 1 μsr). They propose to study the reactions $\bar{n}p$ and $\bar{n}d$, and to measure $\sigma_{ch.ex.}$.
- Proposal by F. Balestra et al.[19] to study $\bar{n}n(d)$ with emission of charged prongs in a streamer chamber, and to measure cross-sections.

5.2 Experiment to measure polarization in $N\bar{N}$ annihilation

P. Dalpiaz and K. Kilian[20] propose to measure polarization distributions between $\sim$ 0.3 GeV/c and $\sim$ 2 GeV/c with an atomic H polarized target in LEAR. With a density of $\rho \sim 10^{-12}$ g/cm^2, a luminosity of 10^{29} cm^{-2} s^{-1} should be reached giving the following rates:

σ_{tot} : $\approx 10^9$ interactions/day;

σ_{el} : $\sim 5 \times 10^8$ interactions/day;

σ_{annih}: into $\pi\pi$, $k\bar{k}$, $n\pi$, ...: $\sim 10^6$ interactions/day.

For σ_{el}, spin and parity should be measured when passing through a baryonium state.

The authors stress that H polarized targets will soon be operational and that the rates allow parasitic operation of LEAR at a 1% level, for instance.

5.3 Experiments on rare annihilation channels of special interest

5.3.1 Study of $\bar{p}p \to 2\pi^0$

This channel is of particular interest since parity conservation forbids it to proceed from even L-waves. A comparison of the annihilation

rate in $\pi^+\pi^-$ which can proceed from L-even or L-odd states, yields the fraction of odd-L contributing to annihilation in two pions. Recent results give a fraction (39 ± 8)% by Devons et al.[21] and (13 ± 3)% by Bassompierre et al.[22] for antiprotons annihilating at rest in liquid hydrogen. Also, $\bar{p}d$ experiments suggest a large p-wave contribution.

This can be explained in Shapiro's approach by the presence of a $\bar{N}N$ p-state near threshold. If this state is weakly bound it can have large dimensions (R ≈ 3-4 fm), and since

$$\Gamma_{na}(p) \simeq \left(\frac{R}{|ra|}\right)^5 ,$$

a relatively large $\Gamma(p)$ can be obtained.

Several proposals have already been made to study this reaction:

- Proposal by P. Pavlopoulos et al.[11] to measure $\sigma_{2\pi^0}$ at rest in a gas target inside the crystal ball.
- Proposal by P. Dalpiaz et al.[23] to measure $\sigma_{2\pi^0}$ at rest and up to LEAR maximum energy with angular distributions, using an apparatus similar to the set-up proposed for electromagnetic form-factor study (see later).
- Proposal by K. Kilian and P. Birien[16] to measure $\sigma_{2\pi^0}$ at very low energy: 5 MeV down to ∿ 0.5 MeV or lower. They suggest that this study could be a way to measure the annihilation radius. The apparatus would consist of the low-energy antiproton spectrometer quoted above, followed by a crystal ball.

5.3.2 Study of $\bar{p}p \to e^+e^-$

As is well known, the rate of this reaction is related to the electromagnetic form factors in the time-like region. This important region (near to the poles of the analytic function) is also accessible via the inverse reaction $e^+e^- \to \bar{p}p$, but the rates foreseen at LEAR should be decisive. Moreover, near threshold the experimental conditions are in favour of $\bar{p}p$ annihilation. Figure 2 shows the experimental situation for $|G_E|$.

In the time-like region, BNL and CERN old limits, ADONE's point, and the two points[24] near threshold (open circles) obtained in 1976 at CERN, are represented. The recent DCI results are not shown. The continuous

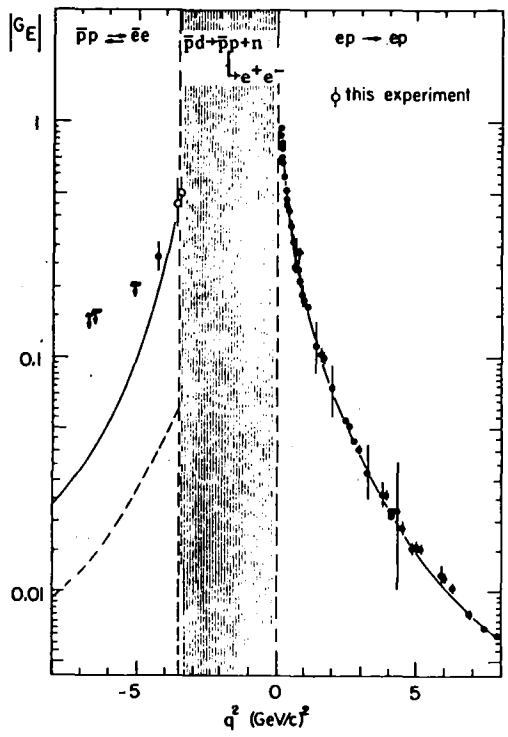

Fig. 2 Present situation of the data on $|G_E|$ for $-8(\text{GeV/c})^2 < q^2 < 8(\text{GeV/c})^2$. The solid line represents a fit to the existing data, based on the VDM model with the contribution of ω, ω', ϕ, ρ, ρ'_{1250}, ρ''_{1600} mesons. An increased statistical weight was given to the time-like data. A VDM fit (dashed line) using only ρ, ω, ϕ mesons is also shown. For $q^2 > 0$, it is superposed on the solid curve.

line represents a rough fit by the authors using six vector mesons and giving increased weight to the time-like points. Clearly, to obtain a model-selective fit requires many more points with high statistics. Moreover, to obtain $|G_E|$ and $|G_M|$ separately, angular distributions are necessary.

P. Dalpiaz, P.F. Dalpiaz, M. Schneegans and L. Tecchio[23,25,26], propose to measure, with the LEAR extracted beam, high statistics points of $\sigma_{e^+e^-}$ from $\sim$ 30 MeV/c to the LEAR maximum energy with angular distributions. At rest, the branching ratio to e^+e^- could be measured in liquid hydrogen and in gas at various pressures to study $G = |G_E| = |G_M|$ and the effect of the Stark mixing. With $\Delta p/p \lesssim 10^{-3}$ and starting from 100 MeV/c antiprotons, they could be all stopped in less than a 1 mm of liquid H_2 and less than 10 cm of gas at atmospheric pressure. The e^+e^- annihilation

widths of the protonium cascade levels could be measured by requiring the X-ray signal in coincidence.

Following rates can be expected for 3×10^6 $\bar{p}$/s:

$p\bar{p}$ [GeV/c]	q^2 [(GeV/c)^2]	σ [nb]	L Target [cm]	$N_{e^+e^-}$ [day]
0	-3.52	$B_{e^+e^-} = 3 \times 10^{-7}$	1	6×10^4
0.3	-3.61	50	10	4000
1.0	-4.3	4	50	1700
2.5	-6.8	≈ 0.07	100	50

These rates can be compared to typical rates obtained in 1976 in the CERN PS m_{14} beam: ~ 3 e^+e^-/day at rest.

Note that P. Dalpiaz et al.[27] have also proposed to study the annihilation into e^+e^- with an internal jet target, which would yield somewhat higher rates.

It is also proposed to study reaction:

$$\bar{p}d \rightarrow \bar{p}p + n \quad (\rightarrow e^+e^-)$$

which should allow $|G_E|$ and $|G_M|$ to be determined below the threshold of the time-like region.

The apparatus for such a study should have a high rejection against the hadronic background, and a 4π coverage is advisable in order to have good angular distributions. Figure 3a shows a possible apparatus where gas Čerenkov counters and lead-scintillator sandwiches would give a rejection of $(10^2 \times 10^2)^2 = 10^8$ against pion pairs at the trigger level. The energy resolution would be $\approx \pm 10\%$ at 1 GeV/c. The electron directions would be measured in wire chambers to $\pm 0.5°$.

Note that a cylindrical geometry around the beam would not be convenient since forward and backward particles would be badly treated. We rather leave open top and bottom which may be closed with detectors if possible.

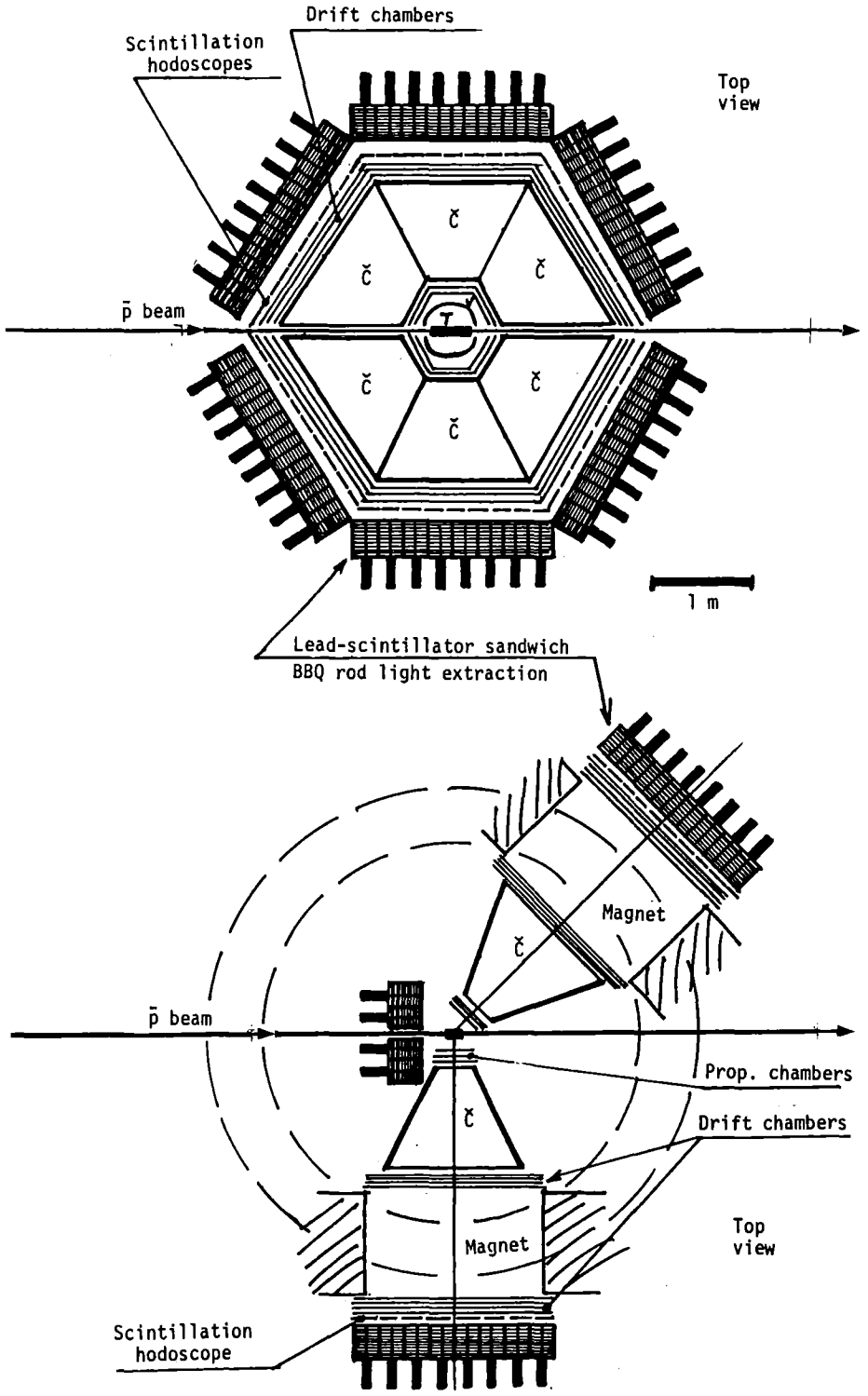
Drift chambers
Scintillation hodoscopes
a)
Top view
Č
p̄ beam
1 m
Lead-scintillator sandwich
BBQ rod light extraction
b)
Magnet
p̄ beam
Prop. chambers
Drift chambers
Top view
Magnet
Scintillation hodoscope

Fig. 3

5.3.3 Study of neutral annihilation modes (same authors)

All neutral annihilation cross-sections could be measured between $\sim$ 30 MeV/c and $\sim$ 2.5 GeV/c with angular distributions in the same apparatus as for e^+e^-, with addition of a veto counter surrounding the target and of lead converters allowing precise measurement of the γ-ray directions in the wire chambers (see Fig. 3a). Some interesting channels are:

$$\bar{p}p \to 2\pi^0$$
$$\to \eta^0\ \pi^0$$
$$\to 2\gamma$$
$$\to \pi^0\ \omega \quad \omega \to \pi^0\gamma$$
$$\to \pi^0\phi \quad \phi \to \eta\gamma$$
$$\to \omega\ \eta \quad \omega \to \pi^0\gamma, \ \eta \to 2\gamma$$
$$\to \phi\ \eta \quad \phi \to \eta\gamma, \ \eta \to 2\gamma$$
$$\to 3\pi^0$$
$$\to \pi^0\ \pi^0\ \eta$$
$$\to E\ \pi^0\ \pi^0 \quad E \to 2\gamma$$

and so on.

Most of these channels are of specific interest. For instance, Chan Hong-Mo suggests measuring the angular distribution on possible structures in $\eta^0\ \pi^0$ production in flight to look for isospin degeneracy. Another example: the observation of $E \to 2\gamma$ would give evidence in favour of E(1400) for being the ninth member of the pseudoscalar nonet.

5.3.4 Vector meson spectroscopy (same authors)[23,25]

A study of the reaction:

$$\bar{p}p \to V^0 + \text{neutrals (mostly 1 or 2 } \pi^0) \quad V^0 \to e^+e^- \text{ (or } \mu^+\mu^-)$$

at rest and in flight allows vector meson spectroscopy from 1 to 3 GeV/c^2.

The theoretical predictions are:

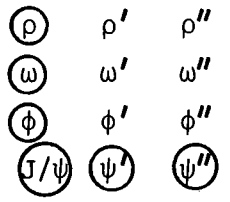

Circle means established

The experimental situation in this mass region is at present rather confused. Several states have been observed:

- 2-3 at ADONE
- ∿ 3 in $\bar{p}p$ at CERN
- ∿ 4 at DCI
- ∿ 2-3 at DESY

but they are difficult to compare and to interpret. We propose to use a double magnetic spectrometer which can identify and measure the angles and energy of the electrons. In this case, we need high rejection ($>10^8$) and the best energy resolution possible. A $\Delta p/p$ of 1% would give a 10 MeV/c^2 mass resolution, which would allow a fine spectroscopy and a complete clarification of this region. Figure 3b shows a possible set-up (with also π^0 detection) where the solid angle has been sacrificed for good rejection and good energy resolution. If these requirements can be met by a 4π set-up, which is under study, it will also allow measurement of the form factors and of the neutral channels.

6. CONCLUSIONS

As a conclusion, I would like to show how much progress can be expected for $N\bar{N}$ annihilation from LEAR extracted beams, depending on the energy range. If we assume the data yield to be proportional to beam intensity and quality, we can make the following guess:

Annihilation energy range	$\frac{\text{Data yield in LEAR AGE}}{\text{Data yield in PRELEAR AGE}}$
$\bar{p}$ STOP EXPERIMENTS	10^3 - 10^6
Very low energy (10 - 300 MeV/c)	∞
Low energy (0.3 - 1 GeV/c)	10^3 - 10^4
Medium energy (1 - 2.5 GeV/c)	10^2 - 10^3 ∞ for rare modes

If we sum up possible experiments concerning $N\bar{N}$ annihilation, baryonium search, protonium studies, charmonium and other spectroscopy, we see that we are facing a large experimental program of 20-30 experiments which may last of the order of 10 years. The number of experiments could of course be reduced by building large sophisticated set-ups, capable of measuring everything and used as a facility by large collaborations. We feel strongly that specific experiments done by small groups will be more fruitful in terms of physics results and also more rewarding to physicists.

I will end with the hope that after a few years of LEAR operation, nuclear forces will be better understood. Also, LEAR results could help in answering the question, Is QCD a good theory?

REFERENCES

1) B. Povh, $\bar{p}$ LEAR Note 63 (1979).

2) H. Koch, LEAR Note 62 (1979).

3) P. Dalpiaz, LEAR Notes 32 and 55 (1979).

4) I.S. Shapiro, Phys. Reports 35C (1978) 129-185.

5) T.E.O Ericson, Proc. Third European Symposium on Antinucleon-nucleon interactions, Stockholm, 1976 (eds. G. Ekspong and S. Nilsson), (Pergamon Press, Oxford, 1977), p. 3.

6) For QCD models, see
Chan Hong-Mo, preprint CERN TH.2540 (1978);
Chan Hong-Mo and A. Högaasen, Phys. Lett. 72B, 400 (1978).
Chan Hong-Mo and A. Högaasen, Nucl. Phys. B136, 401 (1978).

7) H. Muirhead and P.S. Gregory, Proc. Third European Symposium on Antinucleon-nucleon interactions, Stockholm, 1976 (eds. G. Ekspong and S. Nilsson), (Pergamon Press, Oxford, 1977), p. 331.

8) P. Dalpiaz, U. Gastaldi, K. Kilian and M. Schneegans, Memorandum to Workshop of Medium-Energy Physics (14 June 1977).

9) W. Hardt et al., CERN PS/DL/Note 79-1 (1979).

10) F. Balestra et al., LEAR Notes 4 and 5 (1979).

11) P. Pavlopoulos, LEAR Note 27 (1979).

12) M. Macri and F. Silombra, LEAR Note 26 (1979).

13) J. Rafelski, LEAR Note 3 (1979).

14) E. Klempt, LEAR Note 25 (1979);
J. Bailey, LEAR Note 48 (1979).

15) U. Gastaldi, LEAR Notes 9 and 30 (1979).

16) P. Birien and K. Kilian, LEAR Note 45 (1979).

17) C. Voci, LEAR Note 20 (1979).

18) H. Poth, LEAR Note 15 (1979).

19) F. Balestra et al., LEAR Note 47 (1979).

20) P. Dalpiaz and K. Kilian, LEAR Note 31 (1979).

21) S. Devons et al., Phys. Rev. Lett. 27, 1614 (1971).

22) G. Bassompierre et al., Measurement of the $\pi^0\pi^0$ production in $\bar{p}p$ annihilation at rest, presented at the 4th European Antiproton Symposium, Barr, 1978.

23) M. Schneegans, LEAR Note 11 (1979).

24) G. Bassompierre et al., Phys. Lett. 68B, 477 (1977).

25) P. Dalpiaz et al., LEAR Notes 38 and 39 (1979).

26) P. Dalpiaz et al., e^+e^- pairs produced in $\bar{p}p$ annihilation with intense cooled antiproton beams, presented at the 4th European Antiproton Symposium, Barr, 1978.

27) P. Dalpiaz et al., LEAR Note 39 (1979).

CHARMONIUM AND OTHER ONIA AT MINIMUM ENERGY

P. Dalpiaz*)

Istituto di Fisica Superiore dell'Università di Torino
and
INFN, Sezione di Torino, Italy

1. INTRODUCTION

In recent years considerable interest has been focused at CERN[1] on the experimental possibilities offered by the antiproton-proton collisions to answer some of the fundamental questions of the present-day physics.

Various working groups, set up at CERN during the last two years, have examined the physics potentials and the technical feasibility of $\bar{p}p$ colliding devices at various energies. As a consequence of this work, two $\bar{p}p$ projects have already been approved: the ISR $\bar{p}p$ project, and the SPS collider, covering a centre-of-mass energy range from 20 to 540 GeV. The Low-Energy Antiproton Ring (LEAR) project[2], allowing the study of phenomena under the $2m_p$ threshold up to 2.3 GeV, is at present under study. Transforming LEAR into a $\bar{p}p$ minicollider[2], it is possible to reach a centre-of-mass energy of 3.7 GeV.

Considering, then, the $\bar{p}p$ physics facilities at CERN as a whole project, it is seen that the energy range between 3.7 GeV and 20 GeV remains uncovered.

In this report the physics interest of experiments in a centre-of-mass energy range between 2 and 20 GeV will be outlined and the technical feasibility investigated.

2. PHYSICS INTEREST

2.1 Search for new particles and fine spectroscopy

As is well known, in the last years excellent work has been done in the search for new particles using e^+e^- colliding beams. The vector mesons ($J^P = 1^-$) have been produced in formation experiments, where they can profit

*) Visitor at CERN, Geneva, Switzerland.

from the resolution of the order of some MeV, typical of such machines*). The non-$J^P = 1^-$ particles, however, are produced by radiative decay of the vector mesons of higher mass; therefore the resolution achieved is that of the 4π detector spectrometer, i.e. about 50 to 100 MeV. This fact is a clear limitation of the experimental possibilities of e^+e^- machines.

The overwhelming advantages of using $\bar{p}$ cooled beams is that in the $\bar{p}p$ annihilation, the non-$J^P = 1^-$ channels are not depressed, while the resolution that can be reached is always very high. In fact the exceptional $\Delta p/p$ of $\bar{p}$ and p cooled beams is of about 10^{-3}-10^{-5}, which allows a resolution of 1 or 2 orders of magnitude better than that of e^+e^- colliding machines. Furthermore, the high-intensity $\bar{p}$ beam allows a sufficiently high event rate. One of the disadvantages is the presence of a strong hadronic background, but, asking for clear signatures such as

$$e^+e^-, \quad \mu^+\mu^-, \quad \gamma\gamma, \quad e^\pm\mu^\mp, \quad \text{etc.},$$

we can identify the channels.

The search for particles strongly coupled with $\bar{p}p$, such as

$$2N\bar{N}, \quad 2N2\bar{N}, \quad Y\bar{Y}, \text{ and } Y_c\bar{Y}_c,$$

is clearly advantaged in $\bar{p}p$ annihilation.

These features make the $\bar{p}p$ cooled beams a unique tool for performing fine spectroscopy, and several problems, not yet solved by e^+e^- colliding beam experiments, may find a solution.

2.1.1 Charmonium[3-5]

In the charmonium family[6], the two pseudoscalar members have not yet been clearly seen (see Fig. 1). The widths of all the χ particles are not determined: these structures have been investigated with an experimental resolution much larger than their width. Finally, it will be interesting to measure the width of J/ψ, ψ', with a resolution of the same order of magnitude.

---

*) Up to $E_{cm} \sim 5$ GeV the resolution is about 1 MeV. At $E_{cm} \sim 10$ GeV we expect ~ 6 MeV at PETRA, CESR, and PEP, and ~ 10 MeV has been obtained at DORIS.

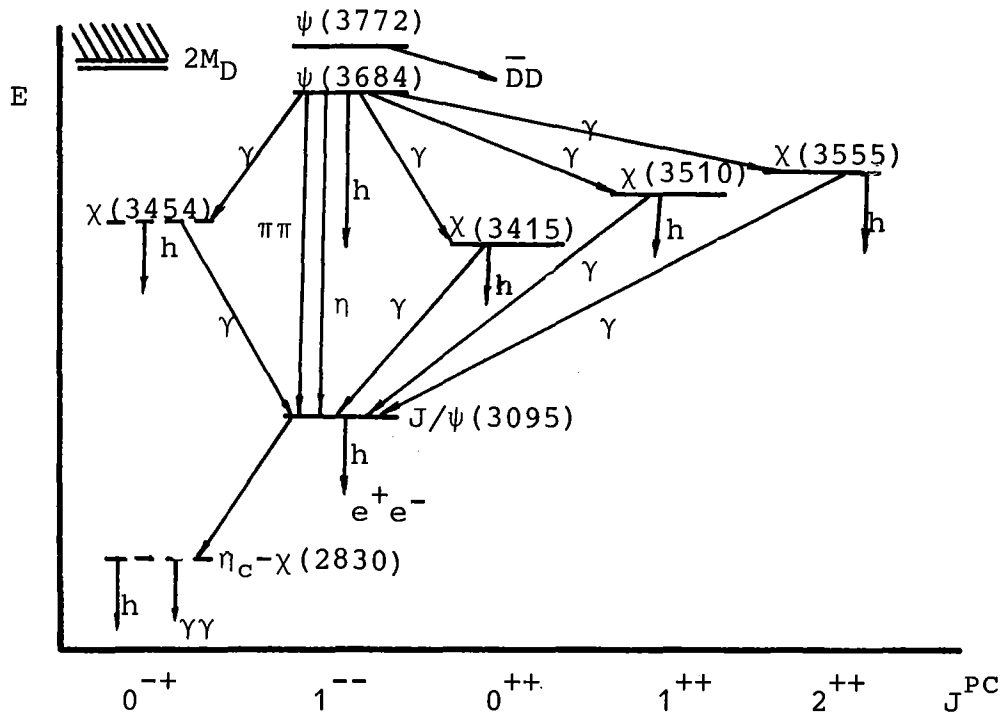

Fig. 1 Charmonium spectrum from Ref. 6

Tuning the $\bar{p}$ momentum to the correct value, it is possible to detect the following processes:

$$J^P = 1^- \qquad \bar{p}p \to J/\psi(\psi', \psi'') \to e^+e^-(\mu^+\mu^-) \ ,$$

$$J^P = 0^{-+},\ 0^{++},\ 1^{++},2^{++} \qquad \bar{p}p \to \chi \to \gamma + J/\psi \hookrightarrow e^+e^-(\mu^+\mu^-) \ ,$$

and

$$\eta_c \ (J^P = 0^-) \qquad \bar{p}p \to \eta \to \gamma\gamma \ ,$$

all of which have a clear signature.

The charmonium production cross-sections may be evaluated, taking into account that

$$\sigma(e^+e^- \to J/\psi \to \text{hadrons}) = 3\ \mu b \cdot MeV$$

$$\sigma(e^+e^- \to \psi' \to \text{hadrons}) = 0.6\ \mu b \cdot MeV \ .$$

From the detailed balance,

$$\sigma_{e^+e^-}(q^2) = (p^*_{\bar{p}}/p^*_e)^2 \times \sigma_{\bar{p}p}(q^2) \ ,$$

and the coupling ratio,

$$(J/\psi \to \bar{p}p)/(J/\psi \to e^+e^-) \ ,$$

and obtain

$$\sigma(\bar{p}p \to J/\psi) = 3\ \mu b \times \Gamma(J/\psi)$$

$$\sigma(\bar{p}p \to \psi') = 0.2\ \mu b \times \Gamma(\psi') \ .$$

We will assume that $\sigma_{\eta_c} \equiv \sigma(J/\psi)$. For the χ-states, interpolating between J/ψ and ψ' we obtain a cross-section from 1 μb and 1.6 μb. QCD predictions favour higher values for the cross-sections, but here we will use more conservative figures. The expected signal-to-background ratio R for J/ψ is

$$R = \frac{\sigma(\bar{p}p \to J/\psi \to e^+e^-)}{\sigma(\bar{p}p \to \text{hadrons})} = \frac{2 \times 10^{-31}}{6 \times 10^{-26}} = 3 \times 10^{-6} \ .$$

For the channels $\psi' \to e^+e-$, $\chi \to e^+e^- + \gamma$, $R = (0.5\text{-}1) \times 10^{-7}$, a rejection of $e/\pi \geq 10^{-4}$ is therefore requested, for each electron.

2.1.2 Bottomonium[3,5]

A new family of high-mass vector mesons T, T′ has recently been discovered at Fermilab[7] in the reaction $pN \to \mu^+\mu^- + X$. The existence of these particles has been confirmed at DORIS[8] in e^+e^-.

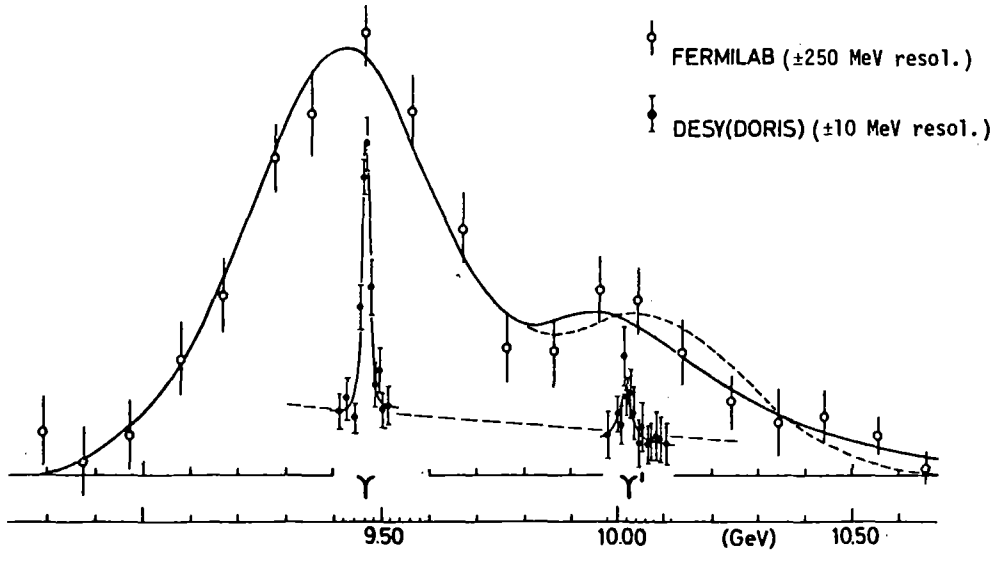

Fig. 2 Comparison of the data on T or T′ obtained at Fermilab and DORIS

Several models predict the existence of an T-family similar to the J/ψ family, but until now only the T and T′ have been detected. The e^+e^- colliding beam machines (PETRA, CESR, or PEP) can investigate these structures with a resolution of ≃ 6 MeV; but it is not clear whether they can detect the "χ_b" states of the T-family as clear structures emerging from the background, as has been the case for the J/ψ family (see Fig. 2).

Using $\bar{p}p$ facilities it is possible to tune the beams on the resonance mass value. In this case we are probably in a better position to investigate the χ_b states.

These particles can be searched for in reactions analogous to those considered in the charmonium case. The expected cross-sections are evaluated as follows: from $\sigma[(e^+e^-) \to T \to \text{hadrons}] \simeq 20$ nb × 10 MeV and $\Gamma(T) \simeq 50$ keV, assuming the same coupling to $\bar{p}p$ as that for the J/ψ, we have $\sigma(\bar{p}p \to T) \simeq 0.2\ \mu b \times \Gamma(T)$. If we assume, to be conservative, that $\sigma(\bar{p}p \to T)/\sigma(\bar{p}p \to J/\Psi) = 1/5$, we have $\sigma(\bar{p}p \to T) \simeq 40$ nb × Γ(T).

2.1.3 The Higgs boson[5)]

In gauge theories the mass of the gauge bosons and the renormalizability are obtained with the introduction of the Higgs fields, at least one of which survives as a physical particle[9)]. In the simplest of these theories, due to Weinberg and Salam, one of these bosons, H^0, with $J^P = 0^+$, has a mass that is practically undetermined: its value lies between 1 GeV and 1 TeV. Spontaneous symmetry breaking is generally obtained introducing a $-\mu^2\phi^2$ term in Higgs potentials, where $m^2_{H^0} = 2\mu^2$, but these quantities are not related to observable parameters. Some years ago Coleman and Weinberg[10)] demonstrated the possibility of setting to zero the $-\mu^2\phi^2$ term in the Higgs potential, and generating the symmetry breaking dynamically through radiative corrections to the effective potential. In this case the m_{H^0} is related to the mass of fermions, vector bosons W, and the Weinberg angle θ_w.

Assuming that

$$m_f \ll m_W \text{ *)} \quad \text{and} \quad \sin^2 \theta_w \simeq 0.2 \ ,$$

then the mass of this scalar boson could be about 10 GeV.

---

*) Where m_f is the fermion mass and m_W the mass of intermediate vector bosons.

Recently, Ellis et al.[11] have calculated all branching ratios for the decay of and into a Higgs boson of mass at about 10 GeV. For $H^0 \to \tau^+\tau^-$ they foresee a branching ratio between 25% and 50%. The evaluation*) of the ratio of couplings $\bar{p}p \to H^0/\bar{p}p \to J/\psi$ is $\sim 10^{-2}$. Assuming $\Gamma(H^0) \simeq 100$ keV we can evaluate

$$\sigma(\bar{p}p \to H^0) \simeq 0.4 \text{ nb to } 2 \text{ nb} \times \Gamma(H^0)$$

Clearly, the search for scalar bosons such as H^0 in $\bar{p}p$ formation experiments is particularly convenient, since it is possible to tune the beam at the wanted mass value and to detect processes with leptons in final states. The process

$$\bar{p}p \to H^0 \to \tau^+\tau^-$$
$$\tau^- \to e^-\nu\bar{\nu}(\mu^-\nu\bar{\nu})$$
$$\tau^+ \to e^+\nu\bar{\nu}(\mu^+\nu\bar{\nu})$$

will be studied, identifying pairs of e^+e^- or $\mu^+\mu^-$ or $e^\pm\mu^\mp$.

In Table 1 the properties of the states considered in Section 2.1 in relation to their study with $\bar{p}$ beams with fixed target or with a minicollider are presented. The event rate per day calculated in the hypothesis of a luminosity of $L = 10^{30}\,cm^{-2}\,sec^{-1}$ is very encouraging.

2.2 High-mass baryonium states

A standard field of research, using $\bar{p}p$ annihilation in the LEAR energy range, is the search for baryonium states and the determination of their properties. Several speakers contributed on the subject at this Workshop. It must be pointed out, however, that baryonium-like states can be produced at energies higher than those reachable by LEAR.

We have precise predictions for these states, which can be summarized as follows:

$2N\bar{N}$[12]: These states have an energy around 3 proton masses (2750 MeV - 2850 MeV). Their width varies between 15 MeV and 100 MeV, and they can be formed in the reactions

*) J. Ellis (private communication) evaluates this ratio using QCD in the hypothesis that $\bar{p}p \to T$ via 3 gluons and $\bar{p}p \to H^0$ via 2 gluons.

Table 1

E_{cm} (GeV)	Investigated particle	J^{PC}	$p_{\bar{p}}$ (GeV/c)		$\sigma(\bar{p}p \to \ldots)$		Branching ratios	Event rate per day with $L = 10^{30}\ cm^{-2}\ s^{-1}$
			Fixed target	Colliding beams	Measure	Model		
2.8	$\eta_c(2.8)$	0^{--}	3.2	1.07	-	$3\ \mu b \cdot \Gamma_{\eta_c}$	0.003	~ 750
3.1	J/ψ	1^{--}	4.2	1.26	$3\ \mu b \cdot \Gamma_{J/\psi}$	-	0.07	~ 18000
3.4	$\chi(3415)$	0^{++}	5.3	1.46	-	$1.6\ \mu b \cdot \Gamma_{\chi}$	0.033×0.07	~ 200
3.45	$\chi(3454)$	0^{--}	5.4	1.47	-	$1.5\ \mu b \cdot \Gamma_{\chi}$	?	-
3.51	$\chi(3510)$	1^{++}	5.5	1.52	-	$1.2\ \mu b \cdot \Gamma_{\chi}$	0.23×0.07	~ 1600
3.55	$\chi(3555)$	2^{++}	5.6	1.54	-	$1.0\ \mu b \cdot \Gamma_{\chi}$	0.16×0.07	~ 1000
3.7	ψ'	1^{--}	6.1	1.60	$0.2\ \mu b \cdot \Gamma_{\psi'}$	-	0.009	~ 170
9.5	Υ	1^{--}	48.0	4.6	-	$200\ nb \cdot \Gamma_{\Upsilon}$ to $40\ nb \cdot \Gamma_{\Upsilon}$	Like J/ψ	~ 1500 to ~ 300
10	Υ'	1^{--}	52.0	4.9	-	?	-	-
$\sim \overline{10.4}$	H^0	0^{++}	~ 57.0	~ 5.1		2 to $0.4\ nb \cdot \Gamma_{H^0}$	$(0.25\text{-}0.5) \times 0.35^2$	1 to 12

$$\bar{p}p \to 2\bar{p}2p \quad (\bar{p}p\bar{n}n)$$

$$\bar{p}d \to \bar{p}pn \ .$$

$2\bar{N}2N$[12]: around $4m_p$ (3375 MeV - 3800 MeV). We can search for such states in the processes

$$\bar{p}p \to \bar{p}p\bar{p}p$$

$$\bar{p}p \to \bar{p}p\bar{n}n \ .$$

$\bar{Y}Y$: Baryonium with hidden strangeness[5,12,13]. Several narrow states are predicted in $\Lambda\bar{\Lambda}$, $\Sigma\bar{\Sigma}$, and $\Xi\bar{\Xi}$ channels, with masses from 2200 MeV to 2800 MeV. They are detected in the reactions

$$\bar{p}p \to \bar{\Lambda}\Lambda$$

$$\bar{p}p \to \bar{\Sigma}\Sigma$$

$$\bar{p}p \to \bar{\Xi}\Xi \ .$$

Some experimental evidence for such states has already[14] been found.

$\bar{Y}_cY_c$: Baryonium with hidden charm: Various structures have been found in the region from 4.2 GeV to 5 GeV in e^+e^- annihilation experiments. Some authors[13,15] attribute some of these structures to baryonium states with hidden charm.

It is indeed very interesting to look for the states in reactions such as, for example, $\bar{p}p \to \bar{\Lambda}_c\Lambda_c$.

2.3 Other interesting physics subjects

2.3.1 Strange particle production[16]

As is well known, strange particles are produced more in $\bar{p}p$ annihilation than in πp or pp reactions. It should be interesting to detect final states such as

	I	$\bar{p}$ momentum (GeV/c)		Cross-section
		Fixed target	Colliding beams	
$\bar{p}p \to \bar{\Lambda}\Lambda$	0	1.44	0.6	100 μb
$\bar{p}p \to \bar{\Sigma}^0\Lambda$ $(\Sigma^0\bar{\Lambda})$	1	1.77	0.71	60 μb
$\bar{p}p \to \bar{\Lambda}nK^0$, $\Lambda\bar{n}K^0$	-	2.35	0.9	-

that are pure I-states. The $\bar{\Lambda}\Lambda$ are self-analysers of polarization, allowing spin determination. Furthermore, we note that in $\bar{p}p \to \bar{\Lambda}\Lambda$, the C and CP invariances demand equal polarization for Λ and $\bar{\Lambda}$ (normal to the production plane). The existing data give an upper limit fixed only at 20%. With the cooled $\bar{p}$ a factor of 10^3 in statistics is easily obtainable.

2.3.2 Charmed particle production

In analogy with the strange particle production, it is possible to look for charmed particle production[4,5,16] in processes such as

$$\bar{p}p \to D\bar{D}$$

$$\bar{p}p \to \Lambda_c\bar{\Lambda}_c \ .$$

Cross-sections of about 1 μb are expected.

2.3.3 Hadronic jets

Hadronic jet production starts in e^+e^- annihilation at a centre-of-mass energy of about 7 GeV. It is interesting to compare the behaviour of this phenomenon in e^+e^- and $\bar{p}p$ annihilations near the threshold in order to understand the mechanism of the jet formation. Several theoretical predictions exist in this field.

All the phenomena outlined in Section 2.2 are strongly coupled with $\bar{p}p$, allowing us to operate with a luminosity of about 10^{27}-10^{28} cm^{-2} sec^{-1}. With an extracted beam we need a momentum range varying between 1.7 GeV/c and about 30 GeV/c. With a $\bar{p}p$ minicollider, on the other hand, it should be enough to operate, at maximum, with beams of 3.5 GeV/c momentum.

3. COMPARISON OF THE DIFFERENT EXPERIMENTAL POSSIBILITIES

We will not consider here the secondary $\bar{p}$ beams from the CERN Proton Synchrotron (PS) and Super Proton Synchrotron (SPS) since they cannot reach a good luminosity and their $\Delta p/p$ is, in the best case, about 10^{-2}. The CERN Intersecting Storage Rings (ISR) $\bar{p}p$ project is not interesting either, because it can reach a luminosity of 10^{28} cm^{-2} sec^{-1}, even with cooled beams, in the energy range with which we are concerned.

We will therefore discuss the following possibilities:

3.1 Cooled $\bar{p}$ beam extracted from the PS

At this Workshop a proposal was presented[4] to study the charmonium family with an $\bar{p}$ cooled beam extracted from the PS. The proponents want to accumulate 10^9 $\bar{p}$ in AA, inject them into the PS*) every hundred seconds, accelerate them at the required momentum, and then extract 10^7 $\bar{p}$/sec for 4-5 seconds. The efficiency of this operation is about 4-5%. The $\Delta p/p$ for $\bar{p}$'s from the PS is about 10^{-3}; with an external measurement they hope to obtain a $\Delta p/p \simeq 2 \times 10^{-4}$. With an external target the luminosity depends on the width of the resonant state searched for. For example, in the case of J/ψ the useful H_2 target is only 0.7 cm.

Assuming that we have 2×10^{11} $\bar{p}$/day, we can calculate the luminosity L corresponding to the various widths; we get:

$\Gamma(J/\psi)$ $\quad L = 0.07 \times 0.7 \times 6 \times 10^{23} \times 2 \times 10^{6} = 6 \times 10^{28}$ cm^{-2} sec^{-1}

$\Gamma(\psi')$ $\quad L \simeq 1.7 \times 10^{29}$ cm^{-2} sec^{-1}

$\Gamma(1$ MeV$)$ $\quad L \simeq 9 \times 10^{29}$ cm^{-2} sec^{-1}

Obviously these luminosities should be multiplied by the efficiency of $\bar{p}$ used (in this case 5%). But the great problem in the study of the charmonium family with an extracted beam ($3.2 < p_p < 6.7$ GeV) is the PS RF transition energy, which is $\simeq 5$ GeV/c, and it is well known that it is difficult to work at ±2 GeV around the RF transition energy.

3.2 Jet H_2 target at the ISR

With the installation of a H_2 molecular jet target of 10^{-9} g/cm^2 in one ring of the ISR[5] with 2×10^{11} $\bar{p}$, we can obtain a very attractive luminosity:

$$L = 4 \times 10^{5} \times 10^{-9} \times 6 \times 10^{23} \times 2 \times 10^{11} = 5 \times 10^{31} \text{ cm}^{-2} \text{ sec}^{-1} ,$$

which is largely sufficient for our purposes. The ISR RF can compensate target energy losses. Cooling the beam stochastically, a $\Delta p/p$ of about 10^{-3}-10^{-4} is obtainable. The ISR should be blind from 7 GeV up to 11 GeV, since the ISR RF transition energy is at 9 GeV. It is still possible, however, to perform the proposed study on charmonium.

---

*) 10^9 p is the minimum bunch that the PS can manage.

A difficulty lies in the fact that, with the use of a jet target at the ISR, only one user at the time is allowed.

3.3 Jet target at the SPS

The installation of a H_2 molecular jet target at the SPS[5], of 2×10^{-9} g/cm^2, gives us a luminosity of 10^{31} cm^{-2} sec^{-1}. This opens up the field of Υ and Higgs bosons. As in the previous case it seems, however, very unrealistic to allow only a single user at a time for the SPS.

3.4 $\bar{p}p$ colliding beams at LEAR[3,5]

The $\bar{p}p$ collision option presented in the "LEAR conceptual study"[2], where LEAR is used as a minicollider, covers a centre-of-mass energy range from 2.3 to 3.8 GeV.

The advantages of using the minicollider instead of a fixed target is the better discrimination from background for all the physical subjects seen before. In fact, the few-body processes go to larger angles than do the products of $\bar{p}p$ fragmentation. In particular for the two-body we can profit from the collinearity. The main features of such a LEAR option are the following:

- The luminosity has been evaluated taking into account the Amman-Ritson limits[2]; with the beam cooled in AA and transferred to LEAR, we have a luminosity on J/ψ of about 2×10^{29} cm^{-2} sec^{-1}, and on ψ' of about 4×10^{29} cm^{-2} sec^{-1}.

With this luminosity we can perform the physics program proposed in Sections 2.2 and 2.3. The charmonium physics can also be investigated, but in this case it is preferable to increase the luminosity.

A way of increasing the luminosity is to use the low-β section. In the LEAR Option, $\beta_\nu^* = 5$ m (the β value in the interaction region). With a low-β section we can reach $\beta_\nu^* = 1$ m with a gain of a factor of 5 in luminosity.

We can also increase the luminosity by cooling the beam continuously with superstochastic or electron cooling. In the calculation of the LEAR Option luminosity, a $\Delta\nu = 0.005$ (beam-beam tune shift) was considered, corresponding to a cooling time of 300 hours. In Fig. 3 we can see the dependence of $\Delta\nu$ on cooling time.

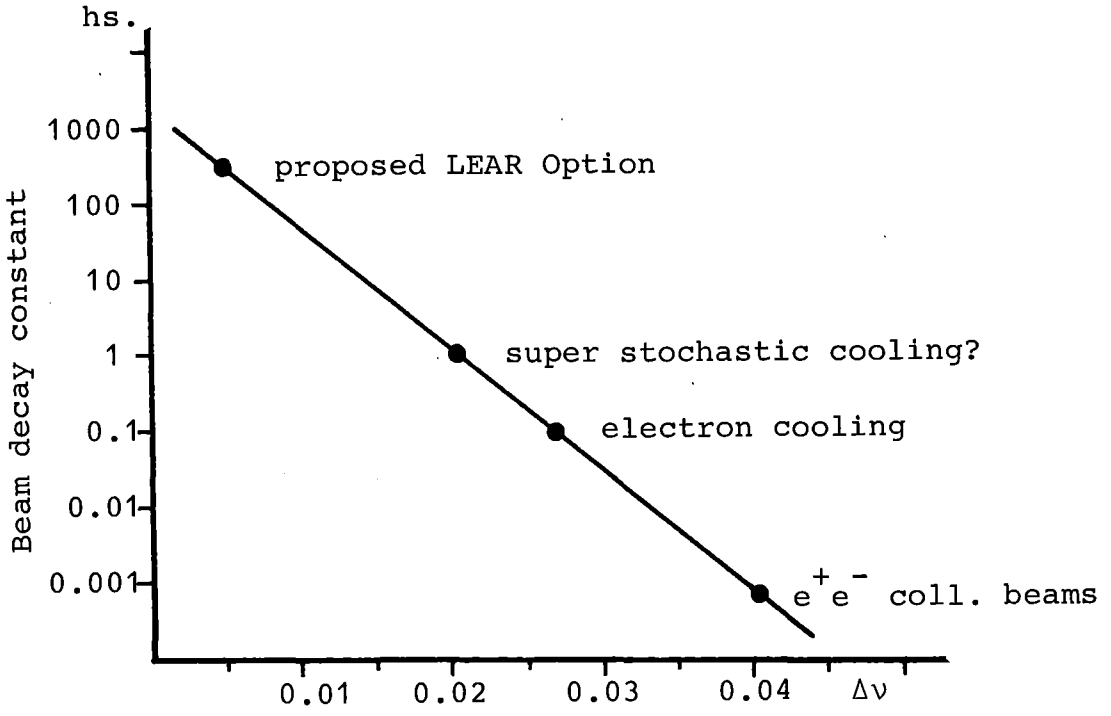

Fig. 3 Variation of $\Delta\nu$ as a function of the beam decay constant

If it is possible to have 1 hour of cooling time with superstochastic cooling, we can have $\Delta\nu = 0.02$, and we gain a factor of 4 in luminosity. With relativistic electron cooling we can probably have 6 minutes of cooling time, which means $\Delta\nu = 0.025$, and a gain of 5 in luminosity.

- In the LEAR Option scheme a momentum dispersion $\Delta p/p$ of 10^{-3} is expected, but it is possible to reach a $\Delta p/p$ of 10^{-4} with superstochastic or with electron cooling.

- One negative point of the actual LEAR Option scheme is the bunch length of 5 m. We can try to decrease the bunch length to about 1 m with some RF gymnastics[17]. Alternatively, we can consider reducing the interaction region length, using the solution of coasting beams.

3.5 Super LEAR[5] (Further LEAR Option)

The whole physics program proposed above can be carried out with a minicollider of $\sim$ 6 GeV/c per beam.

We can obtain this momentum with a ring larger than the LEAR ring or by constructing LEAR with superconducting magnets. In fact these magnets have now been developed for the Fermilab Energy Doubler and for ISABELLE.

The rise-time of such magnets varies from 20 to 60 sec and a field of 4.5 T can be reached. The cost of these magnets is $\sim$ (6000 to 10000) \$/m. For a small ring like LEAR the total cost is not very high.

With a Super LEAR we can work at low energy up to $E_{cm} \sim 3.7$ GeV with a H_2 molecular jet target ($L = 10^{32}$ cm^{-2} sec^{-1}).

With Super LEAR working as a minicollider at $E_{cm} \sim 10$ GeV we can reach a luminosity of 10^{31} cm^{-2} sec^{-1} and this makes the search for χ_b and Higgs bosons (H^0) feasible.

4. CONCLUSIONS

From the arguments outlined in the previous sections it is clearly seen that the LEAR Option is a very promising one, although some more study is necessary in order to have the technical possibilities, to perform all the physics program proposed in Section 2.

We have seen, however, that the reactions strongly coupled with $\bar{p}p$ can be studied with luminosities of about 10^{27}-10^{28} cm^{-2} sec^{-1}: search in this field could profit from a first stage of setting up of the LEAR scheme. The introduction, into the scheme of the minicollider, of the low-β sections will allow work on the charmonium physics in very good luminosity conditions. The addition of superstochastic and/or electron cooling could increase the luminosity and improve the resolution.

The choice of the Super LEAR as a further development should allow us to investigate the Higgs boson and the Υ-family.

The technical requirements which would allow the extension of the LEAR project to cover all physics fields reviewed in Sections 2 and 3 are:

- LEAR momentum not less than 2.0 GeV,
- possibility of acceleration or deceleration,
- good vacuum system,
- tunable stochastic cooling,
- low-β section,
- superstochastic cooling,
- electron cooling and relativistic electron cooling.

REFERENCES

1) C. Rubbia, P. McIntyre and D. Cline, Proc. Int. Neutrino Conference, Aachen, 1976 (eds. H. Faissner, H. Reithler and P. Zerwas) (Vieweg und Sohn, Braunschweig, 1977), p. 683.

2) W. Hardt et al., CERN PS/DL/Note 79-1 (1979).

3) P. Dalpiaz, Electromagnetic annihilation in low energy pp colliding beams, CERN - $\bar{p}p$ Note 06 (1 May 1977).
P. Dalpiaz et al., $\bar{p}p$ colliding beams with cooled antiprotons to perform fine spectroscopy between 2.7 and 11 GeV, to be published in Proc. 4th European $\bar{p}$ Symposium, Barr, France, 1978 (ed. A. Friedman).

4) Edinburgh-Rutherford-Westfield Collaboration, CERN $\bar{p}$-LEAR Note 28 (1979).

5) P. Dalpiaz, CERN $\bar{p}$-LEAR Note 32 (1979).

6) J.D. Jackson, Proc. EPS Conf. on High Energy Physics, Budapest, 1977 (eds. L. Jenik and I. Montvay) (Central Research Inst. for Physics, Budapest, 1977), vol. 1, p. 603.

7) S.V. Herb et al., Phys. Rev. Lett. 39 (1977) 252.

8) C.H. Bergam et al., Phys. Lett. 76B (1978) 243.
C.V. Darden et al., Phys. Lett. 76B (1978) 246.

9) See, for example, J.C. Taylor, Gauge theories of weak interactions (Cambridge Univ. Press, Cambridge, 1976).

10) S. Coleman and E. Weinberg, Phys. Rev. D 7 (1973) 1888.
E. Weinberg, Phys. Rev. D 7 (1973) 2887.

11) J. Ellis et al., CERN TH. 2634 (1979).

12) I.S. Shapiro, Physics Reports 35 (1978) 129.
Chan Hong-Mo and H. Högaasen, Nucl. Phys. B136 (1978) 401.

13) C. Rosenzweig, Syracuse (USA) Preprint COO/3533-106, SU-4211-106 (1977).

14) B. Nicolescu et al., Berkeley Preprint LBL 6701 (1977).

15) C. Rosenzweig, Phys. Rev. Lett. 36 (1976) 697.
C.F. Chew, Berkeley Preprint LBL 5391 (1976) and *in* Antinucleon-nucleon interactions (eds. G. Ekspong and S. Nilsson) (Pergamon Press, Oxford, 1976), p. 515.

16) S. Limentani, CERN $\bar{p}$-LEAR Note 49 (1979).

17) M. Conte, CERN $\bar{p}$-LEAR Note 46 (1979).

ANTINEUTRONS AT LEAR

C. Voci - INFN Padova

(Talk presented at the March 1979 Karlsruhe Meeting on $\bar{p}p$ at low energy)

1. Since the $\bar{n}$ discovery in 1956 at the Berkeley Bevatron, $\bar{n}$ physics has been done essentially in bubble chamber, via the $\bar{p}p \to \bar{n}n$ reaction. The 72" (Berkeley) and the 20" (Brookhaven) chamber have produced the first results, more recently a Bombay-CERN-Neuchâtel-Tokyo collaboration has used pictures from the 81 cm chamber at CERN. Total and elastic $\bar{n}p$ cross sections have been studied as well as $\bar{n}p$ annihilations with ≥ 3 prongs. Statistics are generally low, as compared to $\bar{p}$ induced reactions.

2. The $\bar{n}p$ state is a pure I=1 state; its direct investigation avoids all difficulties related to deuterium targets, where the $\bar{p}n$ state can be produced. Baryonium oriented physics as well as selected annihilation channels can be studied in a much cleaner way. On the other hand the use of deuterium as a target opens the channel $\bar{n}n$ where practically no information are available.

3. In this and in the following section the production of $\bar{n}$'s via $\bar{p}p \to \bar{n}n$ is investigated. Firstly, I consider an internal jet hydrogen target, density 10^{-9} g/cm^2, and a circulating $\bar{p}$ beam of 10^9 particles and $2.2 \cdot 10^6 s^{-1}$ revolution frequency. Assuming a differential cross section of $\sim 10^{-26}$ cm^2/sterad at 0° and 0.5 GeV/c the number of $\bar{n}$'s into 10 μsterad is $13.2 \cdot 10^{-2}$ in one second. With a 25% duty cycle (i.e. $2 \cdot 10^4$ seconds in a day) the number of $\bar{n}$'s is

$$N_{\bar{n}} = 2.64 \cdot 10^3 \text{ (per day into 10 μsterad)}$$

The solid angle value of 10μ sterad corresponds to 6 cm^2 at 8 m from the target and is dictated by the physical dimension of LEAR and the necessity of reduced size for an external target. The improvements

in duty cycle x circulating intensity should easily provide a gain of one order of magnitude, giving

$$N_{\bar{n}} = 2.64 \cdot 10^4 \quad \text{(per day into 10 μsterad)}$$

This $\bar{n}$ beam can then be used in a standard way. For instance, it can impinge on an external hydrogen target, 1 g/cm^2. In one day, over 4π, one can detect

$$N_{ev} = 1.6 \cdot 10^{27}\ \sigma \div 1.6 \cdot 10^{28}\ \sigma$$

and since the total $\bar{n}p$ cross section is about 100 mb one can expect

$$160 \div 1600 \quad \text{ev/day}$$

Something can be gained in target length, but $\sim 10^4$ $\bar{n}p$ interactions/day seems a reasonable upper limit, at the moment.
The $\bar{n}$ beam is essentially mono-energetic; it requires same cooling action and a way out of the ring for the $\bar{n}$'s.

4. An alternative way of producing n's is by an extracted $\bar{p}$ beam impinging on an external target. I consider 10^6 $\bar{p}$ (this is not the only experiment on the floor), 1 cm liquid hydrogen target (to preserve the high momentum resolution and to allow the use of the transmitted $\bar{p}$'s), a solid angle of 100 μsterad (the interaction target can be nearer to the production target). In these conditions $4.2 \cdot 10^{-2}$ $\bar{n}$'s are produced per second into 100 μsterad, ∼30% of the figure for the internal production target. Gains in target length appear to be difficult, since energy losses of primary $\bar{p}$'s and attenuation of secondary $\bar{n}$'s become relevant.
No cooling is required in this option.

5. The $\bar{n}$ beam requires few elements, essentially one sweeping magnet and collimators. About 10% of n contamination seems to be unavoidable; unimportant should be the γ and K°_L contaminations. In principle it should be possible the tagging of $\bar{n}$ production looking at the recoil neutron; however, these neutrons have very low energy, which makes their detection quite inefficient, and are emitted forward (for a $\bar{n}$ angle in the range 1-9 mrad, the neutron angle is in the range 5°-40° at 0.5 GeV/c).
The relative monitoring of beam intensity can be achieved by neutron counting at fixed angle and/or by a downstream $\bar{n}$ calorimeters. A precise knowledge of $(d\sigma/d\Omega)_{cex}$ is in any case essential.
Finally, a "hole" in the main ring is necessary for the extraction of

$\bar{n}$'s in the case of internal target.

6. In this section I will try to guess how one could proceed. A suitable apparatus to measure $\bar{p}p \to \bar{n}n$ differential cross section with high precision will be on the floor, hopefully: it is likely to have a forward sweeping magnet and calorimeter for $\bar{n}$ detection. With a well designed apparatus, in my opinion, one could indeed measure:

a) σ and $d\sigma/d\Omega$ for $\bar{p}p \to \bar{n}n$
b) σ_{TOT} $\bar{p}p$ as a monitor
c) $\bar{p}p \to p\bar{p}$, taking advantage of sweeping magnet and anticounter box
d) $\bar{p}p \to n\bar{n}$, special case of a), properly calibrating the calorimeter.

Then one can install target and detection apparatus for $\bar{n}$ physics. An interesting possibility would be the use of a steamer chamber as proposed in LEAR note
The $\bar{n}$ beam could become a facility that practically does not disturb other users (this is true both for internal or external production).

7. I simply list a few special items that should rise additional interest.

1) If a reasonable increase in intensity can be achieved, $\bar{n}n \to e^+e^-$ could give a rate of few events per day.
2) $\bar{n}n \to \pi^\circ\pi^\circ$ could be studied to investigate the annihilation radius.
3) Very low energy $\bar{n}$ could be produced by degraded $\bar{p}$ to study the behaviour of charge exchange at threshold.

$\bar{p}$ LEAR-Note 66

FUNDAMENTAL PROPERTIES OF ANTINUCLEONS

H. Poth*)
Institut für Experimentelle Kernphysik,
Universität Karlsruhe, Karlsruhe,
Federal Republic of Germany

1. INTRODUCTION

In this talk the experimental knowledge of the lifetime, mass, and magnetic moment of the antinucleons is reviewed. No attention is paid to the experimental determination of the electromagnetic form factors of antinucleons and other particle properties. According to the CPT theorem, the absolute values of these quantities should be equal for particles and antiparticles. Although there are speculations about a particle-antiparticle asymmetry arising from cosmological models, the CPT theorem is confirmed to a very high precision through the study of neutral kaons.

Whenever experimental conditions can be improved by some orders of magnitude, it is instructive to leave theories aside, elaborate the expected experimental precision, and look into new experimental possibilities. Antiproton beams from LEAR[1] (Low-Energy Antiproton Ring) represent such an enormous improvement. In many cases a much higher accuracy can be achieved without any major effort being put into the experimental set-up. In the following, the impact of the much higher antiproton intensities on the precise determination of the particle properties of antinucleons is considered.

2. ANTIPROTON LIFETIME

Until recently no experimental confirmation of the antiproton stability was available. A hydrogen bubble-chamber experiment[2], searching for reactions with an odd number of charges after the disappearance of an antiproton, has found an upper limit of 10^{-4} sec. The first measurement on a macroscopic scale was done in ICE (Initial Cooling Experiment), when a stack of a few hundred antiprotons could be stored in the ICE ring at 2.1 GeV/c. It was possible to detect this low number of stored antiprotons

*) Visitor at CERN, Geneva, Switzerland.

and to monitor the decreasing intensity of the beam in a non-destructive way by picking up a resonant Schottky signal of the circulating antiprotons. The beam lifetime could be extended considerably by permanent stochastic cooling. A new lifetime limit of $\tau > 32$ h $\simeq 10^5$ sec was achieved[3]. This was an improvement of nine orders of magnitude.

In a subsequent measurement[4] it was possible to accumulate antiprotons in ICE and thus increase the number of stored particles. A maximum of 1.5×10^4 antiprotons were accumulated. During the ten days of the measurement an average number of 7000 antiprotons were stored. From the intensity decrease a lifetime limit of 80 h = 2.9×10^5 sec could be deduced. The sensitivity of measurement could be further increased by a direct search for a decay of the stored antiprotons. Within all possible decay channels (violating the fewest conservation laws) the decay into an electron and a neutral pion would be very likely.

In a straight section of the ICE ring eleven lead-glass counters were mounted on each side of the vacuum tube with scintillation counters at their front and rear ends, and at the top and bottom of the vacuum chamber. An event was accepted when at least one lead-glass Čerenkov counter on each side and one internal scintillation counter had fired and no external counter had triggered. The main background contribution was due to cosmic rays. During the ten-day measurement 2 events were observed which survive even more stringent trigger conditions. The cosmic-ray background which was measured under the same trigger conditions, but without beam, produced 4 events in 15 days. The background from antiproton annihilation was at the level of less than 1 event/10 days. Including detection efficiency and solid angle this result improves the lifetime limit again by more than one order of magnitude:

$$\tau_{\bar{p}} > \mathrm{BR} \times 1.7 \times 10^3 \text{ h} .$$

Here BR is the branching ratio of the antiproton decay channel $\bar{p} \rightarrow e^- + \pi^0$. Assuming a branching ratio of 60% as suggested by some theories, the lifetime limit is

$$\tau_{\bar{p}} > 3.7 \times 10^6 \text{ sec} .$$

These measurements represent an enormous gain in accuracy and it is tempting to ask what lifetime limit can be achieved with LEAR. Is it possible to reach a limit comparable to the age of our universe, which is approximately 10^{17} sec?

The sensitivity of direct lifetime measurement in ICE was limited by the beam losses due to rest gas interactions. An improvement of vacuum and beam cooling could overcome this problem; however, the accuracy is then limited by the finite measuring time t and the relative precision η with which the beam intensity can be measured:

$$\tau > t \cdot \eta \cdot \gamma \ , \qquad \text{where } \gamma \text{ is the Lorentz factor}$$

With this method a lifetime limit of 10^{10} sec can probably not be exceeded.

The search for an antiproton decay can increase the sensitivity considerably. Although it depends on assumptions concerning the possible decay channel, this presupposition can be kept rather general. The lifetime limit for the proton was obtained in the same way.

For such a measurement it is essential to cover a large solid angle Ω and to achieve a high detection efficiency ε. Hence a small ring with large straight sections as in LEAR is favourable. The cosmic-ray background can be suppressed by reconstructing the track of the charged particle and by a better energy resolution. The sensitivity of the method depends directly on the number of stored antiprotons and the measuring time:

$$N_{decay} = N_{\bar{p}} \cdot \Omega \cdot \varepsilon \cdot BR \cdot \frac{t}{\gamma \cdot \tau} \ .$$

In LEAR 10^{11} antiprotons and more can be stored. With a similar solid angle and detection efficiency as in the ICE experiment this would immediately push the lifetime limit to $\sim 10^{13}$ sec, if no decay were to be observed. Such a measurement has the great advantage that it can run in parallel with any other measurement and is independent of the operation mode of LEAR. Moreover it does not consume antiprotons at all. The data evaluation would presumably be extremely simple, since there would hopefully be only few events! Such an experiment could also be done in the AA (Antiproton Accumulator) and could run whenever the AA is working. The measuring time could thus be extended considerably. However, it would still be difficult to reach a lifetime limit of the order of the age of the universe.

3. ANTIPROTON MASS

The antiproton mass had been deduced from the X-ray energies of antiprotonic atoms. The energies were in the region between 100 and 300 keV.

The X-ray transitions were measured with solid-state detectors to an accuracy of 15-20 eV. This led to a mass determination[5] of

$$m_{\bar{p}} = 938.179 \pm 0.058 \text{ MeV} .$$

Hence the relative mass difference between proton and antiproton is

$$\frac{m_p - m_{\bar{p}}}{m_p} = (7.6 \pm 3.9) \times 10^{-5} .$$

With the high antiproton rate from LEAR the statistics of such measurements can be improved drastically, allowing for the use of detectors with higher resolution, e.g. small solid-state detectors and crystal spectrometers. A gain in the precision by one order of magnitude can be expected. The intrinsic problem of the mass determination from X-ray measurements however remains. This is the calculation of the energies of the atomic states. Below a level of 10^{-5}, higher-order QED effects and other corrections to the energies of the states come into play in a not well known way.

Because of these problems in the absolute determination of the antiproton mass, and since the proton mass is known only to 2.9 ppm, the emphasis is put on measuring the difference or ratio of proton and antiproton mass. The simultaneous storage of protons and antiprotons allows for a direct comparison of their masses without the roundabout way of an absolute measurement. The idea is to use the relation between the revolution frequency and the mass of a circulating particle[6]. There are several ways to make use of this relation. At low energies the simple formula

$$\omega = \frac{e}{m} B$$

allows a direct determination of the mass ratio through the measurement of the ratio of cyclotron frequencies

$$\frac{m_{\bar{p}}}{m_p} = \frac{\omega_p}{\omega_{\bar{p}}} .$$

For non-relativistic energies this quantity is independent of the orbital radius and of the momentum of the circulating particles. The value of the magnetic field does not need to be known absolutely; however, it has to be

made sure that the circulating particles are exposed to the same field. Cooled antiprotons from LEAR can be injected at low energies (below 100 MeV/c) into a small cyclotron. Protons can be stored in the same cyclotron by injecting them from the other side. The polarity and magnitude of the magnetic field has not to be changed. The revolution frequencies can be measured with Schottky pick-up electrodes. As we know from ICE for a Schottky scan a low antiproton intensity is sufficient and a signal can be obtained within a few minutes. The knowledge of the relative change of the magnetic field in the region of the orbits determines the accuracy. From the g-2 experiment it is known that magnetic fields can be measured to a relative accuracy of 10^{-7}. This leads to a similar precision for the determination of the mass ratio.

During this workshop another method for the determination of the antiproton mass has been suggested[7]. It was proposed to capture antiprotons at extremely low energies into a penning trap. Here again the oscillation frequency is measured and emphasis is put on a direct comparison with the corresponding values for the proton. An estimate for the precision gives 10^{-6}.

4. MAGNETIC MOMENT OF THE ANTIPROTON

The magnitude of the magnetic moment of the antiproton has been deduced from the fine-structure splitting of X-ray transitions in antiprotonic atoms[5]. The sign was determined from the intensity ratio of the fine-structure components. The energy of the X-ray transitions was around 300 keV and the fine-structure splitting was of the order of 2 keV. The X-ray energies were measured with the same accuracy as in the mass measurement and a value of

$$\frac{\mu_p - \mu_{\bar{p}}}{\mu_p} = (0.4 \pm 7.2) \times 10^{-3}$$

was obtained. Again the precision was limited by the statistics and the resolution of the detectors. An increase of one order of magnitude can be expected with the higher antiproton rates, allowing for the use of small high-resolution detectors. Another possibility is to measure the fine-structure splitting in $\bar{p}p$ atoms formed in flight[8], by inducing transitions between fine-structure levels with a laser. This method makes use of the Doppler shift in the transition energies of the moving $\bar{p}p$ system. While fixing the laser frequency the energies can be matched

by tuning the velocity of the $\bar{p}p$ atoms. The sensitivity of this method is then given by the accuracy with which the beam momentum can be measured and taking into account the beam momentum spread.

Also the capture of antiprotons in a penning trap would allow the measurement of the magnetic moment by inducing spin-flip transitions[7]. However, as regards the mass measurement, the antiproton deceleration, the trapping efficiency and the necessity of working at helium temperature complicate the experiment.

5. ANTINEUTRON MASS

The antineutron mass has not been measured yet. With LEAR, tagged antineutrons of moderate intensities can be produced through the charge-exchange reaction[9]. The antineutron mass can be determined by measuring the time of flight of slow antineutrons. With the present time resolution of scintillation counters a precision of the order of 10^{-3} can be anticipated. Owing to the low production rate of antineutrons and the small solid angle the event rate would be very small and background problems may arise.

The antineutron mass can also be deduced from the threshold of the charge-exchange reaction in hydrogen $\bar{p} + p \rightarrow \bar{n} + n$. The invariant mass is determined by the antiproton momentum leading to a boost factor of $\beta_{\bar{p}} \cdot p_{\bar{p}}$ in the energy resolution. Since antiproton beams from LEAR have small $\Delta p/p$ a good energy resolution can be obtained. A large solid angle can be covered and the experiment can be done in parallel with charge-exchange cross-section measurements. A precision below 10^{-3} can be reached depending on the determination of the energy loss of the antiprotons in the charge-exchange target.

6. ANTINEUTRON LIFETIME

The antineutron intensities from LEAR are still too low for a determination of the antineutron lifetime. If the antineutron lifetime is around 1000 sec, less than one decay per day can be observed using a time window of 1 μsec.

7. ANTIDEUTERON MASS

Along with antiprotons also a small number of antideuterons are produced on the production target for the AA. The estimated yield[10] is $10\ \bar{n}/10^{13}$ p. Although this yield is very low, antineutrons can possibly

be accumulated in the AA to give $\sim 10^5$ $\bar{d}$/day. This number would be sufficient for a mass measurement. Again the mass can be deduced from the revolution frequency. Since the absolute value has to be measured, the accuracy depends on the knowledge of the average magnetic field which may lead to a precision of about 10^{-3}.

8. CONCLUSION

With LEAR the particle properties of antinucleons can be measured several orders of magnitude better than before. The largest improvement can be expected for a limit of the antiproton lifetime. High precision can be achieved also for the determination of the antiproton mass in a relative measurement with respect to the proton. An accuracy of the order of 10^{-3} to 10^{-4} can be expected for the magnetic moment of the antiproton and it can be of about 10^{-3} for the mass of the antineutron.

* * *

REFERENCES

1) W. Hardt et al., Conceptual study of a facility for low-energy antiproton experiments, CERN PS/DL/Note 79-1, 1979.

2) S.N. Ganguli et al., Phys. Lett. 74B, 130 (1978).

3) N. Bregman et al., Phys. Lett. 78B, 174 (1978).

4) M. Calvetti et al., Antiproton lifetime measurement in ICE with counter technique, to be published.

5) E. Hu et al., Nucl. Phys. A254, 403 (1975).
P. Roberson et al., Phys. Rev. C 16, 1945 (1977).

6) H. Poth, Phys. Lett. 77B, 321 (1978).

7) G. Torelli, $\bar{p}$ LEAR-Note 16 (1979).

8) U. Gastaldi, $\bar{p}p$ experiments at very low energies using cooled antiprotons, Presented at the IV European Antiproton Symposium, Barr, 26-30 June, 1978.

9) C. Voci, $\bar{p}$ LEAR-Note 20 (1979).
H. Poth, $\bar{p}$ LEAR-Notes 15 and 51 (1979).

10) H. Koch, $\bar{p}$ LEAR-Note 42 (1979).

INVESTIGATIONS ON BARYONIUM WITH STOPPED ANTIPROTONS

H. Koch*)

Institut für Experimentelle Kernphysik,

Kernforschungszentrum und Universität, Karlsruhe, Germany

In this talk a brief review of the evidence for baryonium states below the $\bar{N}N$ threshold (1877 MeV) is given and future experimental possibilities are discussed.

1. THEORETICAL PREDICTIONS

For the $\bar{N}N$-baryonium states the potential model[1] predicts many states near the threshold with widths between 1-100 MeV, while quark models, e.g. the diquark-$\overline{\text{diquark}}$ model of Chan Hong-Mo[2], predict considerably less narrow states. In addition to the $\bar{N}N$ states, the potential model allows also heavier baryonium systems, e.g. $\bar{N}NN$, which may have a surprisingly long lifetime and consequently narrow widths (10 MeV). These heavier systems will not be discussed in this talk.

2. METHODS FOR DETECTING THE $\bar{N}N$ STATES BELOW THRESHOLD

2.1 Experiments on deuterium (spectator technique)

Antiproton-proton systems as well as $\bar{p}n$ systems can be formed from $\bar{p}$ stopping in deuterium. This is illustrated in graphs (a) and (b) below:

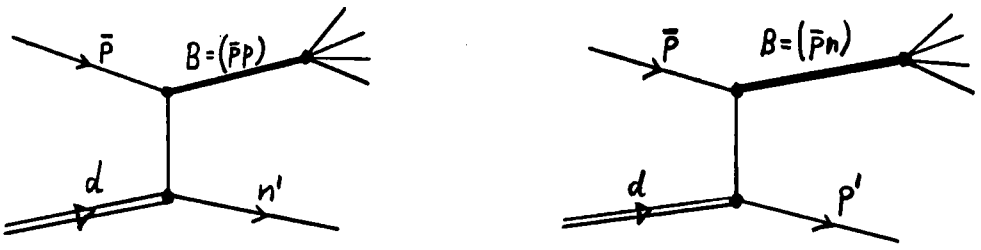

a) b)

An accurate energy measurement on the spectator nucleon (n′ or p′) yields the Q-value of the reaction and thus the mass of the baryonium system B. For (a) there holds the relation: $Q = m_B - 2m_N = -\frac{3}{2} T_{n'}$, with the nucleon

*) Visitor at CERN, Geneva, Switzerland

mass m_N and the kinetic energy of the spectator neutron $T_{n'}$. This very elegant method gave the first hints on baryonium states in the $(\bar{p}n)$ system[3], where the reaction (b) was investigated in a bubble chamber experiment, and two peaks at 1794 and 1877 MeV with widths smaller than 7 and 10 MeV, respectively, were found (see Fig. 1). The only drawback of the method may be possible initial and final-state interactions which may influence the energy spectrum of the spectator nucleon.

At Brookhaven and CERN, two experiments looking for the energy distributions of the spectator nucleons have now started data-taking. While the Brookhaven set-up uses a good neutron TOF detector, the CERN experiment uses a high resolution spectrometer to measure the proton spectrum accurately. Both experiments run not only on stopped antiprotons, but also on antiprotons in flight, which enables them to see the same structure under different kinematical conditions and thus get a first idea of some quantum numbers.

2.2 Monoenergetic γ, $\pi^{\pm}$, and π^0 transitions in the $\bar{N}N$ system

2.2.1 Monoenergetic γ transitions in the $\bar{p}p$ system

How monoenergetic γ-rays can tell us about bound baryonium states is best seen in a simplified energy level scheme of the $\bar{p}p$ system:

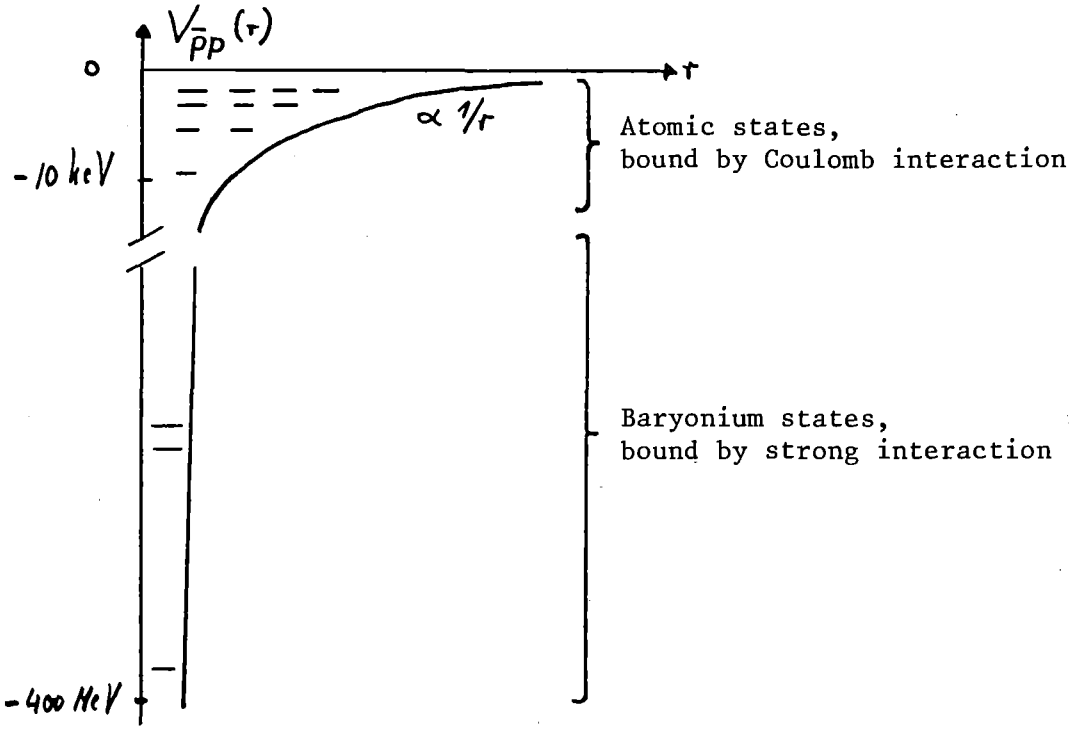

An antiproton which is slowed down in hydrogen is finally captured by a hydrogen atom and forms an electromagnetically bound $\bar{p}p$ system with a maximal binding energy of about 10 keV. In liquid hydrogen, mostly S-states will be populated at low main quantum numbers, while in low-pressure gaseous hydrogen, also states with higher angular momentum will be populated because of the smaller Stark mixing. The dominant decay mode of the atomic levels is the annihilation into $\pi^{\pm}$ and π^0 particles, but it is expected that with a small yield (10^{-2}-10^{-3} per $\bar{p}p$ atom) monoenergetic electromagnetic transitions to a deeply bound baryonium state should occur. If these states have widths below 10-100 MeV, they should be visible as narrow structures on a high background originating from the π^0-decays of the annihilation process.

The first search for such structures was performed at Brookhaven, where only an upper limit of 10^{-2} for the yield of such lines was found[4]. The first positive evidence for such structures has been obtained at CERN, where the inclusive γ spectrum of the $\bar{p}p$ system was measured[5]. As shown in Fig. 2, four narrow structures are visible above the huge π^0 background. One of these structures (γ energy, 130 MeV) probably belongs to the reaction $\pi^- p \to n\gamma$, while the three others, at energies of 183, 216, and 420 MeV, could be interpreted as first hints of baryonium states which then would lie at total energies of 1684, 1646, and 1395 MeV. The same system, but with subtracted smooth π^0 background, is shown in Fig. 3. The yield of the structures is about 7×10^{-3} per $\bar{p}p$ system. At this Workshop an explanation for two of these lines has been offered in terms of reactions of secondary kaons with the hydrogen of the target. As the production rate of kaons in $\bar{p}p$ annihilations is only about 1% and the reactions under consideration have very small yields -- the yield of $K^- p \to \Sigma^0\gamma$ is, for example, less than 4×10^{-3} -- this means a total γ yield of 4×10^{-5}. This value seems to be at least two orders of magnitude too small to give relevant contributions.

The CERN experiment is at present being repeated with an improved set-up (Fig. 4) in an attempt to distinguish between different annihilation channels -- just by counting the charged particles and the gammas in an almost 4π detector -- in order to improve the peak-to-background ratio. This is possible because of the different energy spectrum of neutrals in different channels. The second improvement consists of a much larger NaI

detector with good energy resolution. Because of its modular structure -- it consists of 54 independent modules -- it will allow a good position sensitivity for neutral events and a better understanding of background not originating from the target. The measurements are in progress. The data analysis is far from being complete, so that no definite statements can be made yet.

2.2.2 Monoenergetic $\pi^{\pm}$ and π^0 transitions in the $\bar{N}N$ system

It is quite possible that transitions between two different states of baryonium may be accompanied by the emission of a monoenergetic charged or neutral pion, a process which might be even more probable than the emission of a monoenergetic γ [6,7]. No measurements on the $\bar{N}N$ system have been reported so far, but an experiment at CERN and another at Brookhaven have started to look for monoenergetic charged pions. They use a range telescope and a high resolution spectrometer, respectively.

3. THE SITUATION IN GENERAL

Although some evidence for the existence of baryonium states below threshold has been obtained from past experiments, the situation is far from being clear. This is mainly for two reasons: i) all experiments suffer from too low statistics due to the low intensity of the $\bar{p}$ beams; ii) the coincident background, originating from the annihilation process, consists in general of many charged and neutral particles. With the present detectors it cannot be analysed quantitatively, so that only inclusive measurements were possible. This fact has so far excluded the determination of quantum numbers for the states.

Problem (i) can be overcome by the availability of the Low-Energy-Antiproton Ring (LEAR). Because of the small $\Delta p/p$ of the beam and its high intensity, high-statistic runs on gaseous hydrogen targets will be possible. The change of the gas pressure will allow a change in the population of the atomic states, and so more information can be obtained for the quantum numbers of the baryonium states. Problem (ii) can generally only be solved by the use of a detector for the neutral and charged annihilation products, with a large solid angle which allows a complete reconstruction of the events and the determination of the quantum numbers of the states (exclusive measurements).

How this would work in the search for monoenergetic γ's is illustrated in Fig. 5, which shows a Monte Carlo calculation of a γ-line originating with a yield of 1% in the annihilation channel $\rho^{\pm}\pi^{\mp}$ (2.7%)[8]. The upper spectrum shows the line sitting on a high neutral background ($\rho^{+} \rightarrow \pi^{+}\pi^{0} \rightarrow \pi^{+}\gamma\gamma$). This spectrum corresponds to the present situation, where no distinction between a monoenergetic γ and the two γ's from the π^0 decay is possible. The lower spectrum shows a dramatic increase in the peak-to-background ratio, which can be achieved using a γ detector of nearly 4π solid angle with realistic energy and angle resolution. In more complicated annihilation channels, similarly striking effects are obtained.

From the foregoing it becomes clear that only by the combination of LEAR and improved detection systems can a definite answer about the baryonium states and their quantum numbers be obtained. Although it might be possible to obtain limited information from smaller detector set-ups, a nearly 4π detector seems highly desirable. What this could look like is briefly sketched in the following section.

4. POSSIBLE EXPERIMENTAL SET-UPS

The principle of the set-up is dictated by the physical processes of interest. Around a gaseous hydrogen (deuterium) target, one would like to have a large solid angle counter for low-energy X-rays (1 keV $\leq E_{\gamma} \leq$ 10 keV) which allows triggering on, for example, the atomic 2p $\rightarrow$ 1s state and so makes sure that the event has started from the $\bar{p}p$ ground state. This is probably best realized by a gas-proportional counter of cylindrical geometry, as discussed during the Workshop[9]. Around the proportional chamber a set-up of cylindrical drift chambers would be needed to count the charged particles, to determine their direction (vertex reconstruction), and -- in combination with a magnetic field -- to measure their momenta. The detection of γ's must be done in a nearly 4π counter with the energy and angle resolution that are necessary for reconstructing the π^0 and thus disentangling the π^0-γ's from the single γ's. An instrument with these specifications would be a NaI crystal ball, such as the one at present in use at SLAC. Preliminary results of a test of a part of the crystal ball, in a $\bar{p}$ beam at CERN, look very promising and yield also not too bad performances for the detection of charged pions of not too high energy[10].

Two possible set-ups for such a system are sketched in Fig. 6. The set-up in Fig. 6a is optimized for the detection of neutrals. It would guarantee a very good reconstruction of π^0 events, while the energy determination for charged particles would be only moderate. The set-up in Fig. 6b uses a magnetic field and so there would be a good energy determination of the charged particles. However, the π^0 reconstruction would be very bad. Therefore, for the investigation of baryonium events, a detector of the type shown in Fig. 6a would be highly preferable.

It should be stressed that such a device would not only be of use for baryonium experiments, but could also be useful for different experiments which have been discussed during the Workshop: a) detection of interesting annihilation channels, e.g. $\bar{p}p \to \pi^0\pi^0$ (in flight and at rest); $\bar{p}p \to \eta\pi^0$. b) Charmonium spectroscopy in collider mode: $\bar{p}p \to \chi' \to \chi + \gamma$. c) Search for unknown resonances in neutral annihilation channels. d) HFS of $\bar{p}p$ atomic levels, coincidence with only π^0's.

5. NEEDS FROM CERN

For a complete series of experiments on baryonium, only moderate performances of LEAR are requested. An extracted beam of variable intensity is needed in order to handle the rate problems in the data-taking of the 4π detector. The $\Delta p/p$ of the extracted beam should be as good as possible, in order to be able to stop all antiprotons in a thin hydrogen gas target. However, even if the momentum spread is larger than 10^{-3}, the stop-events can be found with the help of the vertex reconstruction by the drift chambers, so that no big problems would occur there. This means that this type of baryonium experiment could be considered as one of the first experiments at LEAR, because not many sophisticated features are required.

* * *

REFERENCES

1) I.S. Shapiro, Phys. Reports 35 (1978) 129.

2) Chan Hong-Mo, This Workshop.

3) L. Gray et al., Phys. Rev. Lett. 26 (1971) 1491.

4) T. Kalogeropoulos et al., Phys. Rev. Lett. 35 (1975) 824.

5) P. Pavlopoulos et al., Phys. Lett. 72B (1978) 415.

6) C.B. Dover and M.C. Zabek, Brookhaven National Laboratory, BNL-24362 (1978).

7) G. Dosch and B. Povh, MPI-H-1978-V6 (1978).

8) P. Pavlopoulos, LEAR-Note 27.

9) E. Klempt, LEAR-Note 25.

10) M. Suffert, LEAR-Note 41.

Figure captions

Fig. 1 : Momentum spectrum of spectator protons in the reaction $\bar{p}d \to (\bar{p}n) + p_{spect.}$ Upper curve: $2\pi^-\pi^+\pi^+(1667) + 3\pi^-2\pi^+\pi^+(660)$; lower curve: $2\pi^-\pi^+(248) + 3\pi^-2\pi^+(437)$.

Fig. 2 : Inclusive γ spectrum of the $\bar{p}p$ reaction at rest.

Fig. 3 : Same spectrum as Fig. 2, but smooth annihilation background subtracted.

Fig. 4 : Experimental set-up for detection of a monoenergetic γ in coincidence with a selected annihilation channel.

Fig. 5 : Monte Carlo calculations of a single γ-line above a continuous background originating from π^0's.

Fig. 6 : Possible set-ups of a complete experiment for baryonium physics.

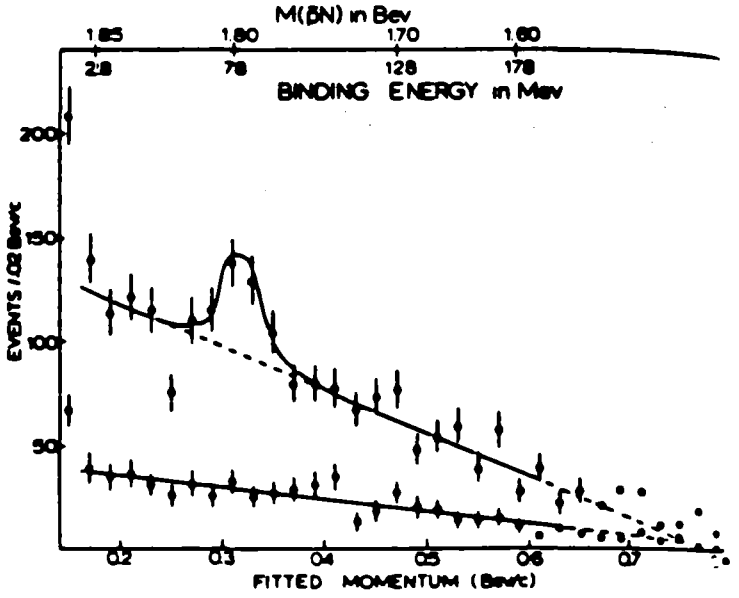
M(ΣN) in Bev
1.85
1.80
1.70
1.60
28
78
128
178
BINDING ENERGY in Mev
200
150
100
50
EVENTS / 02 Bev/c
0.2
0.3
0.4
0.5
0.6
0.7
FITTED MOMENTUM (Bev/c)

Fig. 1

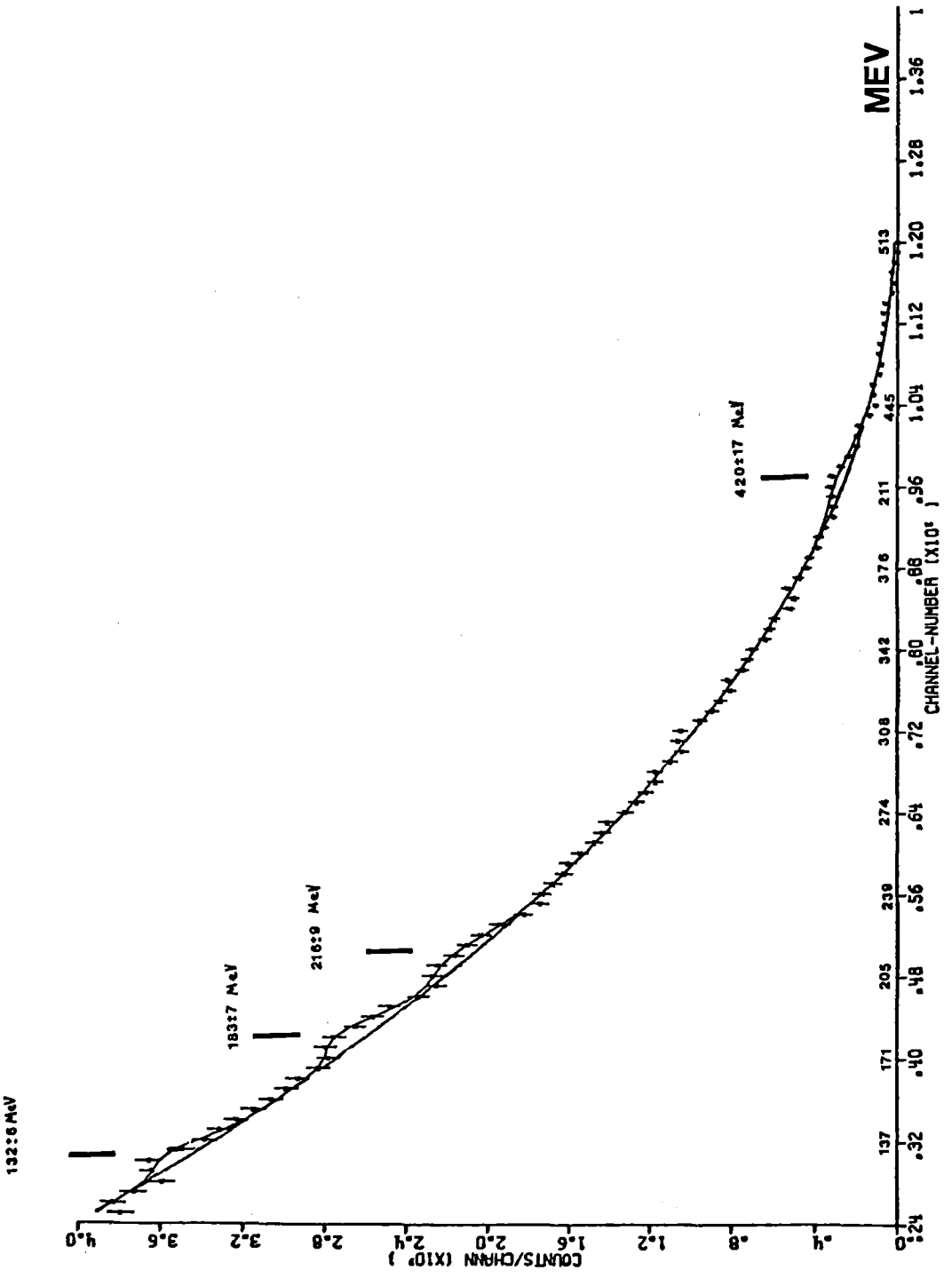
132±6 MeV
183±7 MeV
216±9 MeV
420±17 MeV
COUNTS/CHANN (X10³)
CHANNEL-NUMBER (X10¹)
MEV

Fig. 2

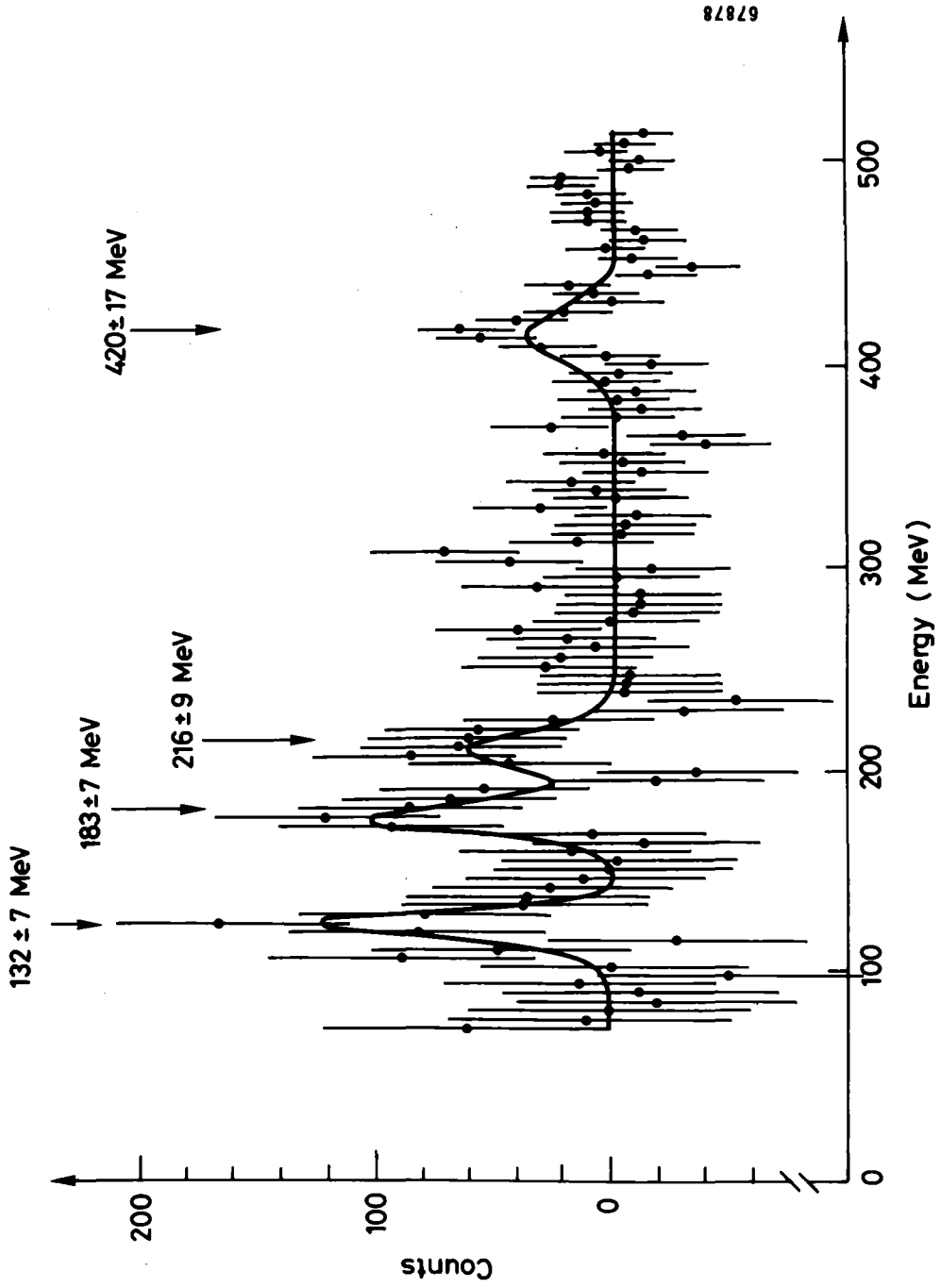
67878
132 ± 7 MeV
183±7 MeV
216±9 MeV
420± 17 MeV
Counts
200
100
0
0
100
200
300
400
500
Energy (MeV)

Fig. 3

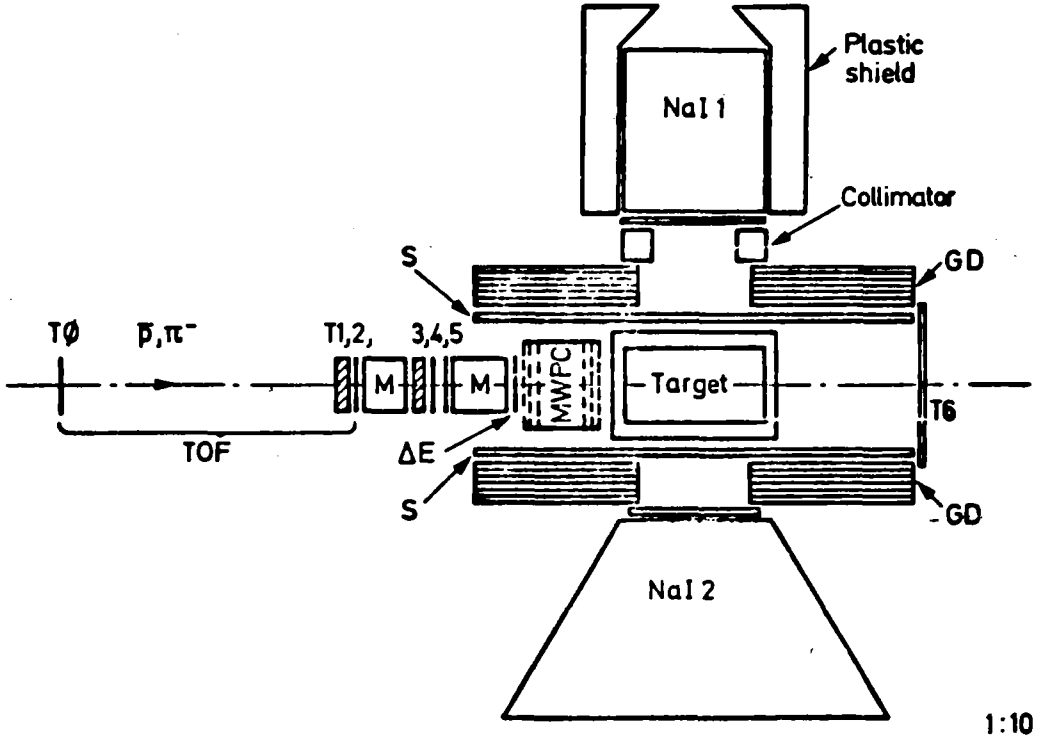

Tø,... T6 : Telescope counters

ΔE : High resolution ΔE-counter

S : Cylindrical scintillation counter

GD : Cylindrical Gamma detector

MWPC: Multiwire proportional chambers

M : Moderator

Fig. 4

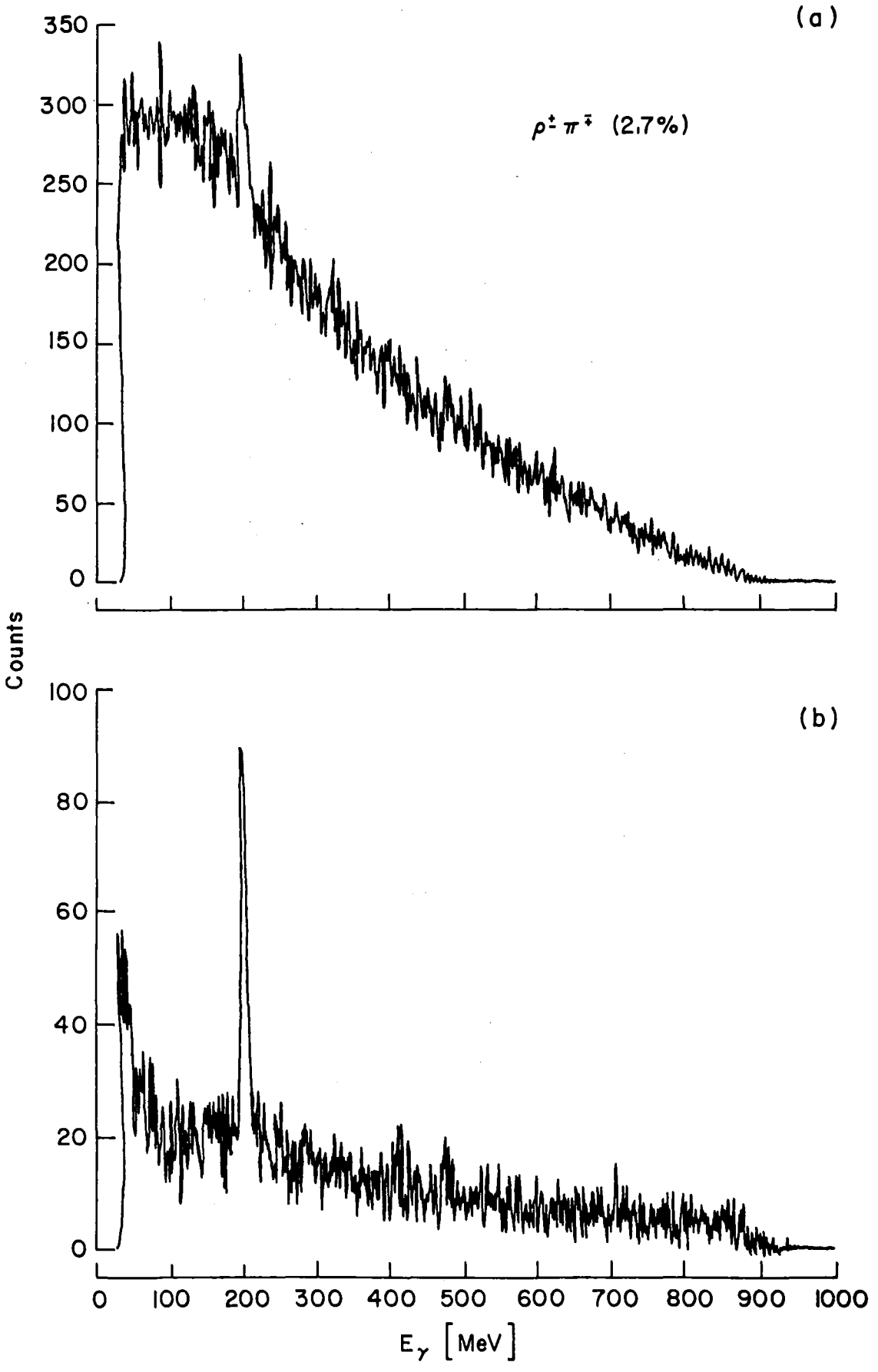
(a)
$\rho^{\pm}\pi^{\mp}$ (2.7%)
350
300
250
200
150
100
50
0
Counts
(b)
100
80
60
40
20
0
0
100
200
300
400
500
600
700
800
900
1000
E_γ [MeV]

Fig. 5

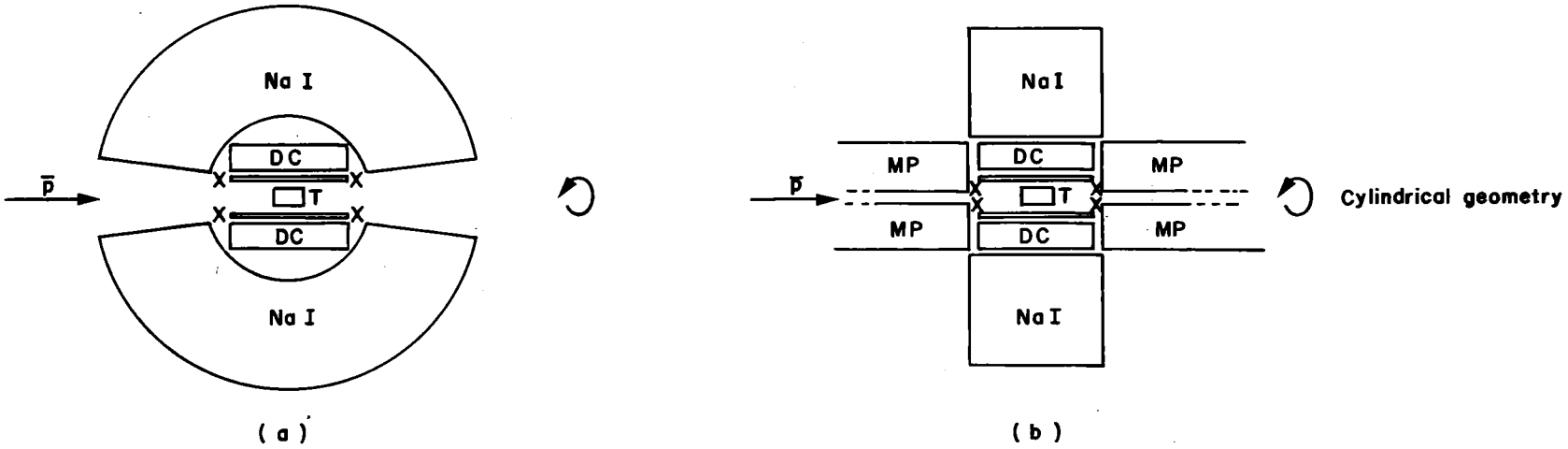

T = Target

X = X-ray prop. detectors

DC = Drift chambers

Na I = Na I- Detectors modular set-up

MP = Magnet poles

Fig. 6

BARYONIUM WITH ANTIPROTONS IN FLIGHT§

B. Povh

Max-Planck-Institut für Kernphysik, D-6900 Heidelberg

Quite some time ago the concept of baryonium states was introduced to antiproton physics based on formal considerations[1]. But it was not before the S resonance was established quite firmly that one started to speculate about the existence of *narrow* baryonium states. Only if this is the case, the investigation of the antiproton-proton system opens the rich possibility of studying the dynamics of quarks in baryons. Let me first start with the nonexotic baryonium states called "T baryonium" by Chan. Averaging the theoretical predictions for the width I concluded that there is no good guess about it. This constitutes our main headache and is the main reason for limiting our optimism concerning baryonium spectroscopy. But the physical concept of the baryonium is so close to our present physical picture of the baryon-antibaryon interaction that it challenges the experimentalist either to establish its existence and properties or to eliminate the subject once for all from the discussions.

In the last few years the numerous theoretical papers on baryonium have kindled this subject. Obviously, there has not been much constraint of experimental data to limit the free imagination of the theoreticians. The poor quality of the experimental data is entirely due to the inadequate quality of the antiproton beams at low energies. This situation can best be demonstrated by reporting on some results on the antiproton-proton cross section measurements.

In the last ten years quite a few resonances have been observed in the antiproton-proton cross section but not many have survived a second, closer inspection. One of the exceptions is the resonance at 1.94 GeV excitation observed

---

§Presented at the workshop on physics with LEAR held at Karlsruhe, March 1979.

in several different experiments - for example, in 1974 in an experiment by a group at Brookhaven[2] - in the total cross section for antiprotons on hydrogen and deuterium. The resonance was found to be quite narrow, with a width of only about 10 MeV. Considering the annihilation channel, which dissipates an energy of 2 GeV, this width is very small. But it is also small if scattering alone is taken into account, since the resonance is 60 MeV above the proton-antiproton threshold. Two groups at CERN have been searching for such narrow resonances in the antiproton-proton formation cross section at antiproton momenta below 700 MeV/c; in this momentum region a good energy resolution can be achieved with the present experimental techniques. Both groups observed[3,4] narrow resonances at 1.94 GeV mass in both the elastic and the annihilation channels, with about equal cross sections. Since the phase space available for the annihilation is much larger than that for the elastic scattering, it is obvious that the 1.94 GeV resonances is predominantly due to the elastic channel.

In all the experiments so far, the experimental resolution has been insufficient to determine the natural width of the resonance. In Figure 1 the results of a Heidelberg group are shown; in this experiment the upper limit for the width is claimed to be 4 MeV. At the Tokyo meeting the bubble chamber results of Brookhaven[5] were presented which display the 1.94 GeV resonance with a width of 3 MeV only. But there were some rumors that the Berkeley group of Tripp could not verify the existence of the S resonance. Is the old story of resonances appearing and disappearing starting all over again? Antiproton beams at 500 MeV/c, where the resonance lies, have an intensity of about 100 $\bar{p}$/s. With a decent beam all these problems could be solved within a few hours.

A production experiment with 9 and 12 GeV pions and protons was performed with the Ω spectrometer at CERN. From all events very few were selected (Fig. 2) according to the requirement that one of the protons be fast and the second slow. For such events one chooses only those which in the rest frame of the slow proton-antiproton system (Jackson frame) have antiprotons moving backwards. Three resonances

were believed to be seen in this experiment (Fig. 2). There is some indication for the S resonance, but the narrow 2.02 and 2.2 GeV resonances were observed for the first time. Unfortunately, the experiment seems to be difficult to reproduce, and we either have to trust or to distrust the results for the time being.

A narrow 2.95 GeV resonance was once reported but soon revoked. The 2.2 GeV and this phantom 2.95 GeV resonance led Chan to devise a model for M baryonium which could explain why such narrow resonances could exist so high above the threshold. In fact, this model is the only one which explains why the baryonium resonances could be narrow - due to color excitation - but we do not know if this type of excitation is found in nature. Figure 3 summarizes the reported narrow antiproton-proton states not yet revoked. In addition to these narrow states broad T, U, and V resonances have been found above the antiproton-proton threshold.

How to search for baryonium? Figure 4 displays the most common reactions used for the search for T baryonium. I will select just two reactions used by the Heidelberg-Saclay-Strasbourg collaboration in its present experiment: (1) $\bar{p} + n \rightarrow p + X$ in knock-out mode; (2) $\bar{p}p \rightarrow \bar{\pi} + x$, equivalent to the $\bar{p}p \rightarrow \pi + \gamma$ reaction reported by Koch. All these reactions are chosen by just one criterion. They should populate preferentially bosonic objects with a geometrical extension larger than that of normal mesons. Independent of the model, baryonium is believed to be more extensive than the simple $q\bar{q}$ mesons. The experiments still are quite simple, measuring just the missing mass and hoping that the baryonium will show up with sufficient intensity in the background of annihilation. It was realized, however, that the question about the existence of baryonium is just one chapter of the annihilation story. And annihilation is a multi-body decay which, unfortunately, has to be studied with all the effort necessary for investigating such reactions. It seems to be more appropriate to attack the annihilation problem as the most fundamental one. It is just below 800 MeV/c that one can study pure annihilation; above this momentum the excitation of the

baryon resonances start to dominate. To study the complicated process of annihilation and hoping also to find the best trigger for baryonium the Heidelberg-Saclay group is preparing a proposal for an apparatus that could determine the decay products with sufficient accuracy. As a vertex detector a cylindrical jet chamber is being considered (Fig. 5) in conjunction with a 0^{o} spectrometer. In this way we may gain much new insight into the decay modes and the angular momenta of the states produced in the proton-antiproton reaction. At the same time, however, we are losing the simplicity and elegance of the low energy experiments and instead are getting closer and closer to the conventional tools of high energy physics.

Concluding, I would like to point out that we learned quite a lot at this workshop or, better to say, between the first workshop last year and the present one. In particular, LEAR - lets hope it will not be as tragic a figure as it was in Shakespeare's time - is not only interesting because of the baryonium but rather for being able to solve a large number of interesting problems with antiprotons, including the annihilation and baryonium. It is an exciting new facility for nuclear physics at CERN. The originality of the machine and the proposed program meet the high standard of nuclear physics performed at CERN in the past.

[1]J.L. Rosner, Phys. Rep. 11C (1974) 189; C. Rosenzweig, Phys. Rev. Lett. 36 (1976) 697; G.F. Chew, LBL Preprint No. 5391 (1976); G.F. Chew, contribution to the Third European Symposium on Antinucleon-Nucleon Interactions (Stockholm, July 1976); G.C. Rossi and G. Veneziano, CERN Preprint TH-2287, to be published in Nucl. Phys. B.

[2]A.S. Carroll et al., Phys. Rev. Lett. 32 (1974) 247.

[3]V. Chaloupka et al., Phys. Lett. 61B (1976) 487.

[4]W. Brückner et al., Phys. Lett. 67B (1977) 222.

[5]S. Sakamoto et al., contribution to the Tokyo Conf. 1978, preprint.

Figure Captions

Fig. 1 The excitation function for the pp annihilation into charged particles and for elastic scattering. The resonance seen at 505 ± 15 MeV/c corresponds to a c.m. energy of 1939 ± 3 MeV.

Fig. 2 The $p\bar{p}$ invariant mass observed in the reaction $\pi^- p \to p_f \bar{p} p \pi^-$ at 9 and 12 GeV pion momenta.

Fig. 3 Narrow baryonium states observed in production and formation experiments. The question marks indicate that the state has been observed in a single experiment.

Fig. 4 Reactions used for the search for T baryonium.

Fig. 5 A layout of an experiment investigating the $\bar{p}p$ annihilation with a 4π detector (jet chambers) and a magnetic spectrometer.

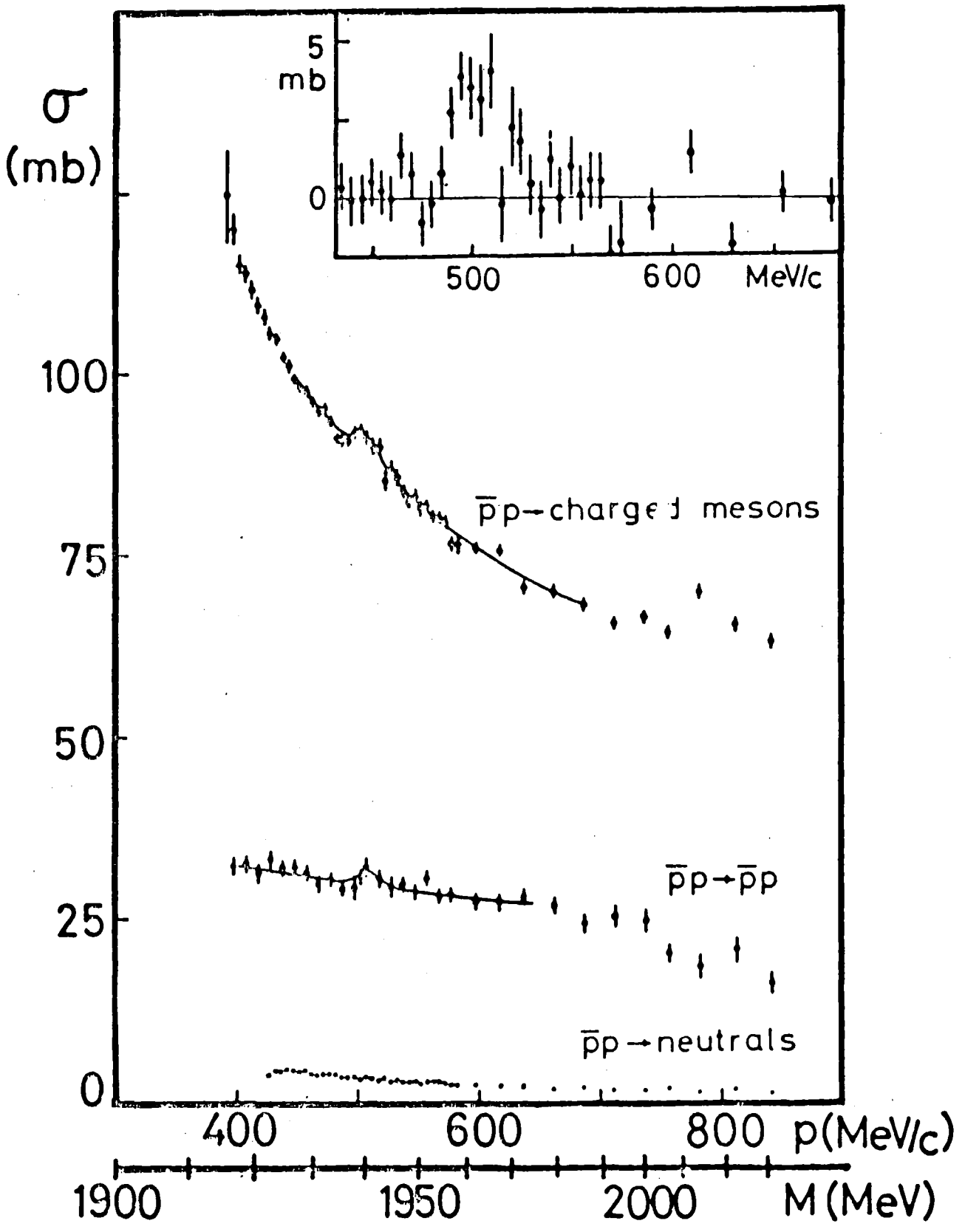
σ
(mb)
5
mb
0
500
600
MeV/c
100
75
50
25
0
p̄p→charged mesons
p̄p→p̄p
p̄p→neutrals
400
600
800
p(MeV/c)
1900
1950
2000
M(MeV)

Fig. 1

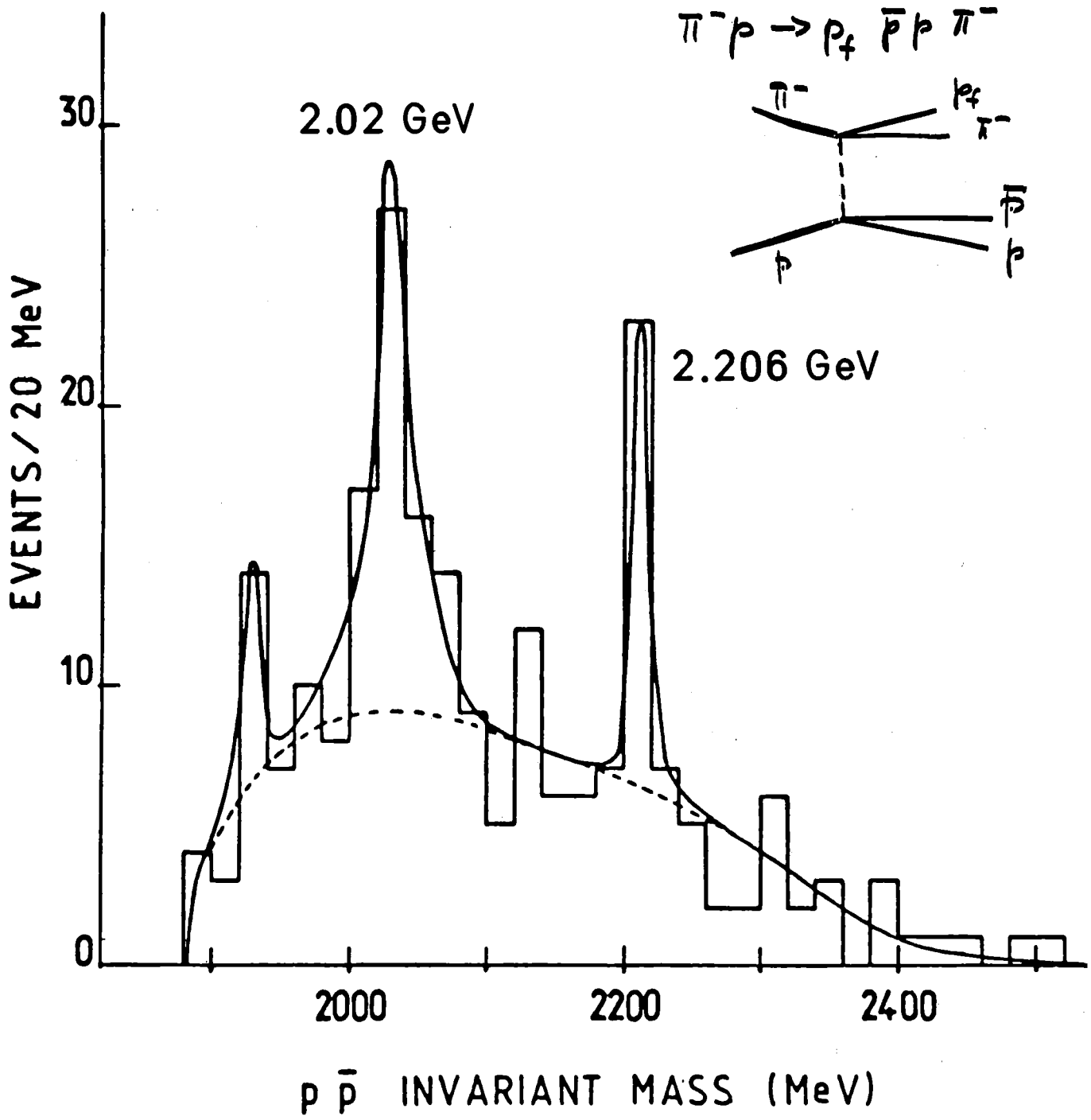
$\pi^- p \to p_f\ \bar{p} p\ \pi^-$
π^-
p_f
π^-
$\bar{p}$
p
p
2.02 GeV
2.206 GeV
EVENTS / 20 MeV
30
20
10
0
2000
2200
2400
p $\bar{p}$ INVARIANT MASS (MeV)

Fig.2

Narrow baryonium states

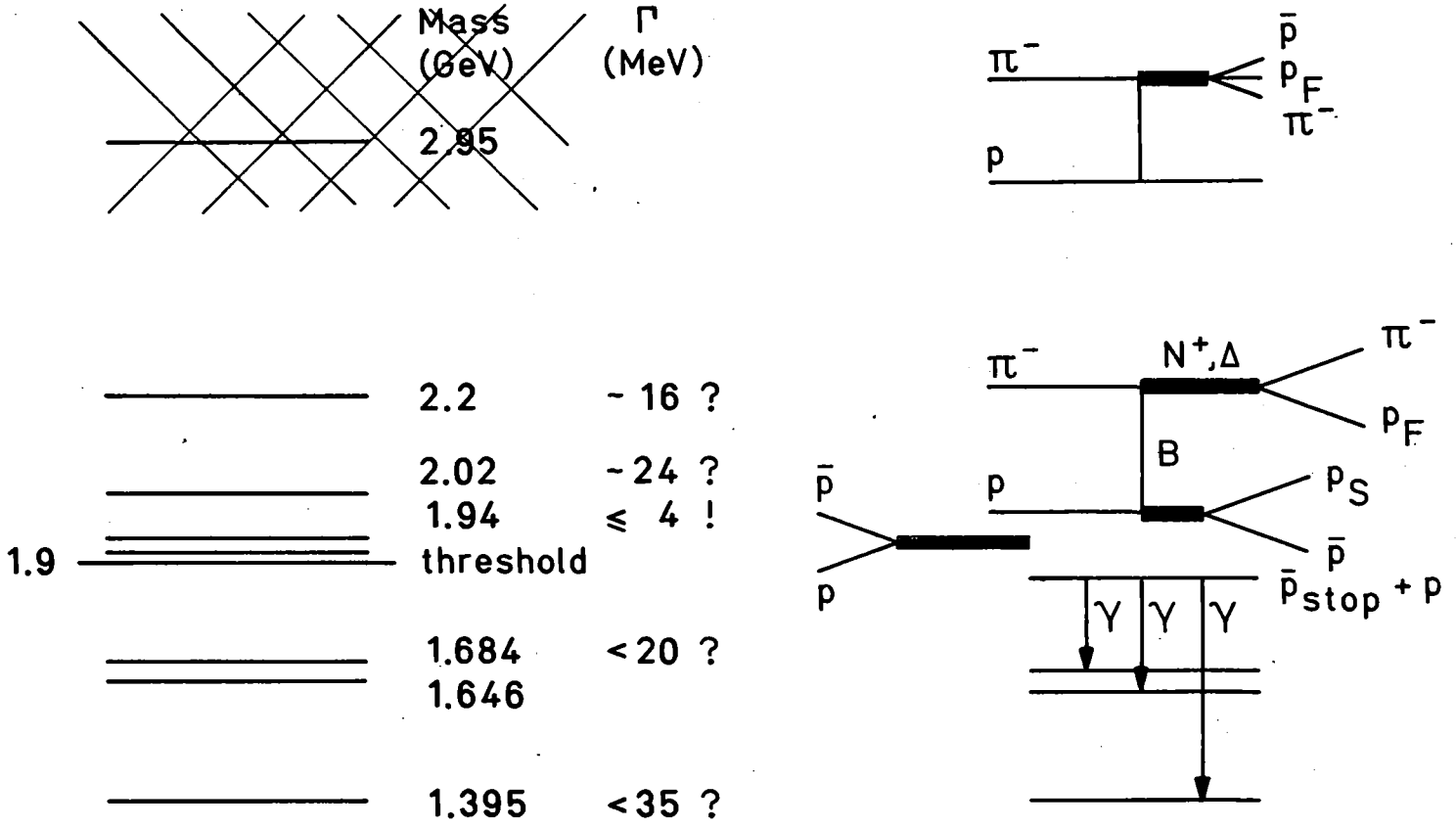

Fig.3

How to search for Baryonium?

1. Looking in the $\bar{p}+p$ decay

a) in formation $\bar{p}+p \to \bar{p}+p$

b) in production $\pi^- + p \to \pi^- + p + \bar{p}\cdot p$

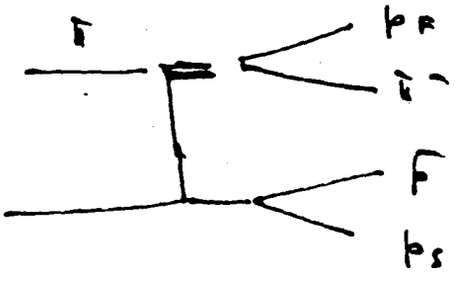

p seen backward in the "Jackson frame"

2.) $\bar{p} + d \to p + X$
$n + X$

$\bar{n} + d \to p + X$
$n + X$

a) Stripping mode

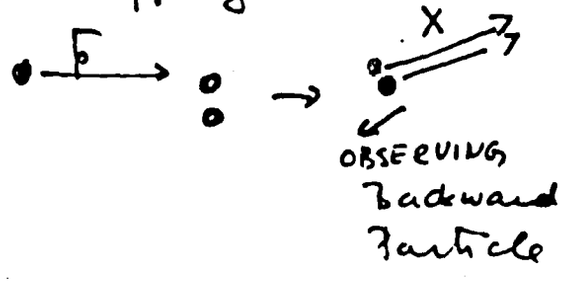

b) Knock out mode

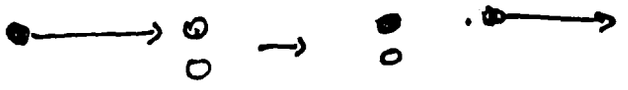

$\frac{d\sigma}{d\Omega} = \frac{d\sigma}{d\Omega}(180°) \neq^2$

3) $\bar{p} + p \to \pi^- + X$
$\gamma + X$

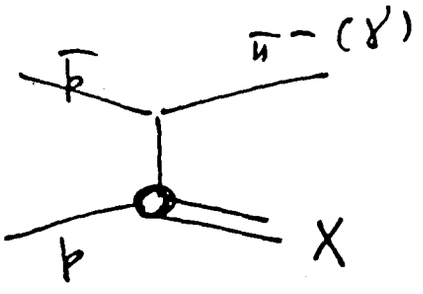

or

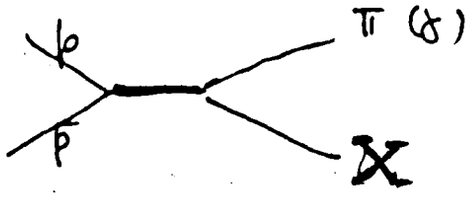

or . . .

Fig. 4

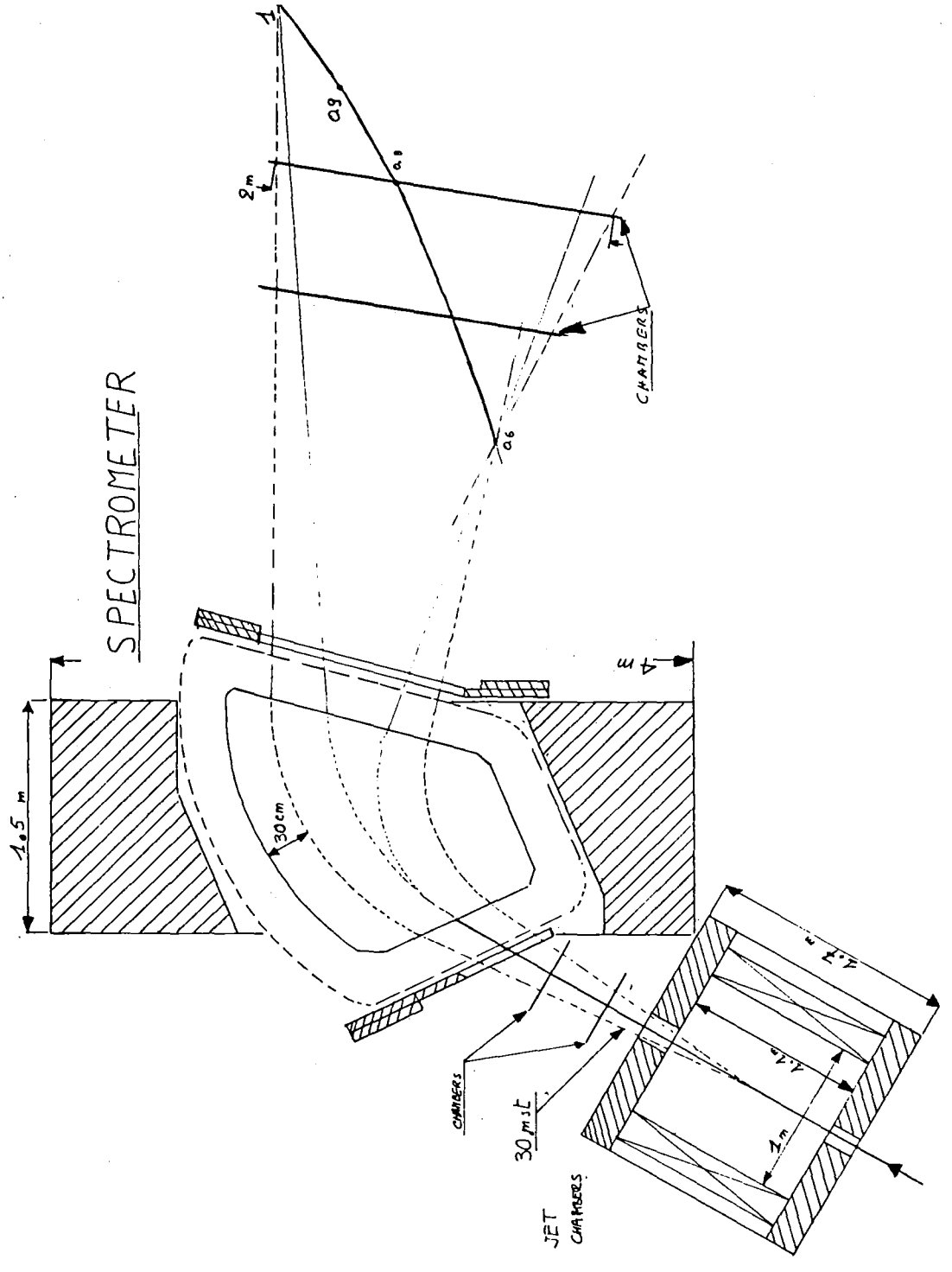
SPECTROMETER
1.5 m
30 cm
4 m
2 m
CHAMBERS
CHAMBERS
30 m st
JET CHAMBERS
1
a9
a1
a6

Fig.5

ANTIPROTONIC ATOMS

$\bar{p}$ LEAR-Note 70

E. Klempt

Institute of Physics, University of Mainz, F R G

I Introduction

The Low Energy Antiproton Ring will place at the experimental physicist's disposal antiproton beams of enormously enhanced quality. [1] Therefore, new experiments will be feasible, and the discovery of new phenomena is to be expected. Yet we have a trustworthy guide to anticipate future developments in the field of atomic physics using antiprotons, because it has only been a few years since meson factories have fully come into operation, and these were accompanied by a similar step in muon and pion beam quality. The meson factories led to a boost in intermediate energy physics using muons and pions, and a similar reinforcement of low energy antiproton physics must be expected.

The field of antiprotonic atoms - which is reviewed in ref. 2) - naturally breaks into two parts, both from the genuine interest point of view and from the experimental techniques. One part covers those antiprotonic atoms where antiprotons are bound by the Coulomb forces of a complex nucleus. Somewhat artificially we define antiprotonic helium to be the low Z limit of this field. Strong interaction effects in a selected choice of these atoms have been measured. By comparision with an optical potential model effective antiproton-nucleon scattering lengths were derived which describe the antiproton-necleus interaction over a wide range of the periodic system. Antiprotonic hydrogen and deuterium - as the second part of the field of antiprotonic atoms- deserve special attention as from these exotic atoms the elementary strong interaction at rest of antiprotons with protons and neutrons can be deduced. Furthermore, these two atoms link the field of atomic physics to the field of elementary paricle physics.

II ANTIPROTONIC ATOMS ($Z \geq 2$)

When antiprotons are brought to rest in matter they are captured by the Coulomb field of nuclei, thus forming antiprotonic atoms. The capture process is influenced by the state of aggregation, by chemical bonds or by effects of solid state physics, resulting in different intensity distributions or cascade times of the emitted X-rays [3]. Even though cascade measurements may expand to a separate field in exotic atom physics we will restrict ourselves to effects caused by the strong interaction between antiprotons and nuclei.

The energy levels of antiprotonic atoms are mainly determined by the Coulomb interaction between antiprotons and nuclei, but they are slightly shifted and broadened by the strong interaction. Effects due to the strong interaction can be observed best in the last circular observable transition of the antiprotonic cascade. A comparison of its measured energy with the energy calculated from QED determines the strong interaction shift E_{Low} of the lower level of this transition. The strong interaction width Γ_{Low} of this level can be determined by fitting the observed line shape by a folded Lorentzian plus Gaussian shape. The intensity of this line can be compared with the total x-ray intensity of x-rays feeding the upper level to derive the strong interaction width Γ_{up} of the upper level. Details of this method can be found elsewhere. [4]

In first order approximation strong interaction effects can be described by adding an optical potential of the form [5]

$$V(r) = -\frac{2\pi}{m_p}\left(1+\frac{m_p}{m_N}\right)^2 \left\{ A^{eff}_{\bar{p}p}\,\rho_p(r) + A^{eff}_{\bar{p}n}\,\rho_n(r) \right\}$$

to the potential due to the electromagnetic interaction (including finite size effects and QED corrections). The effective scattering lengths $A^{eff}_{\bar{p}p}$ and $A^{eff}_{\bar{p}n}$ have to be determined from antiprotonic atoms where the proton and neutron distributions $\rho_p(r)$ and $\rho_n(r)$ are known sufficient precisely. In nuclei where proton and neutron distributions are similar the isospin averaged scattering lengths $A^{eff}_{\bar{p}p}$ and $A^{eff}_{\bar{p}n}$ can be determined. Measurements

on different isotopic species are ideally suited to derive the effective antiproton neutron scattering length.

The effective scattering lengths describe the interaction of antiprotons with nucleons in nuclei. In the elementary scattering lengths $a_{\bar{p}p}$ and $a_{\bar{p}n}$ are to be calculated from these effective scattering lengths, the granularity of nuclei has to be taken into account as well as the fact that the relative momentum between antiproton and nucleon is smeared out by the Fermi motion [6]. Calculations connecting effective and lelementary scattering lengths would certainly benefit considerably if effective and elementary scattering lengths could be determined in independent experiments. The elementary scattering lengths can hopefully be derived from scattering data when LEAR comes into operation, or from strong interaction effects in antiprotonic hydrogen.

A different approach -a black sphere model - to fit strong interaction widths of antiprotonic atoms was chosen by Kaufmann and Pilkuhn. [7] Starting from the effective Coulomb potential of an antiprotonic atom they calculate the barrier penetration factor from an atomic state through the centrifugal barrier into the range of nuclear forces. They get good agreement with experimental data assuming that the chance of rescattering of antiprotons into the atomic orbit vanishes and that the "Nuclear Radius of no Return" is given by the prescription that 1.2 nucleons be outside that radius. So R is defined by

$$1.2 = \int_R^\infty \rho\,(r)\,dr \quad ; \quad \int_R^\infty \rho\,(r)\,dr = N$$

This number of 1.2 nucleons is obtained from Fermi or harmonic well distributions for nuclear densities. It is therefore model dependent. But the number proved to vbe valid for all elements where antiprotonic atom data are available. It will therefore be a powerful tool to discuss isotope nand isotone effects if strong interaction data are available over part of the periodic table.

In the field of muonic atoms it was shown by Fricke and collaborators [8] that measurements of the Barrett equivalent radii $R_k = \langle e^{-\alpha r} r^k \rangle$ of the last muonic transition in an isotope and isotone series of elements provide insight into questions like: how does the nuclear charge distribution change if a proton or neutron is added to a nucleus? What is the effect of the nuclear shell structure on the charge distribution ? Fig. 1 shows the differences in Barrett radii between adjacent nuclei. Nucleons filling the $1f_{7/2}$ nuclear shell obviously result in a much smaller increase in Barrett radius than those added into the $2p_{3/2}$ shell. These shell effects will be much more pronounced in antiprotonic atoms because of the fact that antiprotons scan density distributions dominantly at the nuclear surface.

Until now x-ray transitions from 26 antiprotonic atoms have been observed [9], including the lightest and the heaviest nuclei, hydrogen [10] and uranium. [11] But only for five atoms, for N, O^{17}, O^{18}, P, Zr, the three measurable quantities E_{Low}, Γ_{Low}, Γ_{up}, were simultaneously determined with an at least two or three standard deviation accuracy.

Fig. 2 shows data from antiprotonic oxygen for two isotopic species. [12] From these measurements strong interaction effects for the 3D and 4F level were deduced :

	Γ_{up}	Γ_{Low}	E_{Low}
^{16}O	0.64 (11)	320 (150)	-124 (36) eV
^{18}O	0.80 (12)	550 (240)	-189 (42) eV

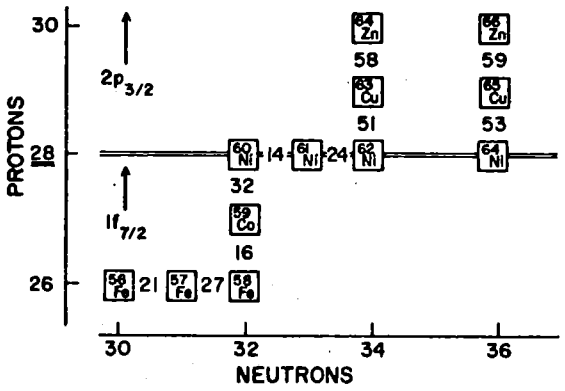

FIG. 1. Differences in the Barrett equivalent radii for adjacent odd-even nuclei (mfm). The experimental uncertainties in these values are typically 0.7 mfm

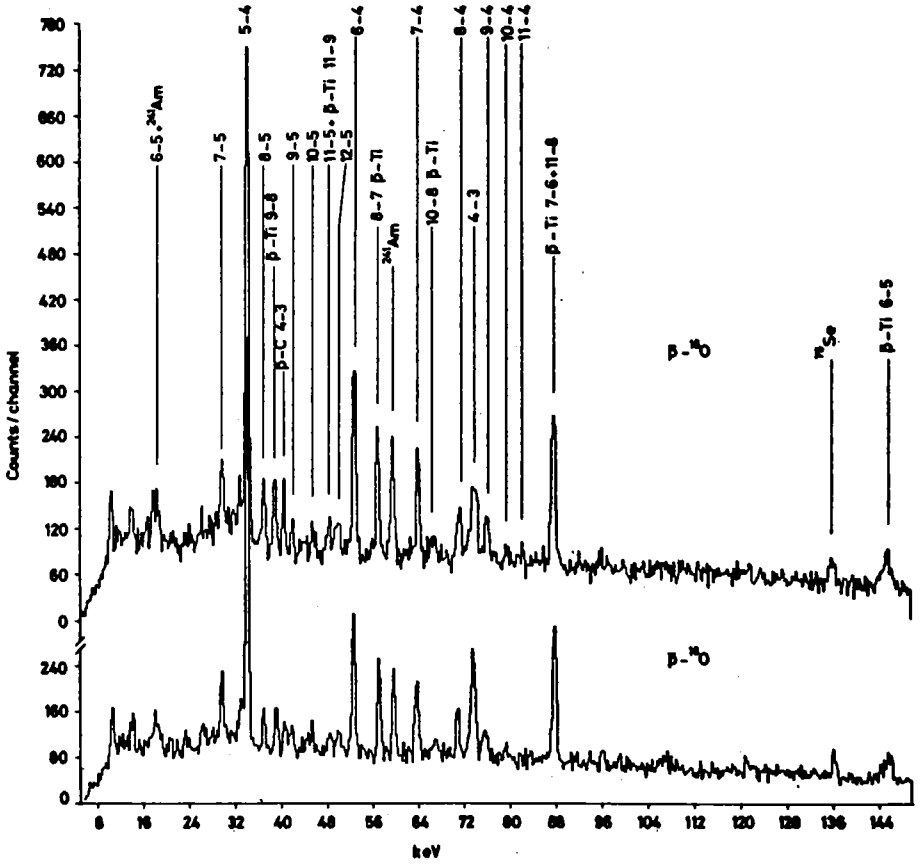

Fig. 2. The $\bar{p}$-^{18}O/^{16}O X-ray spectrum.

The data taking period was about two months. This fact evidences the importance of a substantial increase of antiproton beam intensity if a systematic survey of strong interaction effects in antiprotonic atoms is envisaged.

Evidently, the Low Energy Antiproton Ring will overcome many problems related to beam quality. Experiments will take advantage of the increase in

i) stopping power.
   Thin targets can therefore be used not requiring corrections for self-absorption of x-rays. Gaseous targets can be chosen whenever appropriate. Furthermore, the antiproton beam from LEAR will not contain pions, and the overall background will be reduced.
ii) geometrical beam quality.
   The beam size will be considerably reduced. Therefore small and thin targets can be used allowing to investigate rare and expensive isotopes.
iii) x-ray intensity.
   Therefore strong interaction effects can be measured accurately with high resolution (i.e. small) solid state detectors thus leading to an increase in statistical accuracy and in reliability of the data. Also extremely weak lines which will show large strong interaction effects can be investigated.
iv) data rate.
   Even for small and thin targets good statistical accuracy can be achieved in short running periods so that systematic studies over parts of the periodic table become feasible.

From these data effective antiproton nucleon scattering lengths can be derived with increased statistical accuracy and reliability. Separate determinations of strong interaction effects of the two fine structure components allow to derive the L-S dependence of the $\bar{p}p$ interaction. In high-n atomic orbits strong interaction effects are negligible and the fine structure separation can be used to determine the antiproton magnetic moment [13], while the transition energies can be used to measure the antiproton mass [11].

With the aid of a crystal spectrometer the hyperfine structure of atomic levels will be accessible. As in the case of muonic atoms a wealth of information is hidden there concerning nuclear structure. But for antiprotons there are important differences. Particularly since the $\bar{p}p$ and $\bar{p}n$ interactions are not known precisely measurements of the hyperfine structure separation in antiprotonic atoms could be exploited to study the basic interaction. Since antiprotons interact dominantly at the nuclear surface a new tool for the study of the structure of the nuclear surface will be available.

The measurement of nuclear γ rays as a signature of the nucleus remaining after absorption of the antiproton will give information about the preferential interaction with nuclear protons or neutrons. Coincidence measurements between x-rays and nuclear γ rays may yield partial absorption widths for selected annihilation channels.

III Antiprotonic Hydrogen and Deuterium

The $\bar{p}p$ and $\bar{p}d$ atoms clearly deserve special attention because they are the simplest systems to study nucleon-antinucleon interactions. The energy levels of antiprotonic hydrogen correspond to those of ordinary hydrogen, but the Rydberg constant is scaled by a factor of $m_p/2m_e$ due to the increased reduced mass of the system. The Rydberg constant of $\bar{p}d$ is larger by a further factor of 4/3.

The strong interaction manifests itself dominantly in a shift and broadening of the 1S levels which are, in the case of $\bar{p}p$, in the order of 1 keV. Shift and broadening are related to the complex antiproton proton or antiproton neutron scattering lengths by

$$\Delta E + \frac{i\Gamma}{2} = \frac{4}{a_o} \cdot a_{\bar{p}p} \quad (+ a_{\bar{p}n})$$

The 2P levels will also be shifted and broadened resulting in a reduced K_α x-ray intensity. So the measurable quantities are

identical to those of other antiprotonic atoms with the 1S state as lower and the 2P state as upper levels. But the detection of x-rays from antiprotonic hydrogen and deuterium is more difficult than from other atoms because of a number of experimental reasons :

i) The x-ray energy is low.

The Lyman series (K-line series) has expected energies of about 10 keV, the Balmer series (L-line series) falls into the 2-3 keV energy range. Yet in liquid hydrogen targets the windows have to be covered by superinsulating foils to provide thermal shielding. Thus the effective x-ray window thickness is about 100 μ mylar and the average L line transmission is .2% only.

ii) The Stark effect reduces the intensity.

Antiprotons are captured by the Coulomb field of protons or deuterons in high-n atomic orbits. In collisions with neighbouring molecules $\bar{p}p$ and $\bar{p}d$ atoms will experience large electric fields mixing states of different angular momenta. As annihilation is very strong in S states the number of antiprotons reaching low lying levels is considerably reduced, and the yield of x-rays populating the n=1 and n=2 levels is small. [14] Even in 4 atm gaseous hydrogen and deuterium the population of the 2P level is only 6%. [15] It drops to 4% if the pressure is increased to 8 atm. [16] In liquid hydrogen possible evidence was found for the detection of the K x-ray series from antiprotonic hydrogen [17]. Unfortunately, the energies of the x-rays - which were tentatively ascribed to protonium - coincide in their energy and their width with well known electronic fluorescence lines from Fe, Cu and Zn. Therefore further experiments are needed to establish the x-ray pattern as genuine antiprotonic hydrogen K series.

iii) Annihilation from 2P levels competes with radiative transitions.

From experiment [11] we know that annihilation dominates radiative transitions by at least a factor of 10. Black sphere model calculations, which proved to be very reliable in calculating strong interaction widths of heavier antiprotonic atoms, predict a branching ratio of 1:100 for radiative transitions from the

2P level of antiprotonic hydrogen [18] compared to annihilation. In $\bar{p}d$ the yield of K x-rays is probably reduced to another factor of 10 or 100 due to the bigger size of the deuteron and the more compressed atomic wave function. As the deuteron wave function contains l = 2 waves, some S wave contribution may be mixed into the atomic 3D $\bar{p}d$ wave function, and even annihilation from the 3D state may be appreciable. The yield of K-lines is therefore small, and intensive low momentum antiproton beams are needed to meet the requirement of high stop rates in low density gas.

If K x-rays from antiprotonic hydrogen and deuterium can be detected and their energies be measured, the scattering lengths for antiproton scattering off proton and neutrons can be derived. These scattering lengths can then be compared to theoretical predictions based on One-Boson-Exchange-Potentials for the antiproton-nucleon interaction. Yet the comparison still requires the analysis of isospin mixing in the 1S state, an analysis which, however, seems to be feasible. [19] As soon as low energy antiproton-proton scattering data are available, the scattering lengths from $\bar{p}p$ x-rays can be compared with extrapolated scattering cross sections. Any discontinuity in this comparison would strongly indicate the presence of a $\bar{p}p$ resonance at threshold. The strong $\bar{p}p$ interaction is basically attractive, and an increase of binding energies in the $\bar{p}p$ atom should be expected. A negative interaction shift of the $\bar{p}p$ 1 S state might therefore by itself point to the existence of an S wave nuclear bound state. [20] Yet this interpretation is not unique, as annihilation may be so strong as to push out the atomic wave function resulting in an apparently repulsive interaction. [21] The inference from a negative interaction shift on a nuclear bound state would be much better grounded if the strong interaction shift has different signs for $\bar{p}p$ atoms in the $^1S_0$ and $^3S_1$ states.

Hopefully, the strong interaction widths of the 1S and 2P states can also shed some light on the annihilation range. Neglecting distortion of the atomic wave function the width of the levels is proportional to the $\bar{p}p$ density inside the annihilation range.

Consequently,

$$\frac{\Gamma_{2P}}{\Gamma_{1S}} = \frac{\int_0^{R_a} R^2 \, |\psi_{2P}(R)|^2 \, d\zeta}{\int_0^{R_a} R^2 \, |\psi_{1S}(R)|^2 \, d\zeta}$$

Of course, distortion cannot be neglected, but it can be taken into account once the strong interaction effects in $\bar{p}p$ atoms are measured.

IV Annihilation of $\bar{p}p$ atoms in coincidence with atomic x-rays

The study of annihilation products of the $\bar{p}p$ system in coincidence with atomic x-rays provides a link between investigations of static properties of the $\bar{p}p$ interaction and the dynamics of the annihilation process. This link can be exploited i) to determine the angular momentum state of the $\bar{p}p$ atom from annihilation products, ii) to investigate conservation laws of the strong interaction at very short distances, or iii) to select annihilation channels with specific quantum numbers.

i) Annihilation products can be used to identify the angular momentum state of the $\bar{p}p$ atom when it annihilates. From bubble chamber experiments it was concluded that annihilation occurs predominantly from S states, when antiprotons are stopped in liquid hydrogen targets. [21] Yet in two counter experiments an appreciable annihilation from P states was found, [22] so the question deserves further study. The puzzle can be resolved by measuring the prong distribution in coincidence with K x-rays and L x-rays from the $\bar{p}p$ atom. Because of the strong absorption from the 2P state, annihilation following the emission of an L x-ray will occur from the 2P state in most of the cases (more than 90 %), while the emission of a K line uniquely identifies the final state as S state. Annihilation in liquid hydrogen will thus be decomposed into a superposition of annihilations from S and P states.

From annihilation products in coincidence with K lines the total spin of the $\bar{p}p$ atom can be determined. K x-rays followed by annihilation into neutral pions only identify the final state as ^1S_o state; this annihilation channel occurs with a branching ratio of 3% if antiprotons are stopped in liquid hydrogen. If the requirement is simply that no charged particle should be present in the annihilation the 1^3S_1 state is not completely excluded due to neutral kaonic decay modes including $n\pi^o$, but the frequency for these decays is below 5.10^{-3}. [24] The 1^3S_1 state can unambiguously be determined by its decay modes $\bar{p}p \to \pi^+\pi^-$, K^+K^-, $\bar{K}_L K_S$ or $\bar{K}_S K_L$, which, however, deserve reconstruction of the annihilation process.

ii) We would like to emphasize that the $\bar{p}p$ atom is an ideal system to study conservation laws like C and P invariance of the strong interaction at very short distances. Evidence for C violation was claimed in an experiment comparing the binding energies of $^4_\Lambda H$ and $^4_\Lambda He$ [25]. Parity nonconservation of the nuclear interaction was established by the α decay of the 8.87 MeV state of

^{16}O $(J^\pi = 2^-)$ into the ground state of ^{12}C $(J^\pi = 0^+)$. [26]

The effect is interpreted as self interaction of the strangeness conserving weak hadronic current mediated by ρ exchange. [27] In nuclei the hard core prevents ρ exchange from playing an appreciable role and short ranged parity violating effects are grossly reduced, while in $\bar{p}p$ annihilation the range is of the order of 0.5 fm. Furthermore annihilation offers the possibility to search for parity violating effects in strangeness conserving and in strangeness changing currents by selecting pionic or kaonic decay modes. Table I shows which symmetries are violated if specific decay modes are seen. [28] The observation of $\bar{p}p \to \pi^o\pi^o$ or $\bar{K}_S K_S$ in coincidence with K x-rays immediately establishes violation of a fundamental symmetry. A histogram of x-rays (which can distinguish K x-rays from para- and orthoprotonium) has to be built up in order to ascertain the type of symmetry breaking.

Table I: Symmetry violations allowing for specific annihilation modes. The branching ratios refer to antiprotons stopped in liquid hydrogen where the initial state is not known.

Initial state	Final state				
$\bar{p}p$	$\pi^+\pi^-$	$\pi^o\pi^o$	K^+K^-	$\bar{K}_L K_S$ or $\bar{K}_S K_L$	$\bar{K}_S K_S$ or $\bar{K}_L K_L$
1^1S_o	P	PandC	P	P and C	P
1^3S_1	$32 \cdot 10^{-4}$	PandC	$11 \cdot 10^{-4}$	$5.6 \cdot 10^{-4}$	P and C

iii) As has been pointed out before, the large branching ratio for annihilation from the 2P state of $\bar{p}p$ atoms leads to the conclusion that the detection of an L x-ray provides a reasonably clean trigger for P wave annihilation. A trigger for P wave annihilation is of special interest in experiments searching for radiative or pionic transitions to quasinuclear bound states [29], because these states are more likely to be narrow (and therefore easier to be detected) if they have high angular momenta. The observation of L x-rays in coincidence with annihilation products thus provides a new tool for annihilation studies. A complete experiment on $\bar{p}p$ annihilation at rest will therefore require the detection of atomic x-rays to define the initial state from which annihilation occurred as well as energies and momenta of the charged and neutral annihilation products.

V Unconventional Experiments

Apart from the enormous gain in stopping power which will facilitate experiments which otherwise would use untolerably long running times, atomic physics experiments also have been suggested which either depend on storage of antiprotons or suffer from intensity problems even at LEAR intensities.

First it has been suggested by U. Gastaldi to overlap the stored antiproton beam with an H^- beam: [30] antiprotons from the beam thus will be captured by Auger effect and a neutral antiprotonic hydrogen beam is formed. Its velocity depends on the beam momentum, therefore the x-ray energies can be tuned to coincide with an appropriately chosen x-ray absorption foil, a method exploited in ref. 31). It is claimed that the energy of x-rays from $\bar{p}p$ atoms can therefore be measured with much better precision than by other methods. In addition, the use of high power lasers can provide access to the measurement of quantities which are otherwise not accessible to experiment. The method is exemplified by outlining an experiment to measure the strong interaction effects in the 3P state of the $\bar{p}p$ atom.

Table II shows the energy levels of the n=3 states of the $\bar{p}p$ atom calculated from QED [32]. The strong interaction of the 3S levels leads to shifts and broadenings of the order of 1keV/27 $\simeq$ 40 eV. These levels can therefore be disregarded for our purposes. The strong interaction shifts and widths of the 2P levels were calculated in ref. 17). The shifts and widths of the 3P levels can be calculated by scaling with a factor 2.73.[17] The strong interaction shifts and widths of the 3D levels can also be evaluated following the technique of ref. 16). The results are listed in Table II. Obviously, strong interaction effects are negligible in 3D states. Cascade calculations show that circular transitions are dominant when $\bar{p}p$ atoms cascade in vacuum down to low-lying levels. [33] In passing through the 3D levels a high power laser may drive transitions to 3P levels thus reducing the L x-ray intensity. (The 3P state will dominantly decay by annihilation or by Kβ x-ray emission.) Thus induced 3D → 2P transitions may be observed. The transition has to take place within the lifetime of the 3P states which is 2.10^{-13} sec (average lifetime). Therefore a Laser power similar to the muonic helium Lamb shift experiment is required. Bunching of antiprotons and sudden cascade quenching by electric field discharge may help to increase the number of $\bar{p}p$ atoms in the 3D states when the Laser is "on".

Table II: a) Energy level splitting of states with n=3 in $\bar{p}p$ atoms without strong interaction

3^1S_0 -43.7 meV	3^1P_1 -10.8 meV	3^1D_2 -4.3 meV
	3^3P_2 100.1 meV	3^3D_3 30.1 meV
3^3S_1 1133.9 meV	3^3P_1 - 121.7 meV	3^3D_2 -12.2 meV
	3^3P_0 -232.7 meV	3^3D_1 -55.0 meV

b) Strong interaction effect $\Delta E + i\Gamma/2$ of states with n=3 in $\bar{p}p$ atoms

3^1S_0 ~ 40 eV	3^1P_1 (-10.3+4.4i) meV	3^1D_2 0.02i μeV
	3^3P_2 (0+7.7i) meV	3^3D_3 0.94i μeV
3^3S_1 ~ 40 eV	3^3P_1 (12.8+5.1i) meV	3^3D_2 0.04i μeV
	3^3P_0 (-25.3+35.3i) meV	3^3D_1 1.00i μeV
Radiative width Γ_{rad}	0.20 meV	78 μeV

Furthermore it has been suggested by Torelli and his colleagues to trap antiprotons in a penning trap. [34] Protons and electrons have been trapped for a long time in such a device; the number of trapped particles varied from one to 10^5 .[35] In normal uses the particles to be trapped are created by ionization of the residual gas inside the trap. For antiprotons there will be the difficulty of injection of antiprotons into the trap, techniques for this injection have not yet been tested. If this difficulty can be overcome, the antiproton mass can be measured using techniques exploited in the case of protons,[36] capture processes can be studies in ultra high vacuum, and annihilation can be observed under very clean conditions.

Electrons, protons and their antiparticles can form four types of atoms;

	e^-	$\bar{p}$
e^+	1951	?
p	1766	1978

ordinary hydrogen, revealed in 1766 by Cavendish, positronium discovered by Deutsch [37] in 1951, protonium, which was shown to exist in 1978, [10] and antihydrogen. The detection of antihydrogen will be difficult even with high intensity antiproton beams, because of the low intensity of monochromatic positron beams,and the small radiative cross section for positron capture. A successful search for antihydrogen will therefore possibly require the construction of a Low Energy Positron Ring to over - come the intensity problems.

If the existence of antihydrogen can be established, its binding energies can be compared to those of normal hydrogen, and the invariance of CPT can be tested. It should be pointed out, however, that various tests of CPT exist already, and the assumption seems safe that antihydrogen will never provide the most

stringent test of CPT. But as the simplest atomic system composed of antiparticles only, antihydrogen is clearly a challenge for experimenters to try to verify its existence.

Acknowledgements :

I would like to thank Prof. G. Backenstoss for eluminating discussions and a critical reading of the manuscript.

References

1.) G. Plass, The Low Energy Antiproton Ring, Contribution to this workshop.

2.) G. Backenstoss, Exotic Atoms. In: Prog. Atomic Spectroscopy. Ed. by W. Haule a. H. Kleinpoppen, Plenum Press, 1979.
R. Seki and C.E. Wiegand, Annu. Rev. Nucl. Sci. 25(1975) 241.
H. Koch, Muonic and Hadronic Atoms. In: Nuclear and Particle Physics at Intermediate Energies. Ed. by J. Warren, Plenum Press 1976.

3.) C.E. Wiegand and G.K. Godfrey, Phys. Rev. 9A(1974) 2282.

4.) L. Tauscher, Hadronic Atoms. In: The 1st Course of the Intern. School of Phys. of Exotic Atoms, Erice 1977.

5.) M. Ericson and T.E.O. Ericson, Ann. Phys. 36 (1966) 323

6.) J.F.Haak, A. Lande and F. Iachello, Phys. Lett. 66B (1977) 16.

7.) W.B. Kaufmann and H. Pilkuhn, Phys. Lett. 62B (1976) 165.

8.) E.B.Shera et al., Phys. Rev. C 14 (1976) 731.

9.) H.Poth, Physics Data 14-1 (1979).

10.) E.G.Auld et al., Phys. Lett. 77B (1978) 454.

11.) B.L.Roberts, Phys. Rev. 17D (1978), 358.

12.) H.Poth et al., Nucl. Phys. A 294 (1978) 435.

13.) P. Robertson et al., Phys. Rev. C 16(1977) 1945.

14.) T.B.Day, G.A.Snow and J. Sucher, Phys. Rev. 118 (1960) 864.

15.) E.G.Auld et al., $\bar{p}p$ and $\bar{p}d$ Interactions at Threshold. In: Proc. IV Europ. Antiproton Symposium, Barr 1978 (France).

16.)Preliminary result from the authors of ref. 15.

17.)M.Izycki et al., Results on the measurement of K series x-rays from antiprotonic hydrogen. In: Proc. IV Europ. Antiproton Symposium, Barr (1978) France.

18.)W.B.Kaufmann and H. Pilkuhn, Phys. Rev. C 17(1978) 215. W.B.Kaufmann, Phys. Rev. C 19 (1979), 440.

19.)H.Pilkuhn, private communication.

20.)A.E.Kudryavtsev, V.E.Markushin, and I.S.Shapiro, Soviet Phys. JETP 47 (1978), 225.

21.)S.Caser and R. Omnès, Phys. Lett. B 39 (1972) 369.

22.)R.Armenteros et al., Phys. Lett. 17 (1965) 344. C.Baltay et al., Phys. Rev. Lett. 15 (1965) 532.

23.)S.Devons et al., Phys. Rev. Lett. 27 (1971) 1614. G.Bassiompierre et al., Measurement of the $\pi^o\pi^o$ production in $\bar{p}p$ annihilation at rest. In: Proc. IV European Antiproton Symposium, Barr (France) 1978.

24.)R.Armenteros et al., Phys. Lett. 17 (1965) 170.

25.)A.Bemberger et al., Nucl, Phys. B60 (1973) 1.

26.)K.Neubeck, H. Schober and H.Wäffler, Phys. Rev. C 10 (1974) 320.

27,)M.Gari,H.Kümmel and J.G.Zabolitzky, Nucl, Phys. A161(1971)625.

28.)J.J.Sakurai, Invariance Principles and Elementary Particles, Princeton University Press, 1964.

29.)P.Pavlopoulos et.al., Phys. Lett.72B (1978) 415.

30.)U.Gastaldi, $\bar{p}p$ Experiments at very low energy using cooled antiprotons. In: Proc. IV Europ. Antiproton Symposium, Barr (France) 1978.

31.) J.Bailey et al., Phys. Lett. 50B (1974) 403.

32.) H.A.Bethe and E.E.Salpeter, Quantum Mechanics of One- and Two-Electron Systems. In: Handbuch der Physik, Bd. XXXV.

33.) U.Gastaldi, R.Landua and E.Jacopini, Atomic cascades in vacuum of $\bar{p}p$ atoms formed in flight with the reaction $\bar{p} + H^- \rightarrow \bar{p}p + 2e^-$, Contribution to this workshop.

34.) G.Torelli et al., Unusual approach to the Low energy $\bar{p}p$ physics. Contribution to this workshop.

35.) H.Dehmelt, Adv. At.Mol.Phys. 3 (1967) 53.

36.) G.Gärtner and E. Klempt, Z.Physik A 287 (1978) 1.

37.) M.Deutsch, Phys. Rev. 82 (1951) 455.

LIST OF $\bar{p}$ LEAR - NOTES

(available upon request from U. Gastaldi, K. Kilian and H. Poth, CERN, EP-Division)

---

1. U. Gastaldi and K. Kilian

   Activity of the working groups on LEAR physics preparing the Karlsruhe workshop 19-21 March, 1979, CERN $\bar{p}$ LEAR-Note 01.

2. J. Nassalski, I.P. Zielinski

   Note on the study of the production of light antinuclei ($\bar{p}$: $\bar{d}$) in nuclear interactions, CERN $\bar{p}$ LEAR-Note 02.

3. J. Rafelski

   What can we learn from $\bar{p}$-A annihilation in flight? CERN $\bar{p}$ LEAR-Note 03.

4. F. Balestra, L. Busso, P.F. Dalpiaz, R. Garfagnini, G. Piragino, L. Tecchio, I.V. Falomkin, G.B. Pontecorvo, Yu. A. Shcherbakov, A. Maggiora, C. Guaraldo and R. Scrimaglio

   Fine spectroscopy of baryonic states near threshold, CERN $\bar{p}$ LEAR-Note 04.

5. F. Balestra, L. Busso, P.E. Dalpiaz, R. Garfagnini, G. Piragino, L. Tecchio, I.V. Falomkin, G.B. Pontecorvo, Yu. A. Schcherbakov, M. Yu. Khlopov, Ya. B. Zeldovich, A. Maggiora, C. Guaraldo and R. Scrimaglio

   Low energy antiproton interactions in light nuclei, CERN $\bar{p}$ LEAR-Note 05.

6. J.C. Kluyver

   Is the S-Meson a baryonium state?, CERN $\bar{p}$ LEAR-Note 06.

7. A.H. Sørensen

   Calculations on electron cooling, CERN $\bar{p}$ LEAR-Note 07.

8. A.H. Sørensen

   Influence of a strong longitudinal field on electron cooling, CERN $\bar{p}$ LEAR-Note 08.

9. U. Gastaldi

   $\bar{p}p$ ($\bar{p}d$) interactions at very low kinetic energy with the parallel beam approach, CERN $\bar{p}$ LEAR-Note 09.

10. G.F. Chew, B. Nicolescu, J. Uschersohn and R. Vinh Mau

    Topological quark-gluon structure of elementary hadrons beyond mesons and baryons, CERN $\bar{p}$ LEAR-Note 10 and CERN-TH 2635.

11. M. Schneegans

$\bar{p}$-annihilation, vector mesons and charmonium, CERN $\bar{p}$ LEAR-Note 11.

12. R. Bertini

$\bar{p}$-interaction with nucleons, CERN $\bar{p}$ LEAR-Note 12.

13. G. Backenstoss

Antiprotonic atoms, CERN $\bar{p}$ LEAR-Note 13.

14. H. Poth

Metastable $\bar{p}$-atoms, CERN $\bar{p}$ LEAR-Note 14.

15. H. Poth

$\bar{n}$ beams from external targets, CERN $\bar{p}$ LEAR-Note 15.

16. G. Torelli

Unusual approach to the low energy $\bar{p}$-physics, CERN $\bar{p}$ LEAR-Note 16.

17. W. Kubischta

The CERN polarized atomic hydrogen target, CERN $\bar{p}$ LEAR-Note 17.

18. E. Iacopini and B. Smith

A microprocessor control system for a hydrogen gas target, CERN $\bar{p}$ LEAR-Note 18.

19. U. Gastaldi

Ultraslow $\bar{p}$ ejection from LEAR with H^-, CERN $\bar{p}$ LEAR-Note 19.

20. C. Voci

Antineutron beam at LEAR, CERN $\bar{p}$ LEAR-Note 20.

21. U. Gastaldi, E. Iacopini and R. Landua

Atomic cascades in vacuum of $\bar{p}p$ atoms formed in flight with the reaction $\bar{p} + H \rightarrow \bar{p}p + 2e^-$, CERN $\bar{p}$ LEAR-Note 21.

22. P. Gear

H^- sources for particle accelerators, CERN $\bar{p}$ LEAR-Note 22.

23. F. Bouvier

Preparation of ultrathin windows for soft X-ray gas proportional counters, CERN $\bar{p}$ LEAR-Note 23.

24. C. Zupancic

π^0 Jacobian peak spectroscopy, CERN $\bar{p}$ LEAR-Note 24.

25. E. Klempt

Annihilation of $\bar{p}p$ atoms coincident with x-rays from the atomic cascade, CERN $\bar{p}$ LEAR-Note 25.

26. M. Macri and F. Silombra

Baryonium via missing mass, CERN $\bar{p}$ LEAR-Note 26.

27. P. Pavlopoulos

Baryonium around threshold - discussion of experiments at LEAR, CERN $\bar{p}$ LEAR-Note 27.

28. Edinburgh-Rutherford-Westfield Collaboration

An experiment to measure the widths of the charmonium χ states using the low energy antiproton facility, CERN $\bar{p}$ LEAR-Note 28.

29. M. Bell, J.E. Chaney, F. Krienen and P. Møller Petersen

Report on the CERN electron cooler, CERN $\bar{p}$ LEAR-Note 29.

30. U. Gastaldi

$\bar{p}p$ interactions at very low energy using cooled antiprotons, CERN $\bar{p}$ LEAR-Note 30.

31. P. Dalpiaz and K. Kilian

Polarization with LEAR, CERN $\bar{p}$ LEAR-Note 31.

32. P. Dalpiaz

Charmonium, γ and $2N\bar{N}$, $2N2\bar{N}$, $Y\bar{Y}$ states with $\bar{p}$ at medium energies, CERN $\bar{p}$ LEAR-Note 32.

33. F. Sauli

Applications of the multistep avalance chamber, CERN $\bar{p}$ LEAR-Note 33.

34. K. Runge

The active H_2 gas target with proportional drift chambers at high pressure of the NA6 Fribourg-Moscow Collaboration, CERN $\bar{p}$ LEAR-Note 34.

35. U. Gastaldi

An X-ray drift chamber (XDC) as central core of a general purpose detector for $\bar{p}$ stop experiments, CERN $\bar{p}$ LEAR-Note 35.

36. C. Hill

H^- sources - a summary, CERN $\bar{p}$ LEAR-Note 36 and CERN/PS/LR/ Note 79-6.

37. D.J. Simon

A possible scheme to transfer 50 MeV H^- ions (and protons) from the old PS-Linac to LEAR, CERN $\bar{p}$ LEAR-Note 37 and CERN/PS/MU/BL/ Note 79-10.

38. P. Dalpiaz, P.F. Dalpiaz, M.A. Schneegans and L. Tecchio

Vector mesons and proton electromagnetic form factor with a 4π detector, CERN $\bar{p}$ LEAR-Note 38.

39. P. Dalpiaz, P.F. Dalpiaz, M.A. Schneegans and L Tecchio

Measurement of the proton electromagnetic form factor with an external liquid H_2 or internal H_2 jet target, CERN $\bar{p}$ LEAR-Note 39.

40. H. Herr and D. Möhl

Relativistic electron cooling in ICE, CERN $\bar{p}$ LEAR-Note 40 and PS/DL/Note 78-4.

41. M. Suffert

Detection of 20-1000 MeV γ-rays with NaI(Tα), CERN $\bar{p}$ LEAR-Note 41.

42. H. Koch

Production of antideuterons, CERN $\bar{p}$ LEAR-Note 42.

43. W. Obert

Production of intense condensed molecular beams (cluster beams), CERN $\bar{p}$ LEAR-Note 43.

44. K. Kilian and D. Möhl

Gas jet target in LEAR, CERN $\bar{p}$ LEAR-Note 44.

45. P. Birien and K. Kilian

Experiments with very low energy antiprotons from LEAR, CERN $\bar{p}$ LEAR-Note 45.

46. M. Conte

Head on collisions in LEAR, CERN $\bar{p}$ LEAR-Note 46.

47. F. Balestra, L. Busso, P.F. Dalpiaz, R. Garfagnini, G. Pinagino, L. Tecchio, A. Maggiora, G.B. Ponteconvo and Yu. A. Shchenbakov

Interaction of low energy $\bar{n}$ in D_2, H_2 and in light nuclei (^{3}He, ^{4}He), CERN $\bar{p}$ LEAR-Note 47.

48. J. Bailey

On protonium and baryonium, CERN $\bar{p}$ LEAR-Note 48.

49. S. Limentani

$\bar{p}p$ to final states with (anti)hyperons, CERN $\bar{p}$ LEAR-Note 49.

50. J.C. Kluyver

Investigation of the S-meson with the LEAR facility, CERN $\bar{p}$ LEAR-Note 50.

51. H. Poth

Antiproton charge exchange and antineutron interactions, CERN $\bar{p}$ LEAR-Note 51.

52. H. Koziol

The CERN antiproton accumulator (AA), CERN $\bar{p}$ LEAR-Note 52 and CERN/PS/AA/Note 79-2.

53. H. Koziol

Beam diagnostics for LEAR, CERN $\bar{p}$ LEAR-Note 53 and CERN/PS/AA/Note 79-3.

54. L. Bracci, G. Fiorentini and O. Pitzurra

$\bar{p}p$ atom formation via atomic capture of $\bar{p}$ from H^-, H^o, H^+ hydrogen ions, CERN $\bar{p}$ LEAR-Note 54.

55. P. Dalpiaz

Charmonium and other -oniums at minimum energy, CERN $\bar{p}$ LEAR-Note 55.

56. I.P. Zielinski

On the use of low energy antiprotons for study of the influence of channeling on nuclear reaction yields, CERN $\bar{p}$ LEAR-Note 56.

57. G. Stefanini

ICE beam profile monitors, CERN $\bar{p}$ LEAR-Note 57.

58. H.H. Andersen and E. Uggerhøj

A proposal for channeling and energy-loss measurements at the low-energy facility LEAR at CERN, CERN $\bar{p}$ LEAR-Note 58.

59. U. Gastaldi

Physics with LEAR as a storage ring, CERN $\bar{p}$ LEAR-Note 59.

60. K. Kilian

Physics with LEAR in its first stage, CERN $\bar{p}$ LEAR-Note 60.

61. M. Schneegans

$N\bar{N}$ annihilation, CERN $\bar{p}$ LEAR-Note 61.

62. H. Koch

Investigations on baryonium with stopped antiprotons, CERN $\bar{p}$ LEAR-Note 62.

63. B. Povh

Baryonium with antiprotons in flight, CERN $\bar{p}$ LEAR-Note 63.

64. W. Hardt

Slow extraction from LEAR, CERN $\bar{p}$ LEAR-Note 64 and CERN/PS/DL/ Note 79-4.

65. W. Hardt

Slow ejection based on repetitive unstacking, CERN $\bar{p}$ LEAR-Note 65.

66. H. Poth

Fundamental properties of antinucleons, CERN $\bar{p}$ LEAR-Note 66.

67. G. Carron, H. Herr, G. Lebee, H. Koziol, F. Krienen, D. Möhl, G. Petrucci, C. Rubbia, F. Sacherer, G. Sadoulet, G. Stefanini, L. Thorndahl, S. van der Meer and T. Wikberg

Experiments on stochastic cooling in ICE, CERN $\bar{p}$ LEAR-Note 67 and CERN-EP/79-16.

68. J. Davies

Solid state detectors for low energy X-rays, CERN $\bar{p}$ LEAR-Note 68.

69. M. Calvetti

Tests of a prototype of the UA1 TPC, CERN $\bar{p}$ LEAR-Note 69.

70. E. Klempt

Antiprotonic atoms, CERN $\bar{p}$ LEAR-Note 70.

71. C. Voci

Antineutron physics at LEAR, CERN $\bar{p}$ LEAR-Note 71.

72. R. Baldini-Celio

Experimental results on e^+e^- annihilations below 3 GeV, CERN $\bar{p}$ LEAR-Note 72.

73. D. Möhl

Possibilities and limits with cooling in LEAR, CERN $\bar{p}$ LEAR-Note 73 and CERN PS/DL/Note 79-5.

74. P. Pavlopoulos

A detection system for conclusive studies of $\bar{p}p$-annihilation and baryonium, CERN $\bar{p}$ LEAR-Note 74.

75. Chan Hong Mo

Baryonium, CERN $\bar{p}$ LEAR-Note 75.

LIST OF PARTICIPANTS

1.	H.H. Andersen	Inst. of Physics, Aarhus
2.	E. Aslanides	CNRS, Strasbourg
3.	G. Backenstoss	Inst. f. Physik, Basel
4.	J. Bailey	IKO, Amsterdam
5.	P. Barnes	Saclay/Carnegie-Mellon
6.	C. Bemporad	INFN, Pisa
7.	I. Bergström	Research Inst. of. Phys.,Stockholm/CERN,EP
8.	R. Bertini	CRN, Strasbourg/CERN
9.	P. Birien	CEN Saclay/CERN
10.	R. Bizzarri	Inst. di Fisica, Roma
11.	P. Blüm	CERN, EP-Div./Inst. für Kernphysik, Karlsruhe
12.	E. Boschitz	Institut für Kernphysik, Karlsruhe
13.	E. Borie	Inst. für Theoret. Phys., Karlsruhe
14.	G. Büche	Inst. für Kernphysik, Karlsruhe
15.	D. Bugg	Queen Mary College, London
16.	D. G. Candlin	CERN, EP-Div.
17.	M. Castellano	INFN, Napoli
18.	Chan Hong Mo	Rutherford Lab./CERN-TH-Div.
19.	A. Citron	Institut für Kernphysik, Karlsruhe
20.	M. Conte	Inst. di Scienze Fisiche, Genova
21.	P. Dalpiaz	Inst. di Fisica Superiore
22.	P.F. Dalpiaz	dell' Univ. e INFN, Torino
23.	L. Dick	CERN, EP-Div.
24.	J. Domingo	SIN, Villigen
25.	D. Engelhardt	Inst. für Kernphysik, Karlsruhe
26.	T. Ericson	CERN, TH-Div.
27.	G. Fiorentini	Univ. di Pisa
28.	E. Gabathuler	CERN, EP-Div.
29.	S. Galster	Institut für Kernphysik, Karlsruhe
30.	M. Garçon	CEN Saclay

31.	U. Gastaldi	CERN EP-Div./Inst.of Phys., Mainz
32.	W. Hardt	CERN, PS-Div.
33.	L. Hoffmann	CERN, PS-Div.
34.	I. Khubeis	Univ. Amman/Jordanien
35.	R. Klapisch	CNRS Orsay
36.	E. Klempt	Inst. of Physics, Mainz
37.	J. Kluyver	Zeeman Lab. Amsterdam
38.	K. Kilian	CERN, EP-Div./MPI Heidelberg
39.	S. Kitamura	Tokyo Univ./CERN EP-Div.
40.	H. Koch	CERN EP-Div./Inst. für Kernphysik, Karlsruhe
41.	W. Koziol	CERN, PS-Div.
42.	F. Krienen	CERN, EP-Div.
43.	W. Kubischta	CERN, EP-Div.
44.	W. Kühn	Inst. für Kernphysik, Karlsruhe
45.	R. Landua	Inst. of Physics, Mainz
46.	S. Limentani	Univ. di Padova
47.	P. Litchfield	Rutherford Lab., England
48.	M. Macri	INFN, Genova
49.	B. Mayer	Saclay/CERN, EP-Div.
50.	D. Möhl	CERN, PS-Div.
51.	K.O. Nielsen	Inst. of Phys., Aarhus
52.	P. Pavlopoulos	CERN, EP/Inst. für Physik, Basel
53.	E. Pauli	CERN EP/Saclay
54.	H. Pilkuhn	Inst. für Theoret. Phys., Karlsruhe
55.	G. Piragino	Univ. di Torino
56.	G. Plass	CERN, PS-Div.
57.	H. Poth	CERN-EP/Inst. für Kernphysik, Karlsruhe
58.	B. Povh	MPI, Heidelberg

59.	J. Saudinos	CEN-Saclay
60.	M. Schneegans	LAPP, Annecy-le-Vieux
61.	F. Silombra	INFN, Genova
62.	A. Sørensen	Univ. Aarhus
63.	V. Soergel	CERN/Univ. Heidelberg
64.	M. Suffert	CRN, Strasbourg/CERN-EP-Div.
65.	L. Tauscher	Univ. Basel
66.	L. Tecchio	INFN, Torino
67.	R. Tegen	Inst. für Theoret. Physik, Mainz
68.	G. Tibell	CERN, EP-Div.
69.	G. Torelli	INFN, Pisa
70.	E. Uggerhøj	Inst. of Physics, Aarhus
71.	P. Wånderer	BNL, Brookhaven
72.	W. Weise	Inst. für Theoretische Physik, Regensburg
73.	B.L. White	Vancouver, Dept. of Phys., UBC, Canada
74.	C.A. Wiedner	MPI, Heidelberg
75.	E. Winkelmann	ETH, Zürich
76.	A. Winnacker	MPI, Heidelberg
77.	D. Wolfe	Univ. New Mexico/BNL Brookhaven
78.	C. Zupancic	LMU, München